การสังเคราะห์อนุพันธ์ 1,4-ไดไฮโดรพิริดีนเป็นฟลูออเรสเซนต์เซ็นเซอร์ชนิดใหม่

นางสาวดารณี หอมระรื่น

SYNTHESIS OF 1,4-DIHYDROPYRIDINE DERIVATIVES AS NOVEL FLUORESCENT SENSORS

Miss Daranee Homraruen

A Thesis Submitted in Partial Fulfillment of the Requirements

for the Degree of Master of Science Program in Petrochemistry and Polymer Science

Faculty of Science

Chulalongkorn University

Academic Year 2011

Thesis Title   SYNTHESIS OF 1,4-DIHYDROPYRIDINE DERIVATIVES AS NOVEL FLUORESCENT SENSORS

By   Miss Daranee Homraruen

Field of Study   Petrochemistry and Polymer Science

Thesis Advisor   Anawat Ajavakom, Ph.D.

Thesis Co-advisor   Luxsana Dubas, Ph.D.

Accepted by the Faculty of Science, Chulalongkorn University in Partial Fulfillment of the Requirements for the Master's Degree

………………………………… Dean of the Faculty of Science

(Professor Supot Hannongbua, Dr.rer.nat)

THESIS COMMITTEE

……………………………………Chairman

(Professor Pattarapan Prasassrakich, Ph.D.)

……………………………………Thesis Advisor

(Anawat Ajavakom, Ph.D.)

……………………………………Thesis Co-advisor

(Luxsana Dubas, Ph.D.)

……………………………………Examiner

(Assistant Professor Varawut Tangpasuthadol, Ph.D.)

……………………………………External Examiner

(Vachiraporn Ajavakom, Ph.D.)

ดารณี หอมระรื่น :   การสังเคราะห์อนุพันธ์ 1,4-ไดไฮโดรพิริดีนเป็นฟลูออเรสเซนต์เซ็นเซอร์ชนิดใหม่ (SYNTHESIS OF 1,4-DIHYDROPYRIDINE DERIVATIVES AS NOVEL FLUORESCENT SENSORS) อ.ที่ปรึกษาวิทยานิพนธ์หลัก : ดร. อนวัช อาชวาคม, อ. ที่ปรึกษาวิทยานิพนธ์ร่วม : ดร. ลักษณา ดูบาส, 90 หน้า.

งานวิจัยนี้เกี่ยวข้องกับการสังเคราะห์อนุพันธ์ 1,4-ไดไฮโดรพิริดีนที่มีหมู่แทนที่ที่ตำแหน่งไนโตรเจนต่างๆกัน โมเลกุล1,4-ไดไฮโดรพิริดีนไตรเอสเทอร์ (1) สามารถเตรียมได้จากการปิดวงของโมเลกุลเบต้าอะมิโนอะคริเลทด้วยไททาเนียมเตตระคลอไรด์ที่อุณหภูมิห้อง การทำปฏิกิริยาไฮโดรไลซิสของ 1 ด้วยโพแทสเซียมไฮดรอกไซด์จะเปลี่ยนหมู่ไตรเอสเทอร์เป็นหมู่ไตรคาร์บอกซิลิก (2) ที่สามารถละลายน้ำได้ จากนั้นนำเอาอนุพันธ์ไตรคาร์บอกซิลิกที่สังเคราะห์ได้มาศึกษาสมบัติการดูดกลืนแสงและคายแสงในสารละลายฟอสเฟตบัฟเฟอร์ pH 8.0 โดยมีค่าการดูดกลืนแสงสูงสุดอยู่ในช่วงความยาวคลื่น 280 ถึง 300 และ 347 ถึง 358 นาโนเมตร การคายแสงสูงสุดอยู่ในช่วงความยาวคลื่น 432 ถึง 445 นาโนเมตร   และมีประสิทธิภาพในการคายแสง (Φ_f) เท่ากับ 0.07 ถึง 0.23 โมเลกุล1,4-ไดไฮโดรพิริดีนที่มีหมู่แทนที่เป็นเมทอกซีฟีนิลจะให้การวาวแสงฟลูออเรสเซนต์ที่ดีที่สุดเมื่อมองด้วยด้วยตาเปล่าจึงเลือกนำไปศึกษาต่อในการประยุกต์ใช้เป็นฟลูออเรสเซนต์เซ็นเซอร์ พบว่าสารดังกล่าวสามารถเกิดอันตรกิริยากับปรอทได้อย่างจำเพาะเจาะจง โดยการที่สัญญาณฟลูออเรสเซนต์ลดลงคาดว่ามาจากปฏิกิริยาออกซิเดชันของวงไดไฮโดรพิริดีนที่มีปรอทเป็นตัวเร่งอย่างจำเพาะเจาะจงทำให้เกิดการเปลี่ยนแปลงโครงสร้างไปเป็นพิริดิเนียม การลดลงของสัญญาณฟลูออเรสเซนต์นี้แปรผันตรงกับความเข้มข้นของปรอทด้วยค่าคงที่ของการระงับสัญญาณที่สูง (Ksv = 78,300 (โมลาร์)$^{-1}$) และค่าการตรวจวัดต่ำสุด 0.2 ไมโครโมลาร์ จากผลการทดลองใช้ไตรคาร์บอกซิลิกแอซิด 2 ในการตรวจวัด Fe^{2+} และ Fe^{3+} ด้วยโปรตีน BSA พบว่าความว่องไวในการจับกันของ BSA กับ Fe^{2+} และ Fe^{3+} จะเพิ่มขึ้นเป็นสองเท่าเมื่อมี 2 ไตรคาร์บอกซิลิกแอซิด 2 ยังใช้ในการทดสอบกับสารลดแรงตึงผิวหลายชนิด พบว่าสัญญาณการวาวแสงเพิ่มขึ้นอย่างจำเพาะเจาะจงกับ SDBS และค่า CMC ของ SDBS ที่อธิบายด้วยวิธีนี้มีค่าเท่ากับ 1.4 มิลลิโมลาร์ (ค่า CMC ในรายงานคือ 1.2 มิลลิโมลาร์) นอกจากนี้ความแตกต่างของพฤติกรรมการเรืองแสงของสารประกอบ 2 ใน THF ด้วยสารประกอบวัตถุระเบิดไนโตรอะโรมาติกเช่น ไตรไนโตรโทลูอีน, 4-ไนโตรโทลูอีน และ 2,4-ไนโตรโทลูอีน อาจจะมีประโยชน์สำหรับการตรวจจับวัตถุระเบิด

สาขาวิชา ปิโตรเคมีและวิทยาศาสตร์พอลิเมอร์   ลายมือชื่อนิสิต _____

ปีการศึกษา   2554   ลายมือชื่อ อ.ที่ปรึกษาวิทยานิพนธ์หลัก _____

ลายมือชื่อ อ.ที่ปรึกษาวิทยานิพนธ์ร่วม _____

5272312223 : MAJOR PETROCHEMISTRY AND POLYMER SCIENCE

KEYWORDS : 1, 4-DIHYDROPYRIDINE/ FLUORESCENCE SENSOR/ MERCURY(II) ION

DARANEE HOMRARUEN: SYNTHESIS OF 1,4-DIHYDROPYRIDINE DERIVATIVES AS NOVEL FLUORESCENT SENSORS ADVISOR : ANAWAT AJAVAKOM, Ph.D., CO-ADVISOR: LUXSANA DUBAS, Ph.D., 90 pp.

This research involves the synthetic preparation of a series of 1,4-dihydropyridine (DHP) by varying substituent of nitrogen atom. The DHP triester (**1**) can be easily prepared from the cyclotrimerization of β-amino acrylate by treatment of $TiCl_4$ at room temperature. Hydrolysis of **1** was carried out using KOH to convert triester to tricarboxylic acid (**2**), which readily soluble in aqueous media. The photophysical properties of these DHP derivatives were studied in pH 8.0 phosphate buffer solution. The absorption spectra displayed absorption maximum in the range of 280 to 300 and 347 to 358 nm. All of these compounds exhibited an emission peak in a range of 432-445 nm with fluorescence quantum efficiencies (Φ_f) of 0.07-0.23. Since methoxyphenyl *N*-substituted DHP showed the highest blue emission appearance also observable by naked-eye, it was therefore selected for further investigation in fluorescence sensing applications. This derivative was found to selectively interact with Hg^{2+} and the fluorescent signal decrease was assumed to be the result of an oxidation of the DHP into a pyridinium ring specifically induced by Hg^{2+} that brought about its remarkable selectivity over other metal ions. The decrease of fluorescence signal was proportional to Hg^{2+} concentration with high quenching efficiency (K_{sv} = 78,300 M^{-1}) providing a detection limit of 0.2 μM. According to the results, of the use of tricarboxylic acid **2** Fe^{2+} and Fe^{3+} detection with protein BSA, as the sensitivity of BSA to Fe^{2+} and Fe^{3+} was increased two-fold-higher in the presence of **2**. This tricarboxylic acid **2** was also tested with various types of surfactant. Its fluorescent signal was enhanced selectively by SDBS, and the CMC of SDBS could be determined by this method as 1.4 mM (literature CMC values is 1.2 mM). Additionally, the different fluorescence behavior of compound **2** in THF by nitroaromatic explosive compounds, such as trinitrotoluene, 4-nitrotoluene and 2,4-nitrotoluene might be useful for the explosive detection.

Field of Study : Petrochemistry and Polymer Science   Student's Signature ....

Academic Year : 2011   Advisor's Signature ....

Co-advisor's Signature ....

ACKNOWLEDGEMENTS

First of all, I would like to express my sincere gratitude to my thesis advisor, Dr. Anawat Ajavakom, and my co-advisor, Dr. Luxsana Dubas, for valuable advice, guidance and encouragement throughout the course of this research. Sincere thanks are also extended to Professor Dr. Pattarapan Prasassrakich, Assistant Professor Dr. Varawut Tangpasuthadol, and Dr. Vachiraporn Ajavakom, attending as the committee members, for their valuable comments and suggestions.

I would like to especially thank Associate Professor Dr. Mongkol Sukwattanasinitt for his generous assistance, invaluable guidance and kindness throughout this research. I also would like to thank Assistant Professor Dr. Paitoon Rashatasakhon and Dr. Sumrit Wacharasindhu for his attention and suggestion during our group meeting.

My appreciation is also given to many people in our research group; Mr. Thirawat Sirijindalert for training; Dr. Nakorn Niamnont, Ms. Warathip Siripornnoppakhun, Mr. Watcharin Ngampueng and Ms. Kanoktorn Boonkitpatarakul for their helpful suggestion. Ms. Nattaporn Kimpitak, Ms. Wannapa Yuanboonlim, Mr. Akachai Khumsri, Mr. Pharkphoom Auttapornpitak, Ms. Wanwisa Thongmalai, and everyone in MAPS group for a greatest friendships and encouragement.

In particular, I am thankful to the National Center of Excellence for Petroleum, Petrochemicals and the National Nanotechnology Center and the 90th Anniversary of Chulalongkorn University Fund for supporting my thesis.

Finally, I would like to specially thank my family and friends for their encouragement and understanding throughout. I would not be able to reach this success without them.

CONTENTS

LIST OF TABLES

Page

LIST OF FIGURES

Figure   **Page**

LIST OF SCHEMES

LIST OF ABBREVIATIONS

Ar	aromatic
calcd	calculated
^{13}C NMR	carbon-13 nuclear magnetic resonance
CDCl$_3$	deuterated chloroform
CH$_2$Cl$_2$	Methylene chloride
CuI	Copper iodide
DMSO-d_6	deuterated dimethyl sulfoxide
DMSO	dimethylsulfoxide
d	doublet (NMR)
dd	doublet of doublet (NMR)
ESIMS	electrospray ionization mass spectrometry
EtOAc	Ethyl acetate
equiv	equivalent (s)
FT-IR	fourier transform infrared spectroscopy
g	gram (s)
^{1}H NMR	proton nuclear magnetic resonance
Hz	Hertz
HRMS	high resolution mass spectrum
h	hour (s)
IR	infrared
J	coupling constant
mg	milligram (s)
mL	milliliter (s)
mmol	millimole (s)
m.p.	Melting point
nm	Nanometer (s)
m/z	mass per charge
m	multiplet (NMR)
M.W.	molecular weight

M	molar
MHz	megaHertz
rt	room temperature
s	singlet (NMR)
THF	tetrahydrofuran
TLC	thin layer chromatography
UV	ultraviolet
δ	chemical shift
°C	degree Celsius
μL	microliter (s)
μM	micromolar (s)
ε	Molar absorptivity
λ	Wavelength
Φ	quantum yield
% yield	percentage yield

CHAPTER I

INTRODUCTION

1.1 Introduction of 1,4-dihydropyridines

The 1,4-dihydropyridine (1,4-DHP) is a heterocyclic molecule, in which the parent molecule pyridine, is semi-saturated with two hydrogens replacing one double bond at the position of 1 and 4 of the pyridine ring, as shown in **Figure 1.1**.

The first 1,4-DHP was easily prepared by Hantzsch reaction in the year of 1882 [1]. Since then their derivatives DHP have been used for a variety of applications, from modeling NADH in biochemistry [2] or photosensitive polymers [3]. Some 1,4-DHPs are drugs belonging to the class of pharmacological agents known as calcium channel blockers [4-5]. For instance, the inhibition of calcium ion cell penetration by DHP derivatives was reported to weaken the contractility of the cardiac muscle [5]. These compounds were also shown to be very effective vasodilators and useful in the treatment of hypertension, ischemic heart disease and other cardiovascular disorders [6-8].

The structure of 1,4-DHP consists of the π-conjugated chromophores is endowed by a strongly allowed absorption with the maximum round 350 nm and maximum emission around 450 nm [9-12]. Due to their optical properties the photophysical characteristics of 1,4-DHP have been reported [13-17].
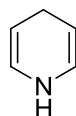
Figure 1.1 Basic structure of 1,4-dihydropyridine (1,4-DHP).

Chen and coworkers [14] synthesized and studied its emission behavior of 1,4-DHP derivative bearing a *N,N*-dimethyl aminophenyl group at 4-position (**1**) (**Figure 1.2**) in aprotic solvents. The absorption and fluorescence spectra of **1** were examined and compared to model compounds $H_2Py–Ph$ (**2**) and $H_2Py–Me$ (**3**). Compounds **2** and **3** showed fluorescence around 420 nm, while **1** exhibits fluorescence around 520

nm due to the intramolecular charge transfer (ICT) state involving the aniline and dihydropyridine groups as donor and acceptor, respectively. However when the amino group in the aniline chromophore is protonated, the electron donating ability of aniline is dramatically reduced; therefore the ICT cannot occur. Transition metal ions also can switch the fluorescence of **1**.
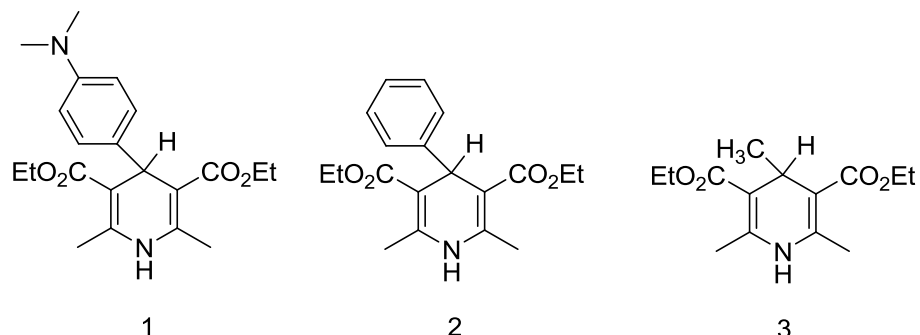
Figure 1.2 Structure of 1,4-DHP **1**, **2** and **3**.

This type of 1,4-DHP derivatives (**4**), as shown in **Figure 1.3** were photophysically and photochemically investigated by Pávez and team [15]. The photophysical properties of substituted 1,4-DHP are mainly dependent on the solvent and the chemical nature of the substituents in the position 4. The chloro substituent at the ortho position of the phenyl ring causes a hindrance to the rotation of the DHP-phenyl C-C bond (CPDHP). The irradiation of the compound bearing a 2-nitrophenyl substituent leads to its decomposition; this is faster in nonpolar solvent. In contrast, the 1,4-DHP derivatives bearing a methyl, phenyl, hydroxyphenyl or 2,3-dichlorophenyl substituent did not decompose under the same experimental conditions.

Name	X	R_1
MDHP	CH_3	CH_3
ADHP	COOH	CH_2CH_3
PDHP	(phenyl)	CH_2CH_3
HPDHP	(phenyl-OH)	CH_3
CPDHP	(dichlorophenyl, Cl, Cl)	CH_2CH_3
NPDHP	(phenyl-NO_2)	CH_3
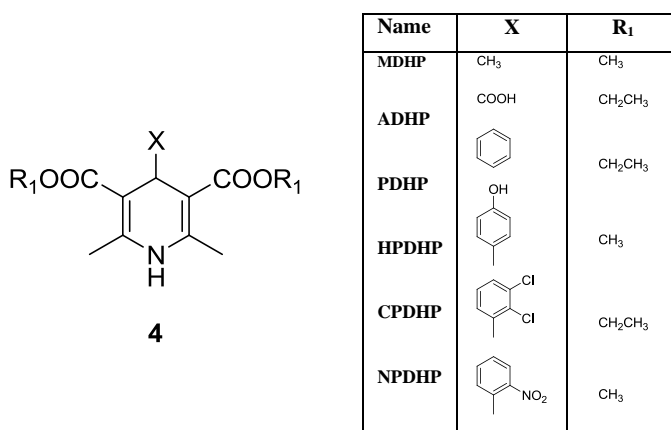
Figure 1.3 Structure of 1,4-DHP **4**.

Moreover, Fang and team [16] studied the formation of an enamine (**5**) and 1,4-DHP (**5**) (**Figure 1.4**) from reaction between malondialdehyde (MDA) and glucosamine (GlcN). The results indicated that GlcN reacted readily with MDA at supraphysiological conditions to form different products, such as a nonfluorescent enamine (**5**) with an absorption peak at 281 nm and a lipofuscin-like fluorescent (Ex. 392 nm/Em. 454 nm) 1,4-DHP (**6**). GlcN also greatly inhibited the formation of lipofuscin-like fluorescence induced by MDA reacted with bovine serum albumin. As a result, the reaction of GlcN with MDA suggested a novel anticarbonylation function of GlcN in pathophysiological situations related to aging-related diseases and provided insight into the reaction mechanism of GlcN in protecting proteins against carbonyl stress.
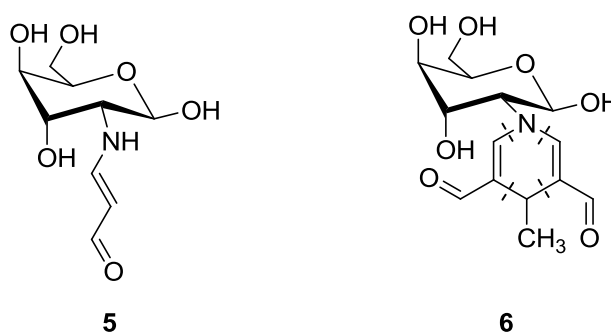
Figure 1.4 Structure of compound **5** and **6**.

In 2006, Vohra and coworker [19] developed the synthetic route of dihydropyridines by using Lewis acids. They carried out Lewis acids to catalyze the addition of β-amino acrylates or β-enaminones to α,β-unsaturated aldehydes leading to the asymmetric DHPs in high yields under mild reaction conditions. However, both substrates had to be prepared prior to the cyclisation.

2a: R^1 = PhCH$_2$, R^2 = OC$_2$H$_5$
2b: R^1 = Ph, R^2 = OC$_2$H$_5$
2c: R^1 = PhCH$_2$, R^2 = CH$_3$

7b-f
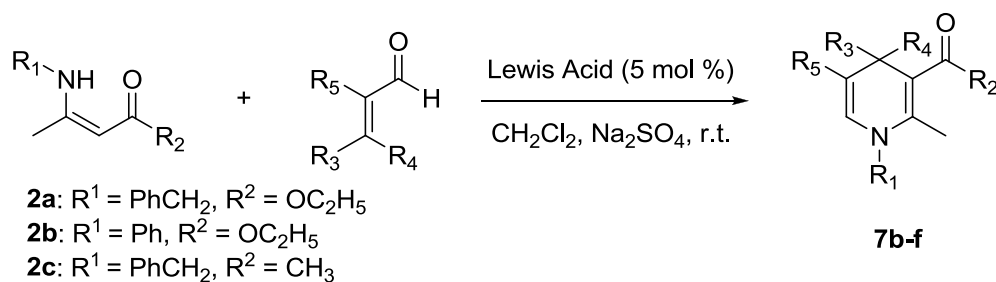
Entry	R^1	R^2	R^3	R^4	R^5	Lewis Acid	Compound	Yield [%]
1	PhCH$_2$	OEt	Ph	H	H	FeCl$_3$·6 H$_2$O	7b	90
2	PhCH$_2$	OEt	Ph	H	H	Sc(OTf)$_3$	7b	75
3	Ph	OEt	Ph	H	H	FeCl$_3$·6 H$_2$O	7c	93
4	Ph	OEt	Ph	H	H	Sc(OTf)$_3$	7c	80
5[b]	PhCH$_2$	CH$_3$	Ph	H	H	FeCl$_3$·6 H$_2$O	7d	99
6[b]	PhCH$_2$	CH$_3$	Ph	H	H	Sc(OTf)$_3$	7d	90
7	PhCH$_2$	OEt	(CH$_3$)$_2$C=C(CH$_2$)$_2$	CH$_3$	H	FeCl$_3$·6 H$_2$O	7e	40
8	PhCH$_2$	OEt	CH$_3$	H	CH$_3$	Sc(OTf)$_3$	7f	87

[b] 0.5 mmol of β-enamino ketone **2c** was used.

Figure 1.5 Structure of compound **7**.

In the past, numerous methods to synthesize DHP derivatives were reported. These methods however required a substituent at a position adjacent to the nitrogen atom in order to gain a better yielding system. Accordingly, Kikuchi and team [18] synthesized 1,4-DHPs bearing a carboethoxy methyl group at 4-position (**8**) from the reaction of anilines with ethyl propiolate catalyzed by Scandium(III) triflate in toluene under reflux conditions (**Figure 1.6**). This method gave DHP product in a GC yield of 42%
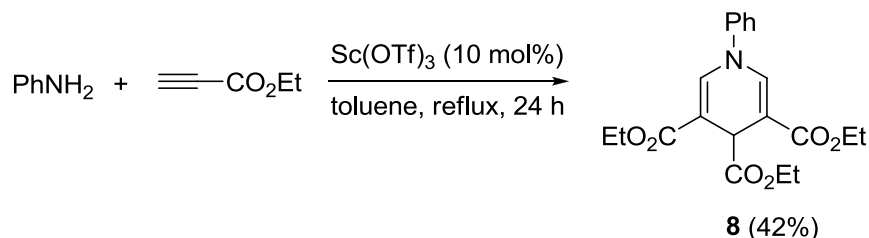
Figure 1.6 The synthetic scheme of 1,4-DHP derivatives **8**.

In 2010, Sirijindalert and coworkers [17] reported the synthesis of 1,4-DHP from β-amino acrylates by using titanium(IV) chloride under facile conditions (**Figure 1.7**). The cyclotrimerization of β-amino acrylates to *N*-substituted 1,4-DHP was achieved by three addition/elimination steps in high to excellent yields (70–83%). Our developed method will be utilized to make fluorescence chemosensor molecules.
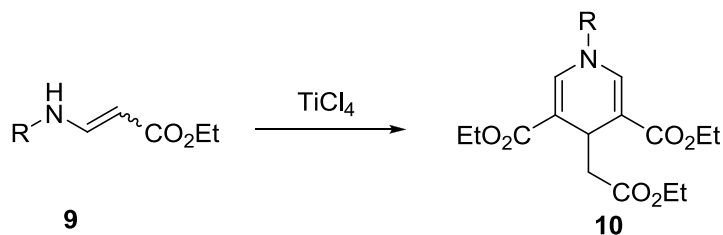
Figure 1.7 The synthetic scheme of 1,4-DHP derivatives **10**.

1.2 Introduction of fluorometry

Fluorometry is a class of techniques that assay the state of a biological chemical system by studying its interactions with fluorescent probe molecules. This interaction is monitored by measuring the changes in the fluorescent probe optical properties. The fluorescence characterizes the relationship between absorbed and emitted photons at specified wavelengths. It is a precise quantitative and qualitative analytical technique that is not only high sensitivity and high specificity but with even greater advantages of rapid testing, inexpensive and easy to use.

Fluorescence is a photon emission process that occurs when a molecule absorbs light photons from the UV visible light, known as excitation, and then rapidly emits light photons as it returns to its ground state. The phenomenon is usually described by the Jablonski diagram [20], which offers a convenient representation of the excited state structure and the relevant transitions, to illustrate possible various molecular processes. A simplified Jablonski diagram shown in **Figure 1.8**, demonstrates that a photon is excited to singlet excited electronic states (S1 or S2) and form an excited photon. The fluorescence signal is observed when an excited electron relaxes to ground singlet electronic state (S0) via photon emission. The time required to complete this whole process takes around nano-second.
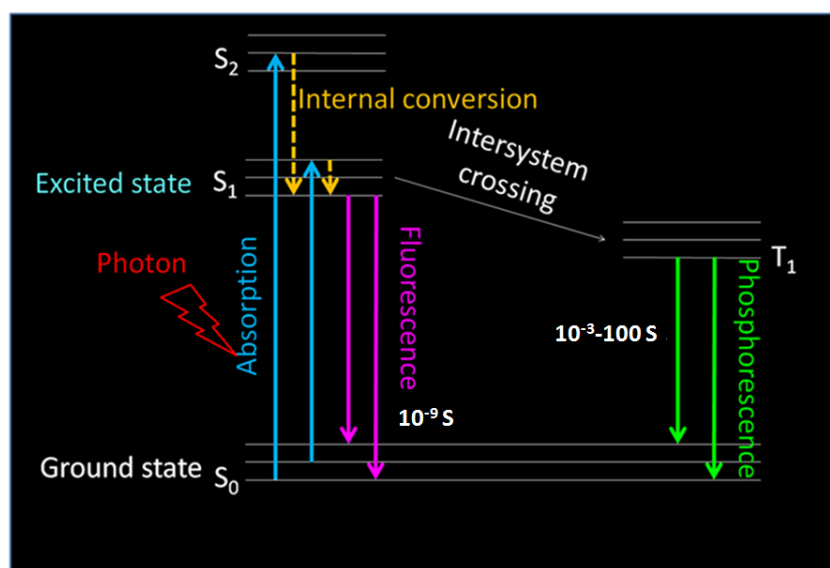
Figure 1.8 Jablonski diagram illustrating fluorescent processes.

1.3   Fluorescence chemosensor

Chemosensors based on fluorescence signal changes are commonly referred to as fluorescent chemosensors [21-25]. A fluorescence signal change normally resulted from the interaction between fluorophore and analysts (target compound), which can be a metal ion, an anion or an organic molecule. Fluorescence chemosensor will then exhibit a new fluorescence behavior, detectable by the fluorometry.

Fluorescent chemosensors are usually composed of three components: a receptor, a fluorophore and a spacer or linker. These three parts do not exactly correspond to the three components shown in **Figure 1.9**. When a fluorescent chemosensor specifically interacts with analyte, the read-out is usually measured as a change in fluorescence intensity, intensity decay lifetime, or a shift of the emission wavelength. An important feature of the fluorescent chemosensors is that signal transduction of the analytes leading to the readout can happen in a very short time and without any other assistances. This makes real-time and real-space detection of the analyte possible as well as imaging associated with analyte distribution.
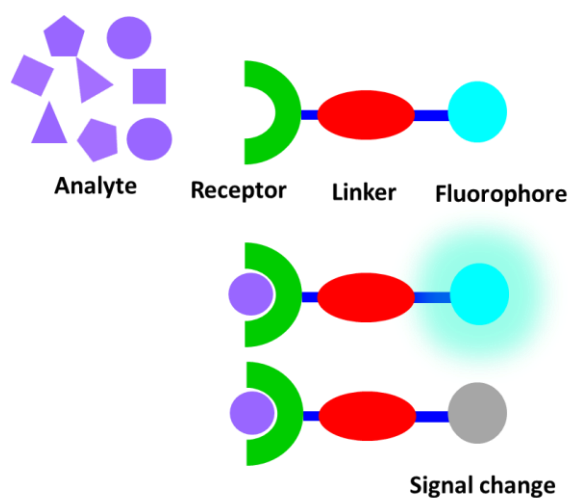
Figure 1.9 Schematic illustration of a sensor device.

1.3.1 Fluorescent small molecule sensors

Fluorescent small molecules sensors have become an important class of materials in a wide variety of applications, including small ions [26] or biomolecules i.e. proteins and nucleic acids [27]. Useful responsive small-molecule ligands that provide immediate optical feedback can overcome such limitations because their use does not require sophisticated instrumentation or sample preparation. The most important considerations influence the design of small molecule ligands for sensing metal ion, the probe should be highly selective for the metal over all other components in the environmental or biological sample. Some examples reported herein show our focus on the design and synthesis of such small-molecule-based metal ion sensors.

In 2007, Korean chemist [28] reported a simple chemosensor dioxaoctanediamide containing two pyrene moieties (**11**). This chemosensor showed a selective fluorescence quenching toward Hg^{2+} ions over other transition-metal ions in an aqueous methanol solution (**Figure 1.10**). The association constant (K_{assoc}) and the detection limit was found to be $6.3 \times 10^4 \, M^{-1}$ and $1.6 \times 10^{-6} \, M$, respectively.
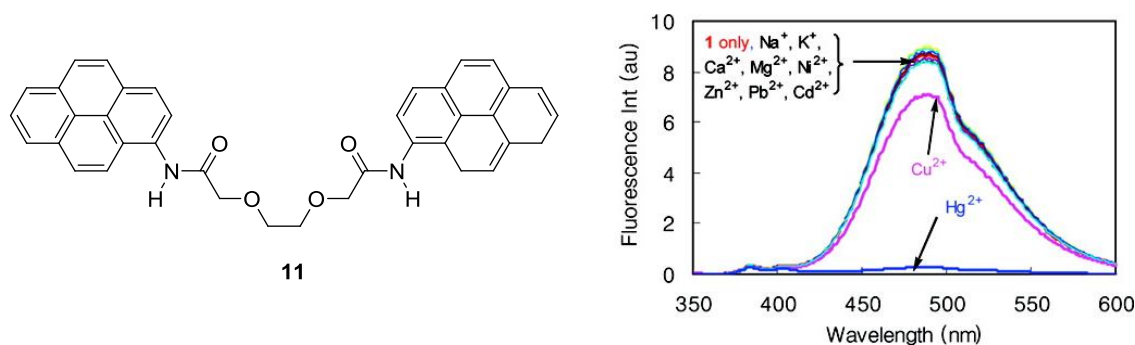
Figure 1.10 Structure of pyrene-appended dioxaoctanediamide **11** and its fluoroionophoric properties in MeOH-H$_2$O.

A novel coumarin-based fluorogenic probe bearing the 2-piconyl unit (**12**) has been developed as fluorescent chemosensor with selectivity toward Cu^{2+} (**Figure 1.11**) [22]. The receptor can be applied to monitoring Cu^{2+}ion in aqueous solution (HEPES/DMSO, 9:1) with pH span of 4-10. The fluorescent changes of this

compound were studied with Cu^{2+} concentration range of 0-50 μM and the detection limit was estimated to be 0.5 μM.

12
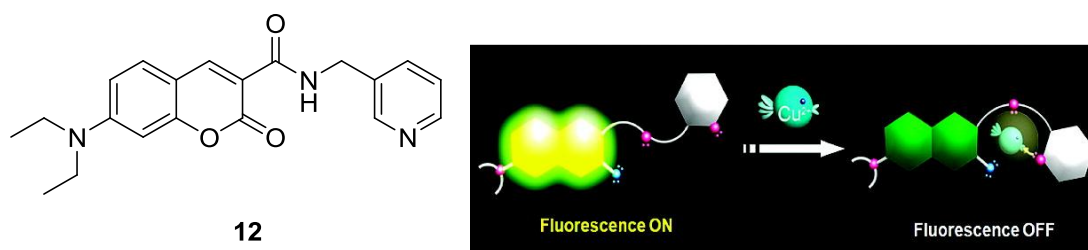
Figure 1.11 Structure of coumarin derivative **12** and proposed the mechanism with Cu^{2+}.

The simple glucose-based C2-derivatized colorimetric chemo-sensor by a one-step condensation of glucosamine and 2-hydroxy-1-naphthaldehyde was designed by Mitra and coworkers (**Figure 1.12**), [26]. The recognition of transition metal ions results in visual color change only in the presence of Fe^{2+}, Fe^{3+} and Cu^{2+} in methanol. However, in an aqueous HEPES buffer (pH 7.2) it is only the Fe^{3+} that gives a distinct visual color change even in the presence of other metal ions, up to a concentration of 280 ppb.

13

Blank Mg^{2+} Ca^{2+} Mn^{2+} Fe^{2+} Fe^{3+} Co^{2+} Ni^{2+} Cu^{2+} Zn^{2+} Cd^{2+} Hg^{2+}
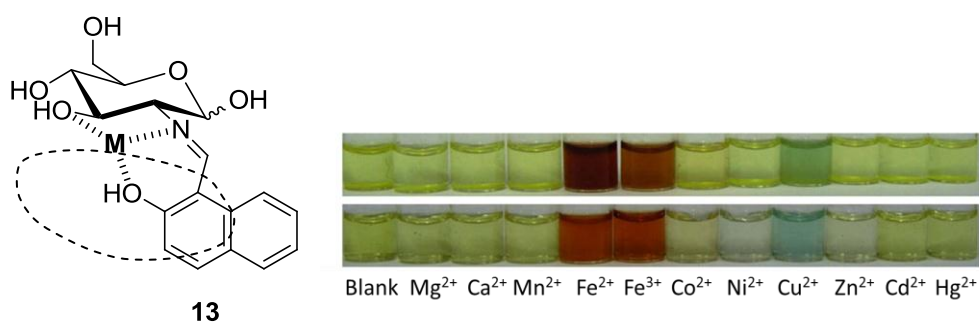
Figure 1.12 Structure of glucose-based derivative **13** and its fluorogenic response in HEPES buffer solutions.

In 2009, Mandal and team [23] reported the fluorescent sensor of pyridine pyrazol based on anthracene fluorophore (**Figure 1.13**) in mixed THF-H$_2$O (2:3, v/v, and pH 7.2, 20 mM HEPES buffer) medium. The results were found to bind four different transition metal ions such as Hg^{2+}, Cu^{2+}, Ag^+ and Ni^2 while binding affinity

towards the Hg^{2+} was revealed to be an order of magnitude higher comparing to other three cations mentioned.
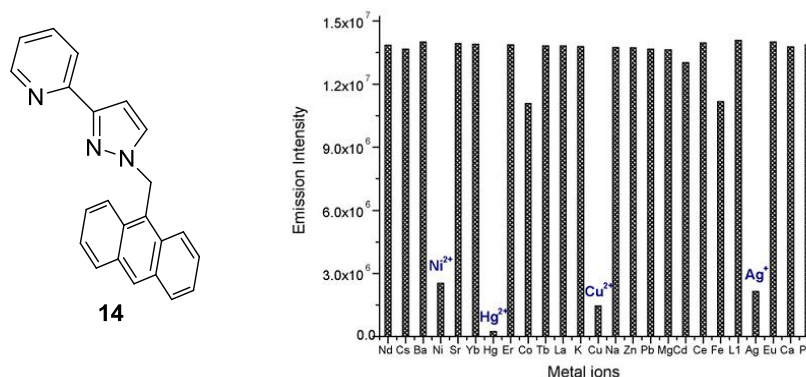
Figure 1.13 Structure of 2-(1-(anthracen-9-ylmethyl)-1H-pyrazol-3-yl)-pyridine **14** and bar diagram represents the fluorescent intensity of **14** for different metal ion.

In the same year, Singh and coworkers [24] synthesized a novel aminobisulfonate receptor joined to a naphthalene fluorophore *via* a methylene spacer (**Figure 1.14**) and developed this fluorescent sensor for the determination of Fe^{3+} in an aqueous solution at pH 7.0. The fluorescence emission of the sensor was quenched upon addition of Fe^{3+}, most likely due to the electron/energy transfer between Fe^{3+} and the excited naphthalene. The sensor displayed good selectivity for Fe^{3+} over other physiologically relevant metal ions.
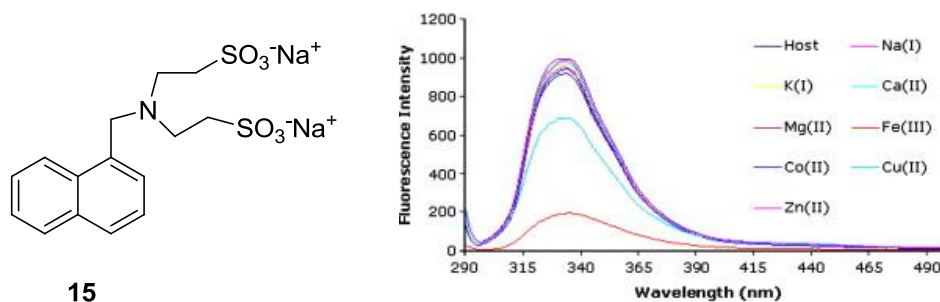
Figure 1.14 Structure of *β*-aminobisulfonate receptor linked naphthalene fluorophore **15** and fluorescence spectra of **15** in the presence of various metal ions.

In 2010, [25] naphthalimide based fluorescent sensor **16** containing an amide-PDA receptor (**Figure 1.15**), has been reported to have strongest affinity with Zn^{2+} among competitive metal ions such as Fe^{2+}, CO^{2+}, Ni^{2+}, Cu^{2+}, Cd^{2+} and Hg^{2+}. This exhibiting excellent fluorescent selectivity for Zn^{2+} was triggered by the amide tautomerization. And for the naked eye detection, **16** can bind both Zn^{2+} and Cd^{2+}, green and blue fluorescent, respectively in aqueous solution (CH_3CN/0.5 M HEPES pH 7.4, 50:50).
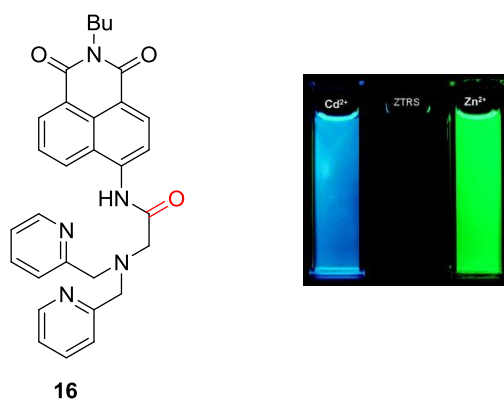
Figure 1.15 Structure of fluorescent sensor naphthalimide containing amide receptor (**16**) and visible emission observed from samples of **16**, **16**/Cd^{2+}, and **16**/Zn^{2+}.

1.4 Mercury sensor

Mercury is considered highly toxic thus the accumulation of mercury in the human body may cause serious health problems, like prenatal brain and nervous system damage, cognitive and motion disorders, and Minamata disease [29-33].

Mercury pollution is a global problem and a major source of human exposure stems from contaminated natural water [34]. Industrial sources of mercury include coal and gold mining, solid waste incineration, wood pulping, fossil fuel combustion, and chemical manufacturing. Emitted elementary mercury vapors are easily transported in the atmosphere, often across continents and oceans, and are eventually oxidized to Hg^{2+}. Atmospheric deposition of Hg^{2+} results in its accumulation in plants, topsoil, and water. Particularly, mercury bioaccumulation in plants and natural waters provides additional routes of entry into the food web [35-36]. The United States Environmental Protection Agency (EPA) has mandated an upper limit of 2 ppb (10 nM) for Hg^{2+} in drinking water [37].

Therefore, the improvement of trustworthy sensing techniques for mercury ions is considerable significance for health diagnosis and environmental analysis. Over the past few years, the analytical techniques developed for the mercury(II) determinations have been reported [38-47]. For instant, there are electrothermal atomic absorption spectrometry [38], controlled-potential coulometry and direct potentionmetry [39-40], high-performance liquid chromatographic method [41-42], inductively coupled plasma mass spectrometry [43-46], capillary electrophoresis [47]. However, these techniques require intricate, multistep sample preparation and/or sophististicated instrumentation

Thus preparation of a highly specific, facile, and cost-effective mercury sensor, which is applicable to the common biological milieux, is an important goal [48]. The fluorometric detections following the changes in the emission of light are more convenient and suitable for monitoring Hg^{2+} in either natural or biological environments. There are multiple advantages in using fluorescence; (i) its powerful visual effects; (ii) its greater sensitivity than that of absorption spectroscopy; (iii) its simple equipment, commonly available in many scientific laboratories.

In 2005, the synthesis of a highly selective fluorescence switch off Hg^{2+} detector in 1:1 MeCN/H$_2$O by introducing a dianthryl cyclam was reported by Youn and coworkers [49]. The addition of 100 equiv of Hg^{2+} caused quenching with a 97% decrease at 417 nm emission band. Titrations of **17** with Hg^{2+} revealed 1:1 binding stoichiometry, a dissociation constant for Hg^{2+} of 11.5 and a detection limit of 3.8 μM. Additionally, reduction of water content in the MeCN/H$_2$O mixtures induced the turn-on mode of detection against Hg^{2+} and Cd^{2+} (5.8-fold and 4.9-fold, respectively).
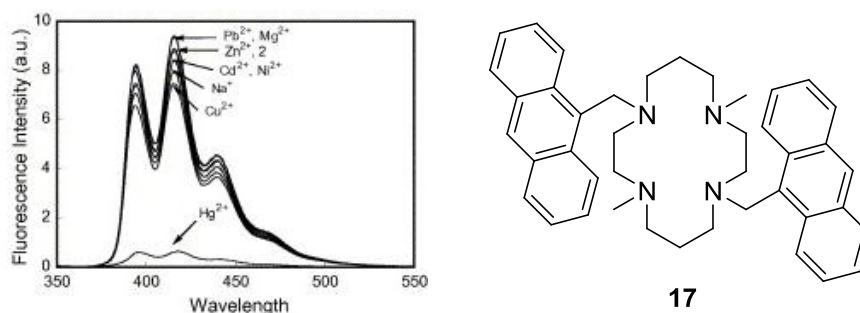
Figure 1.16 Structure of dianthryl cyclam **17** and fluorescence spectra of **17** in the presence of various metal ions.

In 2005, Chinese chemists [50] have synthesized dipyrrolylquinoxaline-bridged macrocycles (**18** and **19**) as shown in **Figure 1.17** into the novel fluorescent chemosensor. Fluorescence quenching was exhibited upon Hg^{2+} addition in aqueous solution buffered at pH 4.5. The coordination between Hg^{2+} and macromolecules **18** or **19** induced blue-shifts of λ_{max} at 506 nm to 460 nm with a ~5- fold (**18**) or ~8-fold (**19**) decrease in emission intensity at 506 nm. Solution studies revealed the specific turn-off response of **18** to Hg^{2+} with 1:1 binding stoichiometry, an apparent dissociation constant of 2.6 μM, and a linear response up to 10 μM Hg^{2+}. A similar selectivity profile of probe **19** and Hg^{2+} K_d value of 2.9 μM were gained.

n = 1, 18
n = 2, 19
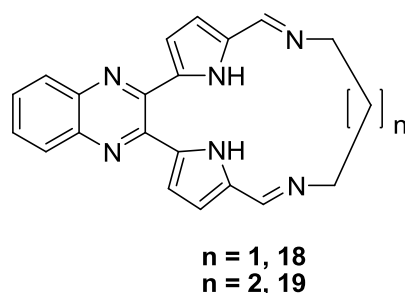
Figure 1.17 Structure of dipyrrolylquinoxaline-bridged macrocycles.

In 2005, Caballero and coworkers [51] developed a pyrene fluorescent Hg^{2+} sensor that incorporates an unsymmetrical 1,4-disubstituted azine. High exhibiting affinity and high selectivity for Hg^{2+} in aqueous environment operated through two different channels, optic/redox and optic/fluorescent were described. Upon addition of one equiv of Hg^{2+} in 7:3 $MeCN/H_2O$, **20** had a quantum yield of 0.005 and 11-fold enhancement of the pyrene excimer emission band centered at 450 nm. Hg^{2+}-binding titrations monitored by fluorescence spectroscopy have revealed the solvent dependent of the Hg^{2+} complex; a dissociation constant of 610 nM in MeCN and 1.1 μM in 7:3 $MeCN/H_2O$.

20
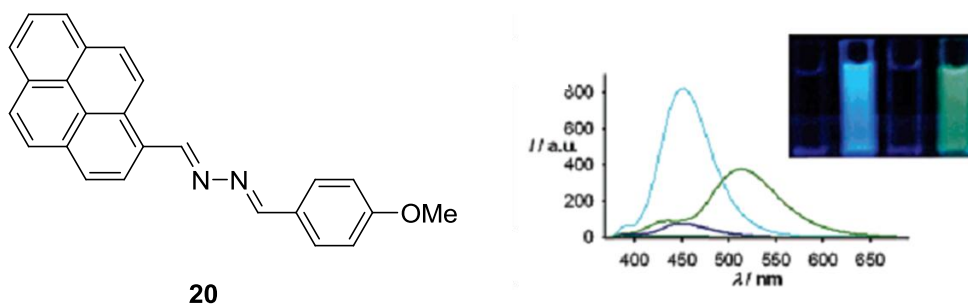
Figure 1.18 Structure of pyrene containing 1,4-disubstituted azine **20** and fluorescence spectra after the addition of 1 equiv of $Hg(ClO_4)_2$ to **20** in CH_3CN/H_2O (7:3) (blue) and in CH_3CN (green).

In 2006, Korean chemists [52] demonstrated that a rhodamine-based chemodosimeter could be employed for monitoring Hg^{2+} in several biological contexts (**Figure 1.19**). Addition of one equiv. of Hg^{2+} to **21** assisted the formation of oxadiazole **22** which showed a $\sim$30-fold fluorescence enhancement and the change of solution color from colorless to bright pink with a ppb detection limit. This *in vivo* type cell permeable sensor was utilized to monitor exogenous Hg^{2+} uptake in C2C12 cells, a mouse myoblast cell line, and in zebrafish in real time, and to image accumulated Hg^{2+} in zebra fish organs. The series of *in vivo* experiments suggested that **21** was feasible will be a versatile Hg^{2+} imaging tool. The only obvious drawback to this Hg^{2+} detector was that the Hg^{2+}-induced fluorescence increase was not reversible.
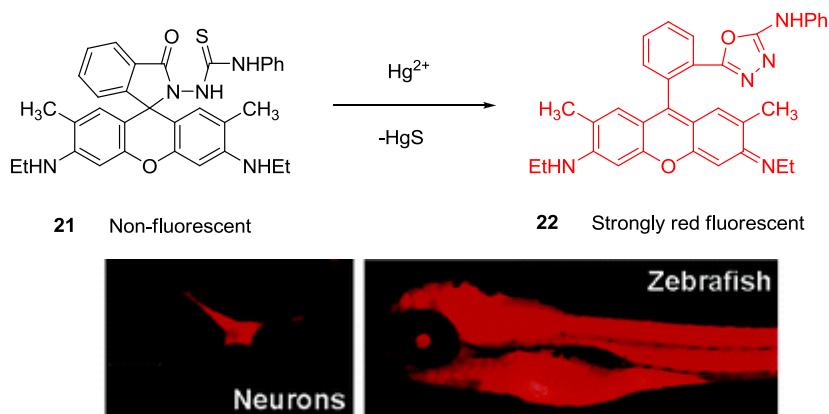
Figure 1.19 Structure of Rhodamine-based chemodosimeter **2**1 for Hg^{2+} that operates in aqueous solution and has been applied to detect exogenous Hg^{2+} in a variety of cell types and in zebrafish.

In 2007, Leray and team [53] reported a new fluorescent molecular sensor for Hg^{2+} based on the phosphane sulfide derivative (**23**) (**Figure 1.20**). Compound **23** showed an intense absorption band in the UV region ($\varepsilon = 1.5 \times 10^5$ L mol^{-1} cm^{-1}) and a fluorescence quantum yield (Φ_F) of 0.1 in CH$_3$CN. A very low detection limit (3.8 nM) in CH$_3$CN−H$_2$O (80:20 v/v) was observed at pH = 4 with a very high selectivity over other interfering cations such as Ca^{2+}, Na$^+$, K$^+$, Mg^{2+}, Pb^{2+}, Cd^{2+}, Cu^{2+}, Ag$^+$.
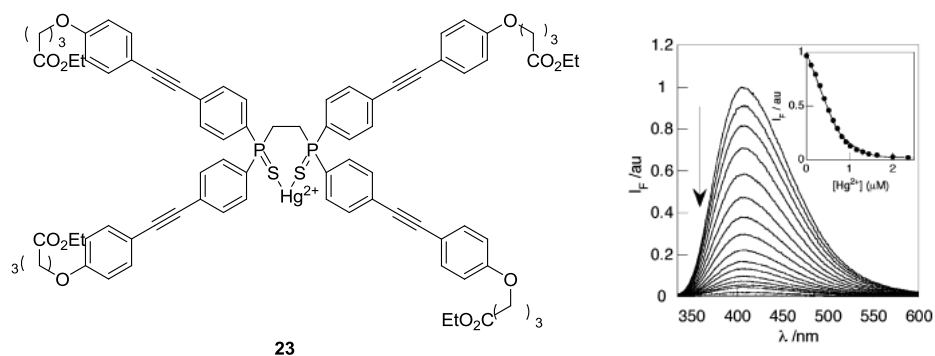
Figure 1.20 Structure of phosphane sulfide derivative (**23**) and fluorescence spectra of **23**.

The selective Hg^{2+} ion detection of Nile blue derivative of **24** in 100% aqueous systems was demonstrated by Lee and colleagues [54] (**Figure 1.21**). Upon its addition into aqueous Hg^{2+} ion solution, this compound **24** exhibited chemodosimetric properties with a considerable blue-shift in its absorption and emission spectra, driven by a desulfurization reaction. Detection at an emission of 652 nm was extremely sensitive (less than 1.0 ppb), and the selectivity and sensitivity of **24** toward Hg^{2+} were not influenced by biologically active metal ions such as highly concentrated Na$^+$, K$^+$, Ca^{2+}, and Mg^{2+} (1.0 mM, 200 equiv), and transition-metal cations such as Zn^{2+}, Cd^{2+}, Co^{2+}, Fe^{2+}, Ba^{2+}, and Ni^{2+}.
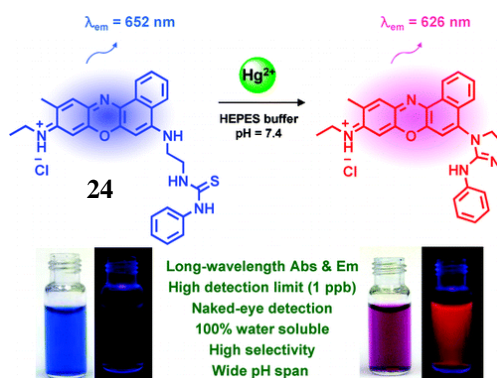
Figure 1.21 A Nile blue-based chemodosimeter

The synthesis and properties of dansyl-L-glutamic methyl diester in HEPES buffer solution (contains 0.1 % DMSO) was studied by Li and his team [55] (**Figure 1.20**). The dansyl-L-glutamic methyl diester was synthesized and its sensing properties aggregated by target Hg^{2+} with a blue-shift and turn-on fluorescence response. After addition 20 µM of Hg^{2+}, a significant emission band at 475 nm appeared with a ~10-fold fluorescence and (10-fold) quantum yield (0.0195 to 0.1895) enhancement. The addition of Hg^{2+} to diester **25** resulted in the reduction of the internal charge transfer (ICT) between the amino group and the dansyl moiety.
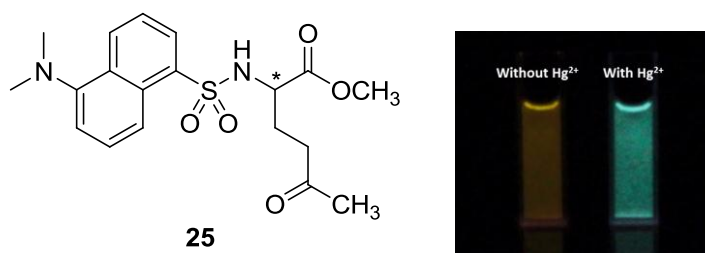
Figure 1.22 Structure of dansyl-l-glutamic acid methyl diester **25** and visible emission observed from **25** with and without Hg^{2+}.

1.5 Statement of problem

The 1,4-DHP (**1**) is considered an easily synthesis via cyclotrimerization of *N*-substituted β-aminoacrylates because it is carried out with mild condition, it also has fluorescent signal and can be apply to fluorescent chemosensor. The structure of DHP **2** consists of tricarboxylic acid is expected to bind with metal ions therefore it is useful in fluorescent sensing applications. However according to the literature reviews of fluorescent chemosensors, there are enormous numbers of reports presenting the fluorescent chemosensing organic molecules. Only a few systems can be used in aqueous media without any presence of organic solvents. So, this project is focused on fluorescent chemosensors from 1,4-DHP in an aqueous media. Hydrolysis of **1** to convert triester to tricarboxylic (**2**) is readily soluble in aqueous media and suitable to use as fluorescent chemosensor.

The design and synthesis of these DHP derivatives by varing substituent at nitrogen atom as electron donating group, electron withdrawing group and aliphatic chain in order to examine the influence to the fluorescent properties; maximum absorption and emission wavelength including fluorescent efficiency. DHP ring, which is fluorescent unit have an effect directly from electrons of substituent at nitrogen atom and interfere to the fluorescent systems. Hydrolysis of **1** to triacid **2** are improve the solubility of these DHP in aqueous system

Hypotheses of this work are an electron donating group stabilizing excited state to give high fluorescent efficiency and exhibited red shift in an absorption and emission wavelength. On the other hand, an electron withdrawing group should affect the fluorescent property differently. For compounds bearing aliphatic *N*-substituted groups, the effects of rigidity of aliphatic and aromatic on the fluorescent efficiency was investigated. Additionally, long chain aliphatic substituent should behave like a surfactant being soluble in the both water and oil, so useful in applications in the cell.

1.6 Objectives of this research

This research involved the synthetic preparation of a series of 1,4-dihydropyridine (DHP) **1** and **2** by varying substituents of nitrogen atom (**Figure 1.23**). The photophysical properties of tricarboxylics (**2**) were investigated in pH 8.0 phosphate buffer solution (PB) and THF, triesters (**1**) were studied in the same manner but without PB. The applications of these tricarboxylic (**2**) for Hg^{2+} sensors were also investigated in PB. Furthermore, this project also focused on the fluorescent sensing of surfactant and nitro aromatic compound by using tricarboxylic (**2**).

a (R = Ph)
b (R = *p*-MeO-Ph)
c (R = *p*-I-Ph)
d (R = Bn)
e (R = *n*-Bu)
f (R = $C_{18}H_{37}$)

Figure 1.23 Target molecules **1** and **2**.

CHAPTER II

EXPERIMENTAL

2.1 Materials and chemicals

Aniline, *p*-methoxy aniline, *p*-iodo aniline, benzylamine, butylamine, ethyl propiolate, $TiCl_4$ and potassium hydroxide were purchased from Sigma-Aldrich and Fluka. Compound **1** was prepared by our previously reported procedure [19]. Dichloromethane (CH_2Cl_2) for anhydrous reactions was dried over CaH_2 and distilled prior to use. Solvents used for extraction and chromatography such as CH_2Cl_2, hexane and ethyl acetate were commercial grade and distilled before use. Ethanol was analytical grade and purchased from Merck. Deionized water was distilled and used in precipitation and all extraction procedures. Milli Q water was used to prepare stock metal and fluorophore solution. Reactions were mostly carried out under positive pressure of N_2 filled in rubber balloons. Thin layer chromatography (TLC) was carried out using Merck 60 F254 plates with a thickness of 0.25 mm. Column chromatography was performed on Merck silica gel 60 (70-230 mesh).

2.2 Analytical instruments

The melting points of all products were acquired from a differential scanning calorimeter (NETZSCH DSC 204 F1). Elemental (C, H, N) analyses were performed on a PE 2400 series II analyzer (Perkin-Elmer, USA). The HRMS was under taken on an electrospray ionization mass spectrometer (microTOF, Bruker Daltonics). Fourier transform infrared spectra (FTIR) were acquired on Nicolet 6700 FTIR spectrometer equipped with a mercury-cadmium telluride (MCT) detector (Nicolet, USA). ^{1}H NMR spectra were recorded on Varian Mercury 400 MHz NMR spectrometer (Varian, USA). ^{13}C-NMR spectra were recorded at 100 MHz on Bruker NMR spectrometer. The UV-Visible spectra were obtained from a Varian Cary 50 UV-Vis spectrophotometer (Varian, USA) using water or THF as a solvent. Fluorescence emission spectra were acquired by using Perkin Elmer precisely LS 45 Luminescence

Spectrometer (PerkinElmer, UK) for metal ion sensing and using a Varian Cary Eclipse spectrofluorometer (Varian, USA) for photophysical property studies.

2.3 Synthetic procedures

2.3.1 Synthesis and characterization of 1, 4-dihydropyridines triester (1a-f)
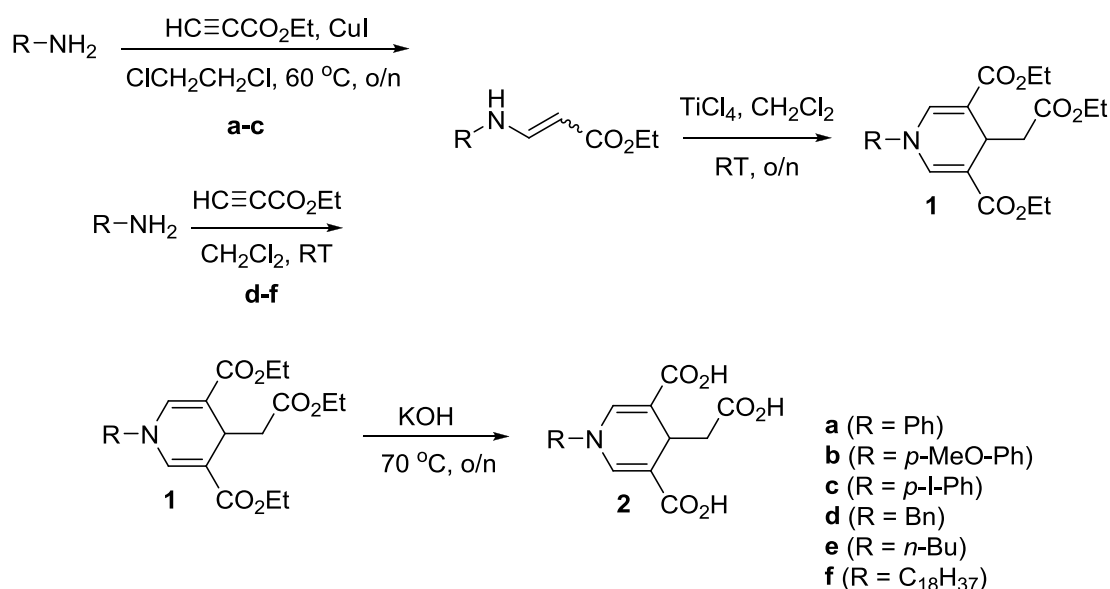
Case of aromatic amines, ethyl propiolate (1.2 equiv) in CH_2Cl_2, copper(I) iodide (0.5 equiv) and aromatic amine (1 equiv) were dispersed and the reaction mixture was stirred for 10 min. The reaction mixture was then heated at 60 °C overnight and filtered. The solvent evaporated to give the corresponding *N*-aromatic β-amino acrylates. In the case of aliphatic amines, the solution of aliphatic amine (1 equiv) in CH_2Cl_2, ethyl propiolate (1.2 equiv) was slowly added and the reaction mixture was stirred overnight at room temperature under nitrogen atmosphere. The mixture was evaporated *in vacuo* to obtain the corresponding *N*-aliphatic β-amino acrylates.

To a solution of *N*-substituted β-amino acrylates (1 equiv) in dried CH_2Cl_2 in an ice bath, $TiCl_4$ (0.2 equiv in the case of *N*-aliphatic β-amino acrylates or 0.5 equiv in the case of *N*-aromatic β-amino acrylates) was added rapidly and the reaction mixture was stirred overnight at room temperature under nitrogen atmosphere. After the solution was quenched with ice, deionized water (25 mL) was added and the

mixture was extracted with CH_2Cl_2 (25 mL). The organic portions were combined and neutralized by addition of 0.1 M aq $NaHCO_3$ solution. The organic phase was washed three times with deionized water (3×25 mL), dried over using $MgSO_4$, and evaporated under reduced pressure. The crude obtained product was purified by column chromatography using EtOAc/hexane with ratio of 1:50 to 1:3 as eluent) to provide the corresponding dihydropyridines (**1a-f**).

Diethyl-4-(2-ethoxy-2-oxoethyl)-1-phenyl-1,4-dihydropyridine-3,5-dicarboxylate (1a), Synthesized according to above general procedure from aniline (1.02 g, 10.97 mmol) as a pale yellow oil (750 mg, 58%); R_f (17% EtOAc/hexane) 0.25; v_{max} (neat) 3063, 2975, 2935, 1734, 1704, 1596, 1586, 1495, 1235, 1204, 1072 cm^{-1}; δ_H (400 MHz, CDCl$_3$): 7.58 (2H, s, CH=C), 7.42 (2H, t, J 7.9 Hz, *meta*-C$_6$H$_5$), 7.30–7.19 (3H, m, *ortho*-C$_6$H$_5$, and *para*-C$_6$H$_5$), 4.30–4.17 (5H, m, DHP–CO$_2$CH_2CH$_3$, and CHCH$_2$CO$_2$Et), 4.03 (2H, q, J 7.1 Hz, CH$_2$CO$_2$CH_2CH$_3$), 2.59 (2H, d, J 4.8 Hz, CH_2CO$_2$Et), 1.30 (6H, t, J 7.1 Hz, DHP–CO$_2$CH$_2$CH_3), 1.17 (3H, t, J 7.1 Hz, CH$_2$CO$_2$CH$_2$CH_3); δ_C (400 MHz, CDCl$_3$): 171.7, 166.7, 143.0, 137.6 , 129.8 , 126.4, 120.8, 108.2, 60.3, 60.1, 40.5, 29.6, 14.4, 14.2;

Diethyl-4-(2-ethoxy-2-oxoethyl)-1-(4-methoxyphenyl)-1,4-dihydropyridine-3,5-dicarboxylate (1b), Synthesized according to above general procedure from *p*-methoxyaniline (1.01 g, 8.22 mmol) as a pale yellow oil (560 mg, 50%), R_f (25% EtOAc/hexane) 0.30; v_{max} (neat) 3079, 3039, 2977, 2934, 1738, 1702, 1599, 1582, 1518, 1229, 1205, 1079 cm^{-1}; δ_H (400 MHz, CDCl$_3$): 7.46 (2H, s, CH=C), 7.15 (2H, d, J 9.0 Hz, *meta*-C$_6$H$_4$), 6.92 (2H, d, J 9.0 Hz, *ortho*-C$_6$H$_4$), 4.28–4.17 (5H, m, DHP–CO$_2$CH_2CH$_3$ and CHCH$_2$CO$_2$Et), 4.04 (2H, q, J 7.1 Hz, CH$_2$CO$_2$CH_2CH$_3$), 3.82 (3H, s, OMe), 2.57 (2H, d, J 4.8 Hz, CH_2CO$_2$Et), 1.29 (6H, t, J 7.1 Hz, DHP–CO$_2$CH$_2$CH_3), 1.18 (3H, t, J 7.1 Hz, CH$_2$CO$_2$CH$_2$CH_3); δ_C (400 MHz, CDCl$_3$): 171.7, 166.8, 158.2, 138.3, 136.6, 122.9, 114.8, 107.5, 60.3, 60.0, 55.6, 40.6, 29.5, 14.4, 14.2;

Diethyl-4-(2-ethoxy-2-oxoethyl)-1-(4-iodophenyl)-1,4-dihydropyridine-3,5-dicarboxylate (1c), Synthesized according to above general procedure from *p*-

iodoaniline (1.18 g, 5.37 mmol) as a pale yellow solid (350 mg, 45%); R_f (20% EtOAc/hexane) 0.20; v_{max} (neat) 3083, 3063, 2974, 2931, 1731, 1704, 1625,1582, 1494, 1229 cm^{-1}; δ_H (400 MHz, CDCl$_3$): 7.72 (2H, d, J 8.4 Hz, *meta*-C$_6$H$_4$), 7.51 (2H, s, C*H*=C), 6.98 (2H, d, J 8.4 Hz, *ortho*-C$_6$H$_4$), 4.30–4.14 (5H, m, DHP–CO$_2$C*H$_2$*CH$_3$, and C*H*CH$_2$CO$_2$Et), 4.01 (2H, q, J 7.1 Hz, CH$_2$CO$_2$C*H$_2$*CH$_3$), 2.59 (2H, d, J 4.7 Hz, C*H$_2$*CO$_2$Et), 1.30 (6H, t, J 7.1 Hz, DHP–CO$_2$CH$_2$C*H$_3$*), 1.16 (3H, t, J 7.1 Hz, CH$_2$CO$_2$CH$_2$C*H$_3$*); δ_C (400 MHz, CDCl$_3$): 171.5, 166.5, 142.7, 138.8, 136.9, 122.4, 108.9, 90.2, 60.4, 60.1, 40.3, 29.5, 14.3, 14.2;

Diethyl-1-benzyl-4-(2-ethoxy-2-oxoethyl)-1,4-dihydropyridine-3,5-dicarboxylate

(1d), Synthesized according to above general procedure from benzylamine (1.00 g, 9.10 mmol) as a pale yellow oil (880 mg, 48%); R_f (25% EtOAc/hexane) 0.25; v_{max} (neat) 3060, 3029, 2979, 2928, 1731, 1698, 1582, 1241, 1186, 1077 cm^{-1}; δ_H (400 MHz, CDCl$_3$): 7.47–7.21 (5H, m, *Ph*), 7.19 (2H, s, C*H*=C), 4.50 (2H, s, NC*H$_2$*), 4.23–4.13 (5H, m, DHP–CO$_2$C*H$_2$*CH$_3$, and C*H*CH$_2$CO$_2$Et), 3.99 (2H, q, J 7.1 Hz, CH$_2$CO$_2$C*H$_2$*CH$_3$), 2.50 (2H, d, J 5.0 Hz, C*H$_2$*CO$_2$Et), 1.27 (6H, t, J 7.1 Hz, DHP–CO$_2$CH$_2$C*H$_3$*), 1.16 (3H, t, J 7.1 Hz, CH$_2$CO$_2$CH$_2$C*H$_3$*); δ_C (400 MHz, CDCl$_3$): 171.7, 166.7, 139.4, 129.0, 128.2, 127.1, 109.9, 106.4, 60.1, 59.9, 58.0, 40.8, 29.5, 14.3, 14.1;

Diethyl-1-butyl-4-(2-ethoxy-2-oxoethyl)-1,4-dihydropyridine-3,5-dicarboxylate

(1e), Synthesized according to above general procedure from buthylamine (703 mg, 9.61 mmol) as a pale yellow oil (655 mg, 54%); R_f (25% EtOAc/hexane) 0.28; v_{max} (neat) 2975, 2957, 2932, 1731, 1699, 1580, 1196, 1081 cm^{-1}; δ_H (400 MHz, CDCl$_3$): 7.12 (2H, s, C*H*=C), 4.23–4.15 (5H, m, DHP–CO$_2$C*H$_2$*CH$_3$ and C*H*CH$_2$CO$_2$Et), 4.03 (2H, q, J 7.1 Hz, CH$_2$CO$_2$C*H$_2$*CH$_3$), 3.30 (2H, t, J 7.2 Hz, NC*H$_2$*), 2.45 (2H, d, J 5.0 Hz, C*H$_2$*CO$_2$Et), 1.66–1.53 (2H, m, NCH$_2$C*H$_2$*), 1.41–1.31 (2H, m, NCH$_2$CH$_2$C*H$_2$*), 1.29 (6H, t, J 7.1 Hz, DHP–CO$_2$CH$_2$C*H$_3$*), 1.20 (3H, t, J 7.2 Hz, CH$_2$CO$_2$CH$_2$C*H$_3$*), 0.95 (3H, t, J 7.3 Hz, N(CH$_2$)$_3$C*H$_3$*); δ_C (400 MHz, CDCl$_3$): 171.7, 166.9, 139.3, 105.7, 60.0, 59.9, 54.7, 40.9, 32.3, 29.5, 19.5, 14.4, 14.1, 13.6

Diethyl-4-(2-ethoxy-2-oxoethyl)-1-octadecyl-1,4-dihydropyridine-3,5dicarboxylate (1f), Synthesized according to above general procedure from octadecylamine (1.01 g, 3.75 mmol) as a pale yellow oil (583 mg, 83%); R_f (25% EtOAc/hexane) 0.20; v_{max} (neat) 2929, 2850, 1736, 1697, 1211, 1175, 1072 cm^{-1}; δ_H (400 MHz, CDCl$_3$): 7.12 (2H, s, CH=C), 4.23–4.15 (5H, m, DHP–CO$_2$CH_2CH$_3$, and CHCH$_2$CO$_2$Et), 4.02 (2H, q, J 7.1 Hz, CH$_2$CO$_2$CH_2CH$_3$), 3.28 (2H, t, J 7.3 Hz, NCH_2), 2.45 (2H, d, J 5.0 Hz, CH_2CO$_2$Et), 1.65–1.55 (2H, m, NCH$_2$CH_2), 1.43–1.11 (39H, m, DHP–CO$_2$CH$_2$CH_3, and CH$_2$CO$_2$CH$_2$CH_3 and N-(CH$_2$)$_2$(CH_2)$_{15}$CH$_3$), 0.87 (3H, t, J 6.8 Hz, N(CH$_2$)$_{17}$CH_3); δ_C (400 MHz, CDCl$_3$): 171.7, 166.9, 139.3, 105.7, 60.0, 59.9, 54.9, 40.9, 31.9, 30.3, 30.09, 30.02, 29.99, 29.93, 29.8, 29.5, 29.3, 26.2, 22.7, 14.8, 14.6, 14.2, 14.1;

2.3.2 Synthesis and characterization of 1,4-dihydropyridines tricarboxylate (2a-f)

1a-f   **2a-f**
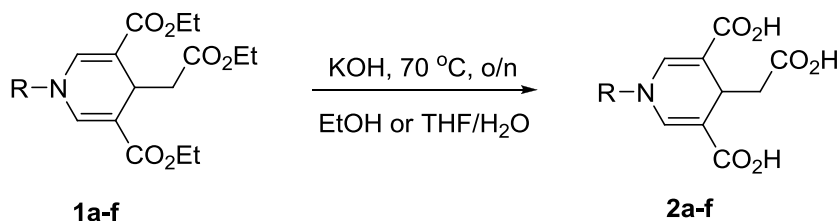
Compound **2** was prepared based on a simple hydrolysis reaction of 1, 4-dihydropyridine triester (**1**) in KOH, H$_2$O and Ethanol or THF at 70 °C. A mixture of compound **2**, excess KOH pellets in THF or ethanol (10 mL) and water (10 mL) was stirred for overnight at 70 °C. The solution was evaporated to gain, which then redissolved in water (15 mL). After addition of approximately 20 g of ice, the aqueous solution residue was acidified by 0.1 M HCl and kept in refrigerator for overnight. The product was precipitated and filtered to afford compound **2a-f**.

4-(Carboxymethyl)-1-phenyl-1,4-dihydropyridine-3,5-dicarboxylic acid (2a), Synthesized from **1a** (205 mg, 0.53 mmol) according to the above general procedure, using THF/H$_2$O as a solvent, to afford a yellow solid (160 mg, 80%); m.p. 185.6 °C;

v_{max} (KBr) 2500-3670, 3070, 2900, 1687, 1666, 1572, 1495, 1431, 1211, 1065 cm^{-1}; δ_H (400 MHz, DMSO-d6): 7.52 (2H, s, CH=C), 7.46 (2H, t, J 7.80 Hz, ArH), 7.32-7.28 (3H, m, ArH), 3.97 (1H, t, J 4.50 Hz, CHCH$_2$CO$_2$H), 2.35 (2H, d, J 4.30 Hz, CH_2CO$_2$H), 12.07 (3H, s, CH$_2$CO$_2$H and CH=CCO$_2$H); δ_C (100 MHz, DMSO-d6): 172.4, 167.5, 142.5, 137.0, 129.8, 126.0, 120.2, 108.1, 39.5, 29.1; Elem. Anal. Found; C, 59.35%; H, 4.35%; N, 4.74% (calcd for C$_{15}$H$_{13}$NO$_6$, 59.41%; H, 4.32%; N, 4.62%); HRMS (ESI): [M+K]$^+$, found 342.0477. C$_{15}$H$_{13}$NO$_6$K$^+$, requires 342.0380.

4-(Carboxymethyl)-1-(4-methoxyphenyl)-1,4-dihydropyridine-3,5-dicarboxylic acid (2b), Synthesized according to above general procedure using THF/H$_2$O as solvent from **1b** (216 mg, 0.51 mmol) as a yellow solid (109 mg, 63%); m.p. 169.9 °C; v_{max} (KBr) 2500-3670, 3068, 2914, 2848, 1697, 1685, 1572, 1514, 1431, 1281, 1213 cm^{-1}; δ_H (400 MHz, DMSO-d6): 7.36 (2H, s, CH=C), 7.21 (2H, d, J 8.91 Hz, ArH), 6.97 (2H, d, J 8.91 Hz, ArH), 3.93 (1H, t, J 4.62 Hz, CHCH$_2$CO$_2$H), 3.74 (3H, s, OMe), 2.30 (2H, d, J 4.51 Hz, CH_2CO$_2$H), 12.00 (3H, s, CH$_2$CO$_2$H and CH=CCO$_2$H); δ_C (100 MHz, DMSO-d6): 172.1, 166.8, 157.0, 137.2, 135.7, 122.0, 114.3, 106.7, 54.5, 39.4, 28.2; HRMS (ESI): [M+K]$^+$, found 372.0561. C$_{16}$H$_{15}$NO$_7$K$^+$, requires 372.0486.

4-(Carboxymethyl)-1-(4-iodophenyl)-1,4-dihydropyridine-3,5-dicarboxylic acid (2c), Synthesized according to above general procedure using THF/H$_2$O as solvent from **1c** (220 mg, 0.43 mmol) as a light yellow solid (132 mg, 72%); m.p. 186.7 °C; v_{max} (KBr) 2500-3670, 2914, 2846, 1693, 1581, 1489, 1215 cm^{-1}; δ_H (400 MHz, DMSO-d6): 7.76 (2H, d, J 7.10 Hz, ArH), 7.47 (2H, s, CH=C), 7.14 (2H, d, ArH), 3.96 (1H, t, J 4.35 Hz, CHCH$_2$CO$_2$H), 2.34 (2H, d, J 3.85 Hz, CH_2CO$_2$H), 12.08 (3H, s, CH$_2$CO$_2$H and CH=CCO$_2$H); δ_C (100 MHz, DMSO-d6): 171.9, 167.2, 141.6, 138.4, 136.3, 121.9, 108.6, 90.2, 40.3, 29.4; HRMS (ESI): [M+H]$^+$, found 429.2488. C$_{15}$H$_{13}$INO$_6$$^+$, requires 428.9708.

1-Benzyl-4-(carboxymethyl)-1,4-dihydropyridine-3,5-dicarboxylic acid (2d), Synthesized according to above general procedure using EtOH/H$_2$O as solvent from **1d** (295 mg, 0.73 mmol) as a light yellow solid (152 mg, 65%); m.p. 163.1 °C; v_{max}

(KBr) 2500-3670, 3008, 2885, 1685, 1647, 1564, 1396, 1284, 1190 cm^{-1}; δ_H (400 MHz, DMSO-d6): 7.25 (2H, s, C*H*=C), 7.40-7.25 (5H, m, Ph), 4.67 (2H, s, NC*H$_2$*), 3.94 (1H, t, *J* 4.70 Hz, C*H*CH$_2$CO$_2$H), 2.22 (2H, d, *J* 4.60 Hz, C*H$_2$*CO$_2$H), 11.79 (3H, s,CH$_2$CO$_2$*H* and CH=CCO$_2$*H*); δ_C (100 MHz, DMSO-d6): 172.4, 167.7, 139.8, 137.4, 128.8, 127.6, 127.3, 105.3, 56.3, 40.3, 29.0; HRMS (ESI): [M+H]$^+$, found 318.1583. C$_{16}$H$_{16}$NO$_6^+$, requires 318.0977.

1-Butyl-4-(carboxymethyl)-1,4-dihydropyridine-3,5-dicarboxylic acid (2e), Synthesized according to above general procedure using EtOH/H$_2$O as solvent from **1e** (300 mg, 0.94 mmol) as a yellow solid (210 mg, 75%); m.p. 139 °C; v_{max} 2990-3680, 2940, 2914, 2858, 1682, 1647, 1186, 1120 cm^{-1} δ_H (400 MHz, DMSO-d6): 7.18 (2H, s, C*H*=C), 3.91 (1H, t, *J* 4.80 Hz, C*H*CH$_2$CO$_2$H), 3.40 (2H, t, *J* 6.8 Hz, NC*H$_2$*), 2.18 (2H, d, *J* 4.70 Hz, C*H$_2$*CO$_2$H), 1.48 (2H, m, NCH$_2$C*H$_2$*CH$_2$); 1.27 (2H, m, *J* 7.6Hz, CH$_2$C*H$_2$*CH$_3$); 0.89 (3H, t, *J* 7.3 Hz, CH$_2$CH$_2$C*H$_3$*); 11.71 (3H, s, CH$_2$CO$_2$*H* and CH=CCO$_2$*H*); δ_C (100 MHz, DMSO-d6): 172.1, 167.5, 139.4, 104.2, 52.8, 38.5, 31.7, 28.6, 18.5, 13.2. HRMS (ESI): [M+H]$^+$, found 284.3321. C$_{13}$H$_{18}$NO$_6^+$, requires 284.1134.

4-(Carboxymethyl)-1-octadecyl-1,4-dihydropyridine-3,5-dicarboxylic acid (2f), Synthesized according to above general procedure EtOH/H$_2$O as solvent from **1f** (280 mg, 0.49 mmol) as a pale yellow solid (212 mg, 89%), m.p. 168 °C; v_{max} 2954-3680, 2916, 2846, 1618, 1070; δ_H (400 MHz, MeOD): 7.24 (2H, s, C*H*=C), 4.08 (2H, t, *J* 4.8 Hz, C*H*CH$_2$CO$_2$Et), 3.36 (NC*H$_2$*, 1H, t, *J* 6.9 Hz), 2.35 (2H, d, *J* 5.0 Hz, C*H$_2$*CO$_2$Et), 1.58 (2H, m, NCH$_2$C*H$_2$*), 1.30–1.21 (15H, m, *N*-(CH$_2$)$_2$(C*H$_2$*)$_{15}$CH$_3$), 0.87 (3H, t, *J* 6.8 Hz, N(CH$_2$)$_{17}$C*H$_3$*); δ_C (100 MHz, DMSO-d6): 172.8, 168.2, 140.1, 105.1, 53.8, 31.7, 31.1, 30.3, 31.9, 30.3, 29.4, 29.3, 29.1, 29.0, 28.9, 27.3, 26.3, 26.0, 22.5, 14.4.

2.4 Analytical experiment

The photophysical property study, metal sensing and surfactant sensing were achieved using pH 8.0 potassium phosphate buffer (PB) (50 mM) and nitroaromatics sensing were attained in THF.

A buffer solution is an aqueous solution used as a means of keeping pH at a nearly constant value in a wide variety of chemical applications. The buffering capacity is the ability of the buffer to resist changes in pH. Buffering capacity increases as the increasing the molar concentration (molarity) of the buffer salt/acid. The phosphates have a very high buffering capacity and are highly soluble in water. Potassium phosphate buffer, the most commonly used buffers, consists of a mixture of monobasic dihydrogen phosphate (KH_2PO_4) and dibasic monohydrogen phosphate (K_2HPO_4). By varying the amount of each salt, a ratio of monobasic and dibasic approximately 1:9 can be prepared that buffer well pH 8.0 [56].

The maximum of buffer concentration should not be exceeded the K_{sp} in order to prevent the precipitation of $HgHPO_4$. The maximum concentration can be calculated by following equation:

$$[HPO_4^{2-}] = K_{sp} / [Hg^{2+}]$$
$$K_{sp} \text{ of } HgHPO_4 = 7.9 \times 10^{-14} \text{ [57]}$$

2.4.1 Photophysical properties study

The stock solution of **1** was prepared by dissolving 5 µmol of **1** in THF to get the concentration of 0.1mM of compound **1** stock solution (50 mL). The stock solution of **2** was prepared in the same manner in THF and also in pH 8.0 PB to get the 0.1 mM compound **2** stock solution (50 mL).

2.4.1.1 UV-Visible spectroscopy

The stock solutions of **1** and **2** (0.1 mM) were diluted to 100 µM. The UV-Visible absorption spectra of the DHP were recorded from 200 nm to 600 nm at ambient temperature.

2.4.1.2 Fluorescence spectroscopy

The stock solutions of fluorophores were diluted into the concentration of 1 µM. The emission spectra of fluorophores were recorded from 380 nm to 600 nm at

ambient temperature using an excitation wavelength at 347 nm (**2a**), 352 nm (**2b**), 353 nm (**2c**), 357 nm (**2d**) and 358 nm (**2e**).

2.4.1.3 Molar extinction coefficient (ε)

The molar extinction coefficient (ε) of **2s** were calculated from the UV-Visible absorption spectra in pH 8.0 PB of analytical samples at varied concentrations. The maximum absorbance of all samples should never be more than value of 1. The absorption maximum wavelengths (λ_{max}) of each compound were plotted against the concentrations at the respective excitation wavelengths. Each plot should be a straight line go thorough origin. The molar extinction coefficient (ε) can also be calculated from plotting of absorption maximum (A) *vs* concentration (C) represented into the following equation:

$$A = \varepsilon bC$$

2.4.1.4 Fluorescence quantum yield (Φ_F)

The fluorescence quantum yield of **2** were performed in phosphate buffer pH 8.0 by using quinine sulfate in 0.1 M H_2SO_4 ($\Phi = 0.54$) as a reference. The UV-Visible absorption spectra of analyte and reference samples at varied concentrations were recorded. The maximum absorbance of all samples should never exceed 0.1. The fluorescence emission spectra of the same solutions using appropriate excitation wavelengths selected were recorded based on the absorption maximum wavelength (λ_{max}) of each compound. Graphs of integrated fluorescence intensities were plotted against the absorbance at the respective excitation wavelengths. Each plot should be a straight line with 0 interception and gradient *m*.

In addition, the fluorescence quantum yield (Φ_F) was obtained from plotting of integrated fluorescence intensity *vs* absorbance represented into the following equation:

$$\Phi_X = \Phi_{ST}\left(\frac{\text{Grad}_X}{\text{Grad}_{ST}}\right)\left(\frac{\eta_X^2}{\eta_{ST}^2}\right)$$

The subscripts Φ_{ST} denote the fluorescence quantum yield of a standard reference which used quinine sulfate in 0.1 M H_2SO_4 ($\Phi=0.54$) and Φ_X is the fluorescence quantum yield of sample and η is the refractive index of the solvent. In all cases achieved in this thesis only aqueous systems were selected for the quantum yield calculation.

2.4.2 Metal ion sensor

Stock solutions of each metal ion with the concentration of 1 mM was prepared in Milli-Q water using acetate salt except for iron and cadmium which the ferric nitrate (Fe^{3+}), ferrous sulfate (Fe^{2+}) and cadmium sulfate (Cd^{2+}) were used instead. .

2.4.2.1 Selectivity study

To attain the fluorescence quenching profile, the **2b** and metal solution were diluted to 1 μM and mixed with metal ion 50 μM in a ratio of 1:50. The mixture was allowed to stand at room temperature for 30 min. The response was collected from 380 nm to 600 nm at ambient temperature by fluorescence spectrophotometer. To achieve the visible fluorescence response and photographed under black light, the stock solution of **2b** were dilute to 0.1 mM and mixed with metal ions in a concentration of 1 mM.

2.4.2.2 Time-dependent quenching study

The fluorescence quenching by Hg^{2+} proceeded gradually, therefore, the fluorescence intensity was monitored for 60 minutes. By fixing ratio of **2b**:Hg^{2+} at 1:50, the mixtures were allowed to stand at room temperature for 0 to 60 min. The spectra from 380 nm to 600 nm at ambient temperature were recorded by using fluorescence spectrophotometer. Time-dependent quenching of **2b** to Hg^{2+} was shown by plotting I/I_0 and time.

2.4.2.3 Fluorescence and UV-vis titration

To reach the fluorescence titration spectra, the mixtures of **2b**/Hg^{2+} was prepared with the ratio of 1/0-100 and allowed to stand at room temperature for 30 min. The spectra were recorded as described previously. In order to gain insightful information about the quenching mechanism, UV–vis metal binding titration was performed in the similar fashion in the study of fluorescence titration but the concentration of **2b** was changed to 24 μM.

2.4.2.4 ^{1}H NMR experiment

Compound **2b** (26 mg, 0.08 mmol) was dissolved in a pH 8.0 PB solution (0.4 mL). Into this aqueous solution, the solution of Hg(OAc)$_2$ (24 mg, 1 equiv) was added and shaken thoroughly. ^{1}H NMR experiment was then conducted immediately with a NMR spectrometer (Bruker, 400 MHz). The spectra of this experiment at the times of 0 min, 30 min, and 2 days were illustrated for the comparison.

2.4.2.5 Effect of pH

Since the pH affects the solubility of **2b** and the quenching of with Hg^{2+}, the effect of pH were studied. The stock solutions of **2b** were prepared in the concentration of 100 μM with varied pH of PB ranging from 6 to 10. The **2b** and Hg^{2+} solutions were diluted and mixed in a ratio of 1:50 and allowed to stand at room temperature for 30 min and recorded spectra from 380 nm to 600 nm at ambient temperature by fluorescence spectrophotometer.

2.4.2.6 Interference study

The mixture of fluorophore/Hg^{2+}/others metal ions with ratio 1/20/200 was used to investigate competitive quenching from other metal ions in the **2b**·Hg^{2+} system.

2.4.2.7 Job's Method

Job's plot was used to determine a ratio of mercury to react with fluorophore. Job's Method experimentally, one prepares a series of solutions containing a fixed total number of moles of **2b** and Hg^{2+}, but in which their mole fractions were varied (3:0 to 0:3). The data was achieved from plotting of mole fraction of Hg^{2+} (X_B) and $y_0 - y(1-X_B)$ where; y_0 is maximum fluorescent intensity of **2b**, y is maximum fluorescent intensity of **2b** after added metal ion at X_B). The maximum on the plot corresponds to the stoichiometry of the two species. The emission spectrum of fluorophore was recorded using an excitation wavelength of 352 nm.

2.4.2.8 Detection limit (DL)

DL is the lowest amount of analyte in a sample that can be detected, but not necessarily quantitated as an exact value. The DL may be expressed as:

$$DL = [I_0/(I-3SD)-1] \,/S$$

Where;

SD is the standard deviation of the response deriving from the maximum intensity of fluorophore at 1 µM of 9 samples.

S is the slope of the calibration curve obtained from fluorescence titration spectra.

I and I0

2.4.3 Surfactant sensor

The photophysical properties toward three types of surfactants, anionic, cationic and non-ionic surfactants were investigated. The stock solution of **2a** was diluted to 1 µM in PB buffer pH 8.0. The stock surfactants were prepared in phosphate buffer pH 8.0. The surfactant solutions with the concentration of 0.1, 1, and 10 mM were diluted from the stock solution (20 mM). The surfactants were added to the **2a** solutions. The final volumes of the mixtures were adjusted to 5 mL to get the final concentration of 0.1, 1, and 10 mM. The emission spectrum of **2a** was recorded

from 367 nm to 600 nm at ambient temperature using an excitation wavelength at 347 nm.

2.4.4 Nitroaromatic sensor

The stock solutions of nitroaromatic compounds were prepared in THF at 100 µM. DHP **2a** solutions were diluted from the 100 µM stock solution to 1 µM and nitroaromatic solutions were added to the final concentration of 1 µM. After the solution was mixed, fluorescence spectra were measured with an excitation wavelength of 347 nm at room temperature. Fluorescence spectra were recorded from 367 to 600 nm.

2.4.5 Protein/metal sensor

Because of the bovine serum albumin (BSA) is normally used as fluorescent sensor for metal ions, such as Fe^{2+}, Fe^{3+} and Cu^{2+} in which the binding between metal ion and quench the fluorescent signal. The sensor performance of the compound **2a** was tested against protein, bovine serum albumin (BSA) as well. The solution of 100 µM compound **2a** was prepared in 10 mM sodium phosphate buffer saline (PBS, pH 7.4). Bovine serum albumin (BSA) protein stock solution was prepared by dilution of BSA with PBS until the absorbance of BSA at 280 nm (A_{280}) being 0.4. Stock solutions of each metal ion (1 mM) were prepared in Milli-Q water by using metal acetate for all metal ions except for ferric nitrate (Fe^{3+}), ferrous sulfate (Fe^{2+}) and cadmium sulfate (Cd^{2+}). The **2a**, protein and metal ions were mixed. The fluorophores with 1 µM, BSA concentration with 15 µM and metal ions were used in a concentration of 10 and 100 µM. The sensor response toward metal ion was monitored using fluorescence spectrophotometer with the excitation wavelength of 347 nm. The emission was recorded from 367 to 600 nm at ambient temperature.

CHAPTER III

RESULTS AND DISCUSSION

3.1 Synthesis of 1, 4-dihydropyridine derivatives

The synthetic route for 1,4-DHP derivatives is presented in **Scheme 3.1**. The synthesis of 1,4-DHP **1d-f** began with the reaction of ethyl propiolate and aliphatic amine in CH_2Cl_2 at room temperature, the reaction mixture was completed overnight to get N-aliphatic β-amino acrylates. For N-aromatic DHP **1a-c** were synthesized from the reaction of aromatic amines, ethyl propiolate and copper(I) iodide in CH_2Cl_2 at 60 °C overnight to achieve N-aromatic β-amino acrylates as an adduct. Subsequence cyclisation of these β-amino acrylates catalyzed by $TiCl_4$ afforded the products in moderate yields of 45-70%. This step showed lower yield of product than it should be because starting material did not purified before use. In addition, the synthetic of 1,4-DHP tricarboxylate (**2a-f**) was achieved by base hydrolysis of **1a-f** to convert the ethyl ester to carboxylic acid (63-80%). All compounds were characterized by ^{1}H NMR spectroscopy, ^{13}C NMR spectroscopy and IR spectroscopy.

yield (%)	1	2
a (R = Ph)	66	80
b (R = p-MeO-Ph)	52	63
c (R = p-I-Ph)	45	72
d (R = Bn)	60	65
e (R = n-Bu)	67	75
f (R = $C_{18}H_{37}$)	70	80
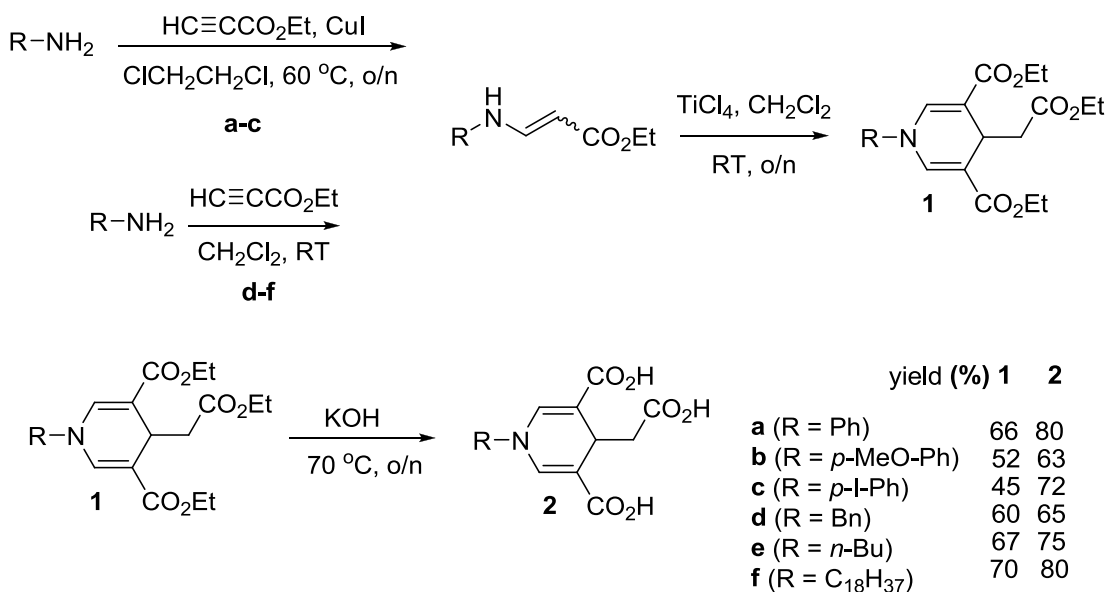
Scheme 3.1 Synthesis of 1,4-DHP derivatives (**1a-f**)

The ^{1}H NMR spectra of compound **1a** and **2a** in CDCl$_3$ and DMSO-d6 are shown in **Figure 3.1**. All signals could be assigned to all protons in each corresponding structure. As the evidence of the 1,4-DHP ring formation, the alkene peak and alkyl peak appeared at 7.58 ppm as a singlet signal and around 4.26 ppm (according to the 2-D results), respectively. The triplet signal at 7.42 ppm and multiplet signals at 7.19-7.30 ppm correspond to the aromatic protons of aryl moiety. The doublet signal of methylene protons appeared at 2.59 ppm. The signal of ethyl ester protons appeared at 4.23 and 4.03 ppm including triplet signals at 1.21 ppm and 1.34 ppm. The complete hydrolysis of **1a** to tricarboxylic acid **2a** was evidenced by the total disappearance of the ethyl ester proton and also found the carboxylic protons were performed at 12.07 ppm.
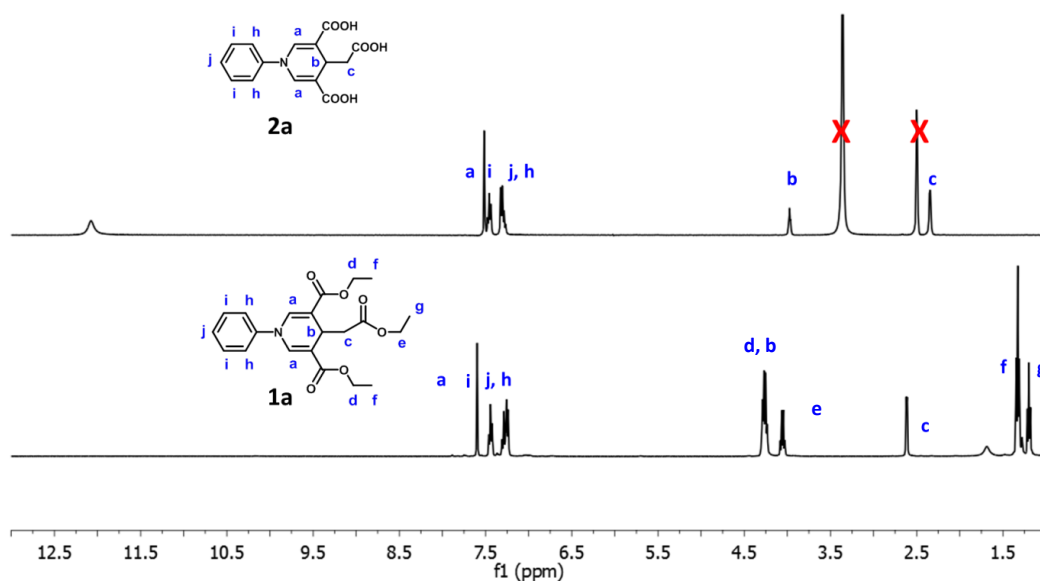
Figure 3.1 ^{1}H NMR (400 MHz) of compounds **1a** (CDCl$_3$) and **2a** (DMSO-d6).

The ^{1}H NMR spectra of compound **1b** and **2b** in CDCl$_3$ and DMSO-d6 are shown in **Figure 3.2**. All the signals can be assigned to all the protons in each corresponding structure. In the formation of dihydropyridines ring were achieved the characteristic of alkene peak as a singlet at 7.46 ppm and the alkyl peak at around 4.19 ppm. It also found that, the two doublet signals at 7.15 and 6.92 ppm corresponding to the aromatic protons and the methoxy protons are appears the singlet signal at 3.82 ppm. The doublet signals of methylene protons appeared at 2.57 ppm. Similarly, the ethyl ester protons are shows at the same position as **1a**. The ^{1}H NMR

spectra clearly indicated complete hydrolysis of **1b** to tricarboxylic acid **2b** with the disappearance of the ethyl ester proton at 4.23, 4.04, 1.29 and 1.18 ppm.
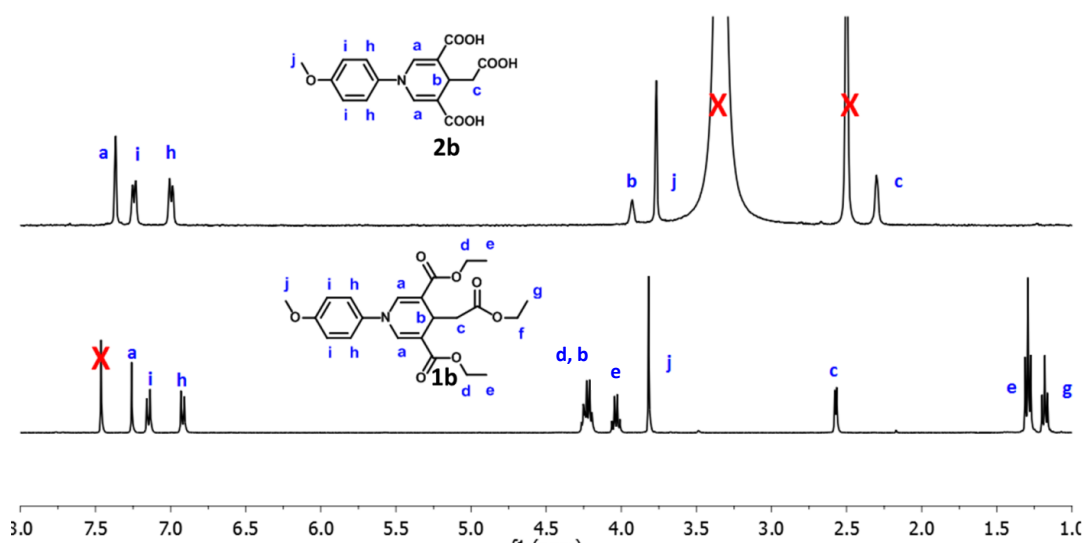
Figure 3.2 ^{1}H NMR (400 MHz) of compounds **1b** (CDCl$_3$) and **2b** (DMSO-d6).

For Iodo compounds **1c** and **2c** were dissolved in CDCl$_3$ and DMSO-d6 respectively, in the same manner as **a** and **b** series. Their ^{1}H NMR spectra demonstrated the same patterns (**Figure 3.3**) as shown in the case of *p*-methoxy DHP derivatives **1b** and **2b**; the singlet peak of alkene protons and signals of alkyl protons within 1,4-DHP ring was observed at 7.51 ppm and around 4.18 ppm, respectively. The aromatic protons were displayed as two doublet signals at 7.72 ppm and 6.79 ppm and the doublet signals of methylene protons appeared at 2.59 ppm. The signals of six CH$_2$ ethyl ester protons appeared at 4.22 and 4.01 ppm and 6 and 3 protons of two types of CH$_3$ ethyl ester groups corresponded to the triplet signals at 1.16 ppm and 1.30 ppm. Comparing both ^{1}H NMR spectra, the conversion from the ethyl ester to carboxylic acid was clearly confirmed by the appearance of new signal at 12.12 ppm and disappearance of all protons corresponding to the ethyl ester groups.
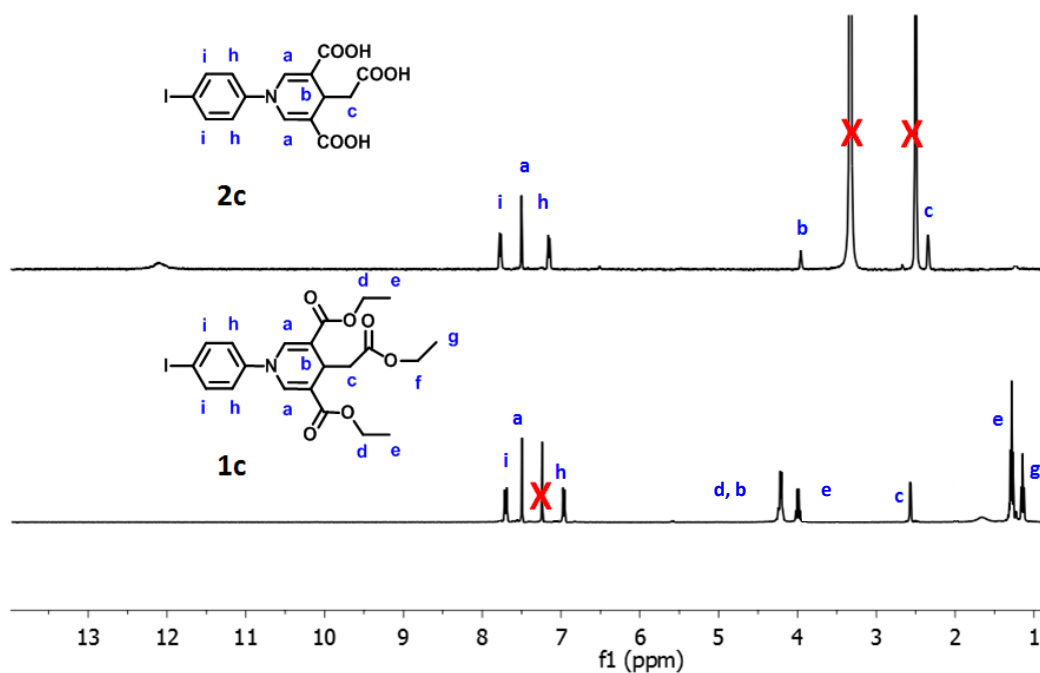
Figure 3.3 ^{1}H NMR (400 MHz) of compounds **1c** (CDCl$_3$) and **2c** (DMSO-d6).

The *N*-benzyl DHP derivatives **1d** and **2d** were conducted by ^{1}H NMR in CDCl$_3$ and DMSO-d6, respectively (**Figure 3.4**). Again in the same interpreting manner with other series, a singlet peak at 7.19 ppm corresponding to the alkene protons of 1,4-DHP. The aromatic protons were observed as the multiplet signals at the range of 7.47-7.21 ppm, and the methylene protons adjacent to nitrogen atom appeared as singlet signal at 4.50 ppm representing of the benzyl group. The signals of ethyl ester protons of **1d** were shown around 4.18 and 4.09 ppm as multiplet and as triplets at 1.16 ppm and 1.27 ppm. The total disappearances of these protons together with the existence of the carboxyl proton near 11.79 ppm assured the complete hydrolysis of above compound to tricarboxylic acid **2**.

Figure 3.4 ^{1}H NMR (400 MHz) of compounds **1d** (CDCl$_3$) and **2d** (DMSO-d6).

All signal in the ^{1}H NMR spectra of compound **1e** and **2e** in CDCl$_3$ and DMSO-d6 shown in **Figure 3.5** could be assigned to all protons in each corresponding structure. For 1,4-DHP **1e**, a singlet signal (a) of the alkene protons and the signal (b) of -C*H* proton appeared at 7.12 ppm and around 4.18 ppm, respectively. Two types of ethyl ester protons appeared as the quartet signals (d) at 4.03 and (f) at 4.19 and 4.02 ppm and two triplets (e and g) at 1.20 and 1.29 ppm. The aliphatic protons of the butyl group in the spectrum of compound **1e** were observed as two triplet signals (k, 3H and h, 2H) at 0.95 and 3.30 ppm and as the multiplet (i, 2H and j, 2H) at 1.41-1.31 ppm. The evidence for the completion of hydrolysis of above compound to tricarboxylic acid **2** was left by the total disappearance of all ethyl ester proton signals, and additionally, the new carboxyl proton near 12 ppm was found.
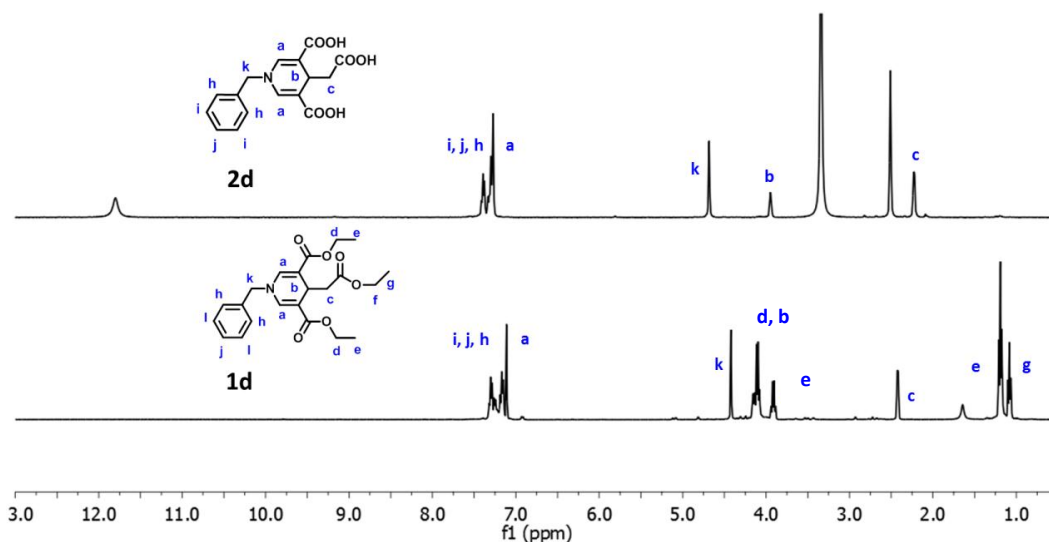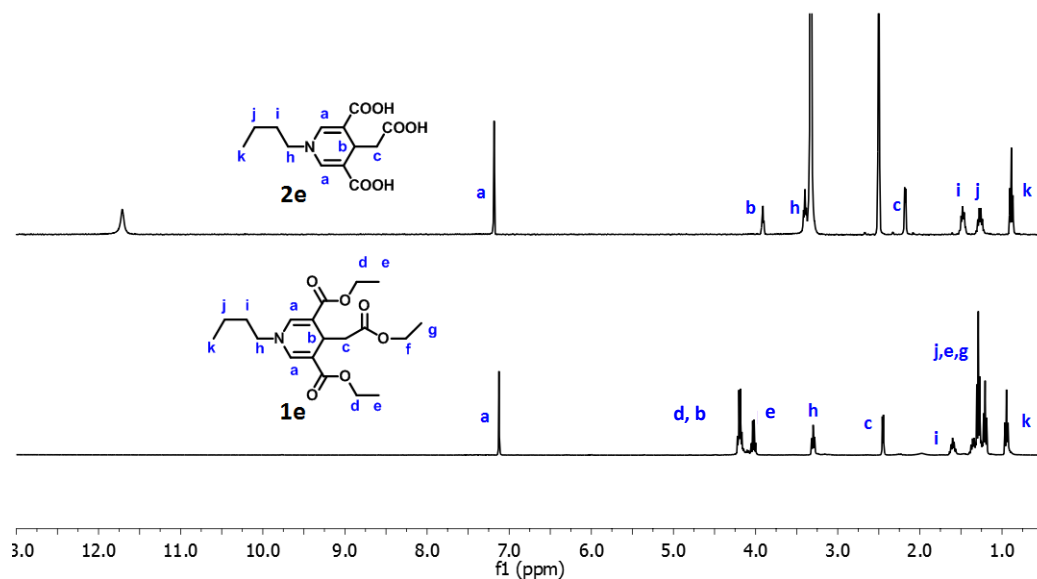
Figure 3.5 ^{1}H NMR (400 MHz) of compounds **1e** (CDCl$_3$) and **2e** (DMSO-d6).

The ^{1}H NMR spectra of compound **1f** and **2f** in CDCl$_3$ and CD$_3$OD are shown in **Figure 3.6**. For 1,4-DHP **1f**, a singlet signal (a) appeared at 7.12 ppm and the signal (b) at around 4.21 ppm were assigned to be of the alkene and CH proton, respectively. The chemical shift of methylene protons exhibited a doublet signal (c) at 2.45 ppm and the ethyl ester protons as the quartet signals (d and f) at 4.19 and 4.02, multiplet signal (e and g) at 1.11-1.43 ppm. The protons of long C$_{18}$ aliphatic chain appeared as a multiplet (i and j) in the range of 1.55-1.65 and 1.41-1.31 ppm (overlapping with the signal of ethyl ester protons) and two triplet signals (h, 2H and l, 3H) at 3.60 and 0.87 ppm. The signal of ethyl ester protons completely disappeared in the **2f** spectrum, indicating the complete hydrolysis of triester **1f** into the tricarboxylic acid **2f**.
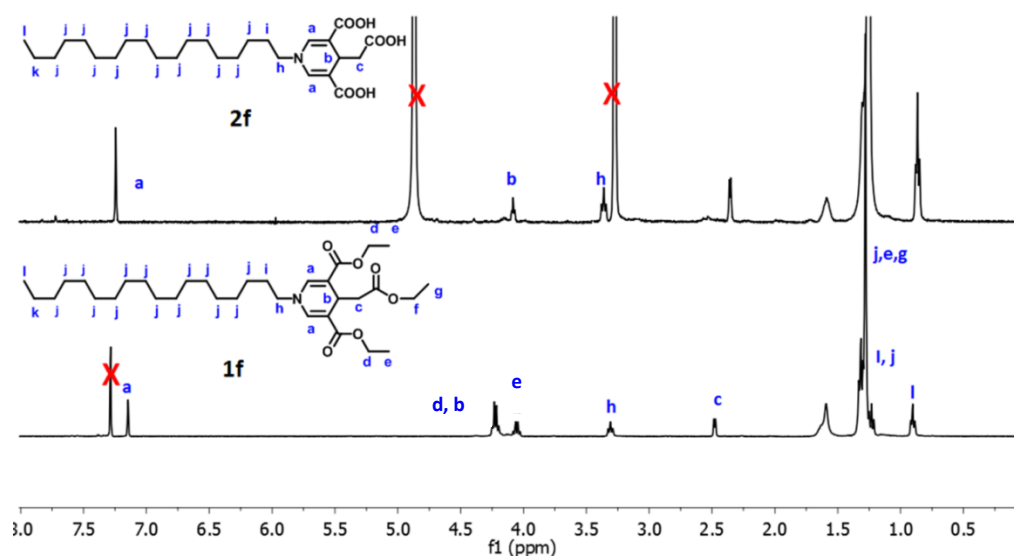
Figure 3.6 ^{1}H NMR (400 MHz) of compounds **1f** (CDCl$_3$) and **2f** CD$_3$OD.

The IR spectra of 1,4-DHP derivatives are shown in **Figure A.27-A.32**. For compounds **1a** and **2a** showed a peak at 1596, 1586, 1495 cm^{-1} which indicated the presence of C=C stretching of aromatic compound. The spectrum displayed that two bands appeared at 2976 and 2914 cm^{-1}, which corresponded to the typical asymmetric and symmetric C-H stretching vibration. Moreover we founded the characteristic peak of ester at 1701 and 1716 cm^{-1}. The IR spectra of **2a** showed the appearance of the new broad OH stretching band appearing at 3670-3000- cm^{-1} and a shift of C=O stretching band to lower energy, 1687 and 1666 cm^{-1} concurred well, consistent with the successful hydrolysis of the ester groups to the carboxylic groups.

The IR spectra of **1b** and **2b** showed a peak at 1599, 1582, 1518, 1442 cm^{-1} which indicated the presence of C=C stretching of aromatic compound. The spectrum displayed that three bands appeared at 2978, 2918 and 2848 cm^{-1}, which corresponded to the typical asymmetric and symmetric C-H stretching vibration. The appearance of carbonyl vibration peaks at 1693 and 1716 cm^{-1} corresponding to the characteristic peak of ester. The IR spectra of **2b** showed the appearance of the new broad OH stretching band appearing at 36700-3000 cm^{-1} and a shift of C=O stretching band to lower energy, 1685 and 1697 cm^{-1} concurred well, consistent with the successful hydrolysis of the ester groups to the carboxylic groups.

Corresponding to the strong peaks IR spectra of compounds **1c** and **2c,** the bands appearing at 1701 and 1714 cm^{-1} correspond to C=O stretching of two type of carbonyl groups. The appearance of a new broad OH stretching band at 3670-3000 cm^{-1} and a shift of C=O stretching band to lower energy, (1695 cm^{-1}) concurred well with the successful hydrolysis of the ester groups to the carboxylic groups.

The stretching peaks of the carbonyl group were perceived clearly at 1697 and 1712 cm^{-1} in the IR spectrum of compound **1d**. The appearance of a new broad OH stretching band at 3670-3000 cm^{-1} in IR spectrum of compound **2d** additionally with shift of C=O stretching band to lower energy, 1647 and 1685 cm^{-1} indicated a complete hydrolysis reaction from ethyl ester to the carboxylic groups.

The IR spectrum of compounds **1e** showed the characteristic peak of ester at 1701 and 1711 cm^{-1} corresponding to C=O stretching. Going from compound **1** to compound **2**, the IR spectra showed a new broad OH stretching band appearing at 3680-3000 cm^{-1} and a shift of C=O stretching band to lower energy, 1620 cm^{-1}.These facts also demonstrated that the ethyl ester had been hydrolyzed to the carboxylic groups.

The IR spectrum both of the 1,4-DHP **1f** and **2f** show C=O peaks at 1734 and 1701 cm^{-1}. A large broad band along the range of 3000 and 3680 cm^{-1} of the **2f** spectrum attributed to the presence of the O–H stretching of carboxylic groups and also a shift of C=O stretching band to lower energy, 1616 cm^{-1} were concurred. These facts suggested that triester **1f** were successfully hydrolysis to the tricarboxylic acid **2f**.

3.2   Photophysical property study

3.2.1 Photophysical property study of 1, 4-dihydropyridines triester (1a-f)

The photophysical properties of fluorophores **1a-f** were studied at concentration of 100 μM in THF. The maximum absorption wavelengths (λ_{max}) of the compounds **1a-f** were recorded from their UV-vis spectra scanned in the range of 200-600 nm. In THF, they displayed λ_{max} ranging from 359 to 368 nm which are the characteristic peaks of DHP moiety (**Figure 3.7**) [10-12] with molar extinction coefficients of 4.8×10^3-7.0×10^3 M^{-1} cm^{-1}. According to the results, DHP **1a-c** exhibited the strong absorption bands in the range of 285 to 292 nm with molar extinction coefficients of 3.4×10^3-1.9×10^4 corresponding to the *N*-substituted aryl moiety, while DHP **1d-f** exhibited weaker absorption bands than those of **1a-c**. All absorption parameters are summarized in **table 3.1**.
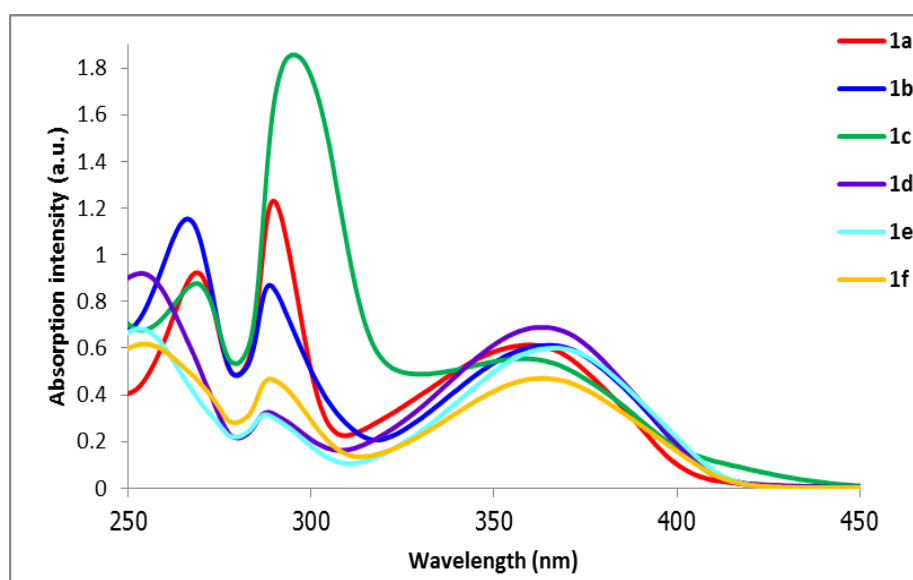

Figure 3.7 Absorption spectra of compounds **1a-f** 100 μM in THF.

Table 3.1 Absorption data of compounds **1** and **2** in THF

Compound	R	1		2	
		λ_{max} (nm)	ε (M^{-1} cm^{-1})	λ_{max} (nm)	ε (M^{-1} cm^{-1})
a	Ph	287	1.3×10^4	284	1.8×10^4
		360	6.2×10^3	361	5.1×10^3
b	p-MeO-Ph	289	9.3×10^3	280	8.3×10^3
		366	6.2×10^3	360	3.2×10^3
c	p-I-Ph	292	1.9×10^4	287	5.1×10^3
		359	5.7×10^3	356	9.0×10^3
d	Bn	285	3.6×10^3	-	-
		363	7.0×10^3	363	1.7×10^4
e	n-Bu	285	3.4×10^3	-	-
		367	6.1×10^3	362	5.0×10^3
f	$C_{18}H_{37}$	289	4.8×10^3	n/a	n/a
		364	4.8×10^3		

The maximum emission wavelengths of all fluorophores (**1a-f**) were determined at a concentration of 0.1 μM in the range between 380 to 550 nm. The results showed that the maximum emission wavelengths of all DHP fluorophores appeared at 409-431 nm (**Figure 3.8**). In the case of DHP **1b,** their fluorescence emission maximum shifted to longer wavelength comparing to these of DHPs which mainly depends on the electronic donating property of the methoxy group present in the aromatic ring. However, there was no such phenomenon occurred in the case of electron donating N-benzyl DHP **1d**. N-butyl and $C_{18}H_{37}$ groups in aliphatic N-substituted DHPs are also responsible for the higher λ_{max} value. For the DHP **1a** and **1c**, its emission wavelength exhibited the shorter wavelength approximately 15 nm

than others. Furthermore, the visible fluorescence emissions of DHP **1a-f** at concentration 10 μM in THF were observed under blacklight at room temperature by using the digital camera,the results showed that all DHP fluorophores responded in blue color (**Figure 3.9**).
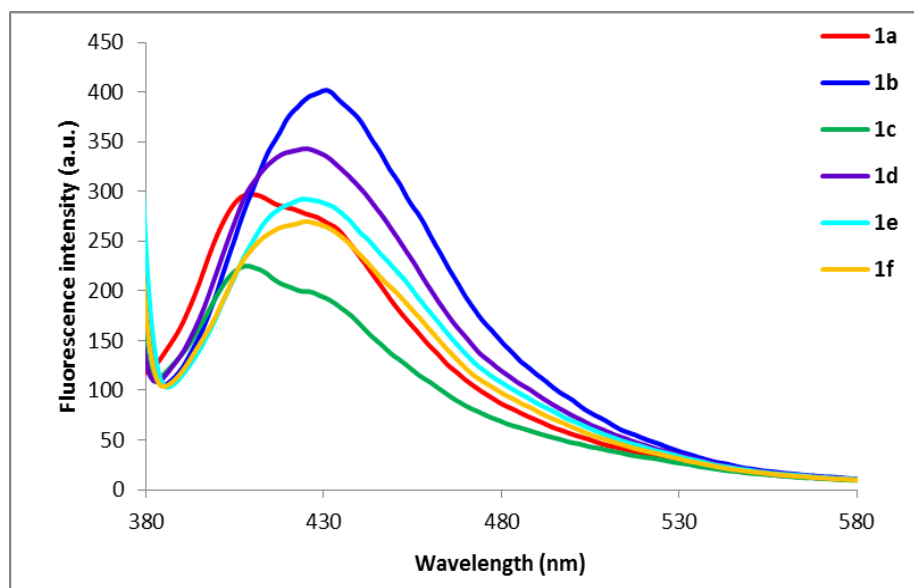

Figure 3.8 Fluorescence spectra of compounds **1a-f** 0.1 μM in THF

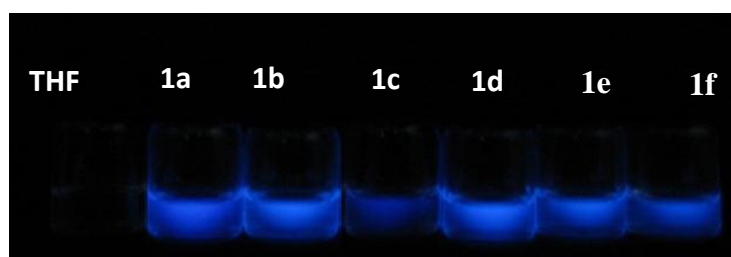Excitation at 360 nm (**1a**), 366 nm (**1b**), 359 nm (**1c**), 363 nm (**1d**), 367 nm (**1e**), 364 nm (**1f**)

Figure 3.9 Visible fluorescence emission response under blacklight of **1a-f** 10 μM in THF.

3.2.2 Photophysical property study of 1, 4-dihydropyridines tricarboxylate (2a-e)

The photophysical properties of the compounds DHP **2a-e** were studied in THF by UV–vis and fluorescence spectroscopy. The absorption and emission spectra were similar to those observed in DHP triester cases. Their UV–vis spectra with the concentration of 100 µM, exhibited the absorption wavelengths in the range of 356 to 363 nm, with the hypsochromic shift around 12 -25 nm, comparing to those of triesters (**Figure 3.10**). Moreover, the UV–vis spectrum of each DHP **2a-c** consists of the strong band in the region between 279 and 287 nm, probably due to its *N*-substituted aryl moiety. The fluorescence spectra of this DHP series are recorded from 380-550 nm, in which the maximum wavelengths located in the range of 402 to 427 nm (**Figure 3.11**). In the case of DHP **2d**, due to its high absorpbance, DHP **2d** showed strong emission band (over 1000 a.u.).
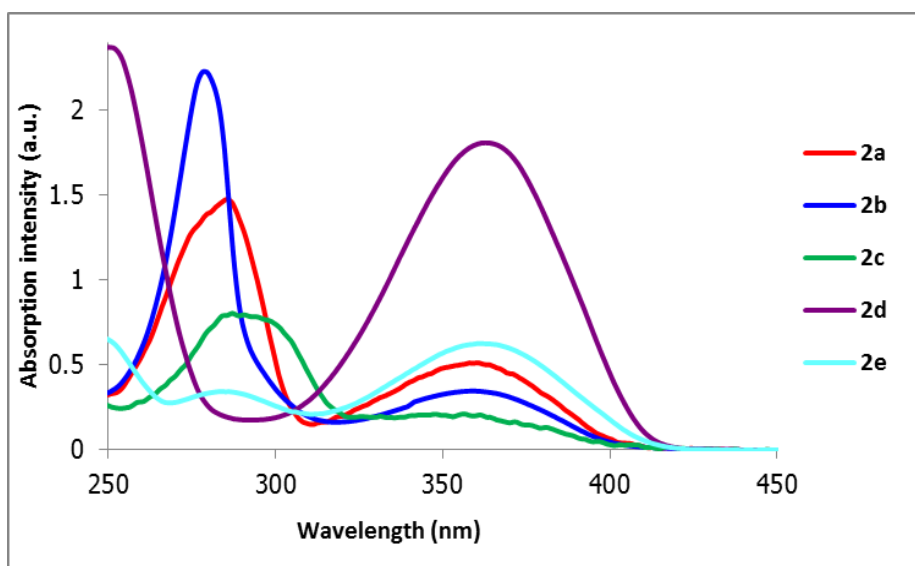

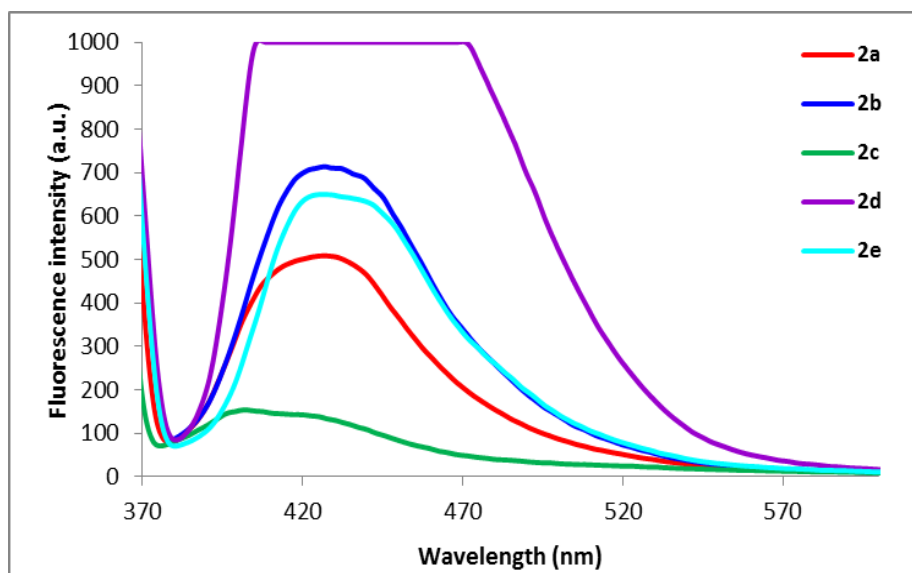**Figure 3.10** Absorption spectra of compounds **2a-e** 100 µM in THF.

Figure 3.11 Fluorescence spectra of compounds **2a-e** 1 μM in THF.

Excitation at 361 nm (**2a**), 360 nm (**2b**), 356 nm (**2c**), 363 nm (**2d**), 362 nm (**2e**)

The photophysical properties of DHP **2a-e** were mainly studied in aqueous solution at the concentration of 1 μM. **Figure 3.12** shows the absorption spectra of DHP **2a-e** in pH 8.0 phosphate buffer (PB). The maximum absorption wavelengths (λ_{max}) were observed as the characteristic peaks of DHP ring appearing in the range of 347 to 358 nm corresponding to π-π* transition. The molar extinction coefficient of this transition for **2a-d** were in a range of 4.67×10^3 - 6.74×10^3, but only 4.11×10^2 for **2e**. The difference in the molar extinction coefficient suggests that the presence of phenyl substituent can facilitate the electronic transition within the DHP ring. The strong bands in the range of 280 to 300 nm were found only in the aromatic *N*-substituted DHP **2a-c**, indicating the characteristic peak and the λ_{max} corresponding to the *N*-substituted aryl moiety. The occurrence of electron donating methoxy group on DHP **2b**, the λ_{max} displayed the hypsochromic shift around 7 nm, comparing to DHP as a result of the decreasing in electron delocalized toward the DHP ring. For DHP **2c** the absorption wavelengths displayed at 300 nm, with the bathochromic shift around 12 nm resulted from an electron withdrawing on aromatic ring caused by the increasing of delocalized electron density in the conjugate system.
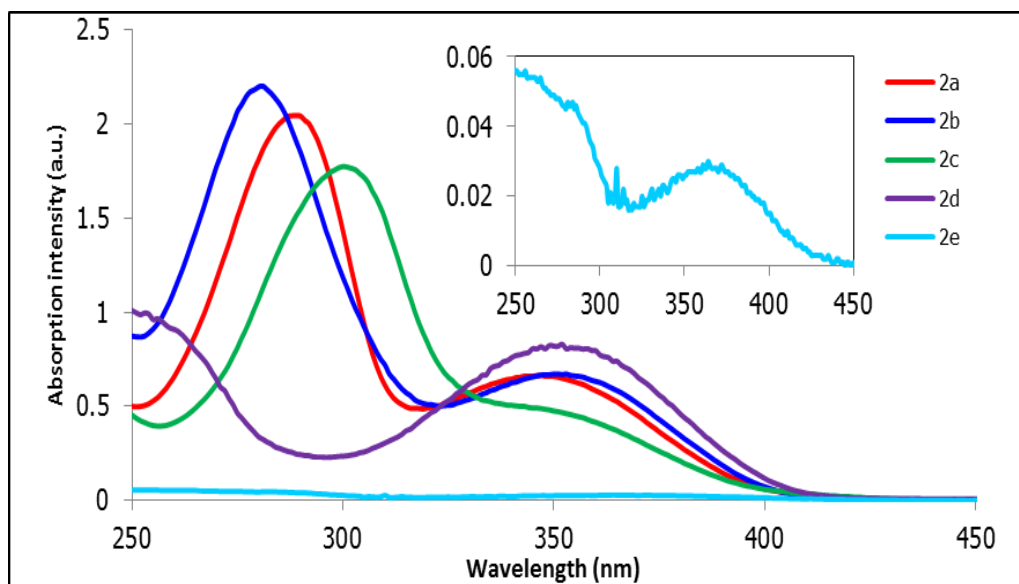
Figure 3.12 Absorption spectra of compounds **2a-e** 100 µM in pH 8.0 PB solution.

The emission spectra of the DHP **2a-e** fluorophores were determined by scanning in the range of 370-600 nm. The maximum emission wavelengths of the DHP fluorophores appeared in the range of 432 to 445 nm (**Figure 3.13**). The λ_{max} of the emission spectra in the aqueous media are correspondingly similar to those in THF. The bathochromic shifts of DHP tricarboxylate around 12-25 nm may result from the stabilizing effect of water to the excited state of DHP tricarboxylate.

The fluorescence quantum efficiencies (Φ_F) of DHP derivatives were measured pH 8.0 in PB solution (A<0.1) at room temperature by using quinine sulfate ($\Phi_F = 0.54$) as a standard. Their fluorescent quantum efficiencies were in the range of 0.07-0.23 in aqueous media. The emission efficiency in dilute solution largely depends on the molecular structure. The lower quantum yield of **2a-d** comparing with **2e** confirms that the benzene ring can stabilize the DHP excited state. Hence, the lower stability of **2e** excited state can lead to faster radiative decay process which in turn gives the higher quantum efficiency. As DHP **2b** possessed an electron donating methoxy group on aromatic ring, it showed a better Φ_F of 0.14 comparing to DHP **1a** and DHP **1c** fluorophores. The different emission behavior of these compounds indicated the dependence of fluorescent efficiency on the molecular structure DHP.

The photophysical properties of DHP **2f** could not be investigated since due to

its relatively low solubility in the condition used. The visible response were significant, their response was detected in the concentration 100 μM (**Figure 3.14**).
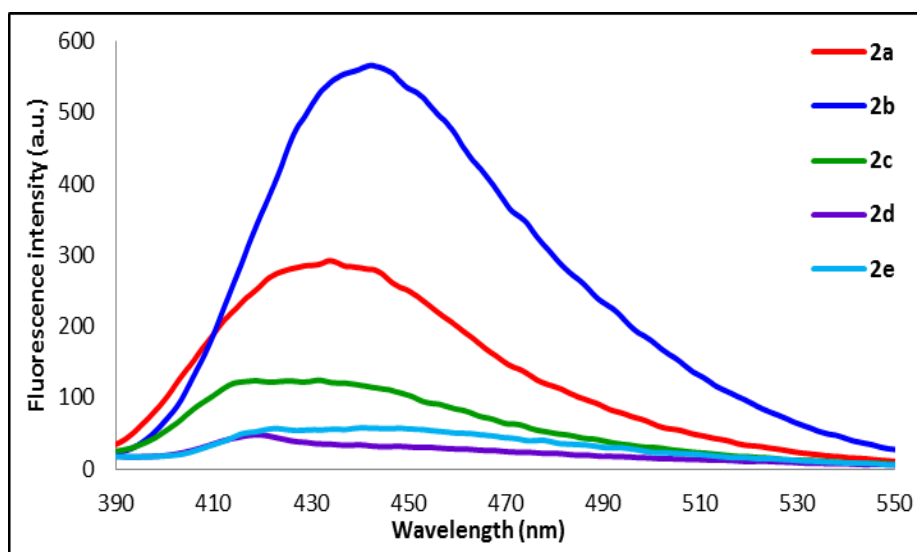

Figure 3.13 Fluorescence spectra of compounds **2a-e** 1 μM in pH 8.0 PB solution. Excitation at 352 nm (**2a**), 347 nm (**2b**), 353 nm (**2c**), 357nm (**2d**), 358 nm (**2e**)
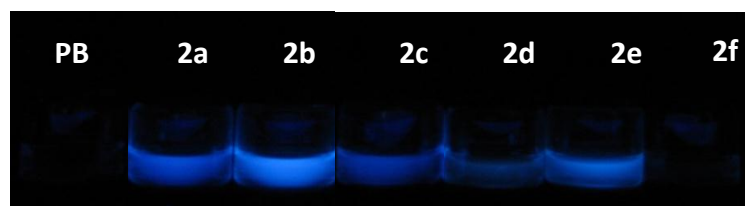

Figure 3.14 Visible fluorescence emission response under blacklight of **2a-e** 1 mM in pH 8.0 PB solution.

Table 3.2 Photophysical properties of compounds **2a-e** in pH 8.0 PB solution

DHP	R	Absorption		Fluorescence	
		λ_{max} (nm)	ε (M^{-1} cm^{-1})	λ_{max} (nm)	$\Phi_f{}^a$
2a	Ph	288	1.8×10^4	435	0.08
		347	6.0×10^3		
2b	*p*-MeO-Ph	281	2.2×10^4	443	0.14
		352	6.7×10^3		
2c	*p*-I-Ph	300	1.7×10^4	432	0.07
		353	4.7×10^3		
2d	Bn	357	6.4×10^3	439	0.09
2e	*n*-Bu	358	4.1×10^2	445	0.23

^{a}Quinine sulfate in 0.1 M H$_2$SO$_4$ ($\Phi_f = 0.54$) was used as the reference.

Excitation at 352 nm (**2a**), 347 nm (**2b**), 353 nm (**2c**), 357 nm (**2d**), 358 nm (**2e**)

3.2.3 Solvent effect on the photophysical property of 1,4-dihydropyridines

The DHP **1** was insoluble in water and thus its absorption and emission spectra were acquired from its THF solution. All DHP **2** were good soluble in water and THF, except for DHP **2f** that could be partially dissolved in water. Accordingly the photophysical properties of DHP **1** and **2** in different solvents were investigated. The tricarboxylic acid (DHP **2)** in THF gave the maximum absorption and emission wavelength in the range of 356-363 and 402-427 nm, respectively. In pH 8.0 PB solution, DHP **2** was found to fluorophores exhibited absorption and emission peak around 347-358 and 432-445 nm, respectively. As the absorption and emission spectra of DHP **1** and **2** in THF were not significantly different, it is likely that their energy levels in ground state and excited state are quite similar. Furthermore, compound DHP **2** display a hypsochromic shift about 14 nm in the pH 8.0 PB

solution. This observation may be explained by the possibility that excited state of DHP **2** mostly exists in the carboxylate form which can be stabilized in the basic aqueous system.

In the case of the triester DHP **1b** in THF, the molar extinction coefficient and quantum efficiency were measured to be 6.2 x 10^3 $M^{-1}cm^{-1}$ and 0.41 at 366 nm, respectively. On the other hand, the tricarboxylic acid DHP **2b** displayed the molar extinction coefficient in THF and in pH 8.0 PB solutions around 3.2 x 10^3 $M^{-1}cm^{-1}$ and 6.7 x 10^3 $M^{-1}cm^{-1}$, respectively with the quantum efficiencies of 0.33 in THF and 0.14 in phosphate buffer. All physical properties of the methoxy phenyl *N*-substituted DHP derivatives are summarized in **table 3.3**.

Table 3.3 Photophysical properties of compound **1b** and **2b** in THF and pH 8.0 PB solutions

DHP	Solvent	Absorption		Fluorescence	
		λ_{max} (nm)	ε (M^{-1} cm^{-1})	λ_{max} (nm)	Φ_f^a
1b	THF	289	9.3×10^3	431	0.41
		366	6.2×10^3		
2b	THF	280	8.3×10^3	427	0.33
		360	3.2×10^3		
2b	pH 8.0 PB solution	281	2.2×10^4	442	0.14
		352	6.7×10^3		

3.3 Metal ion sensor

3.3.1 Fluorescence emission response against metal ions

Since compound **2b** has high extinction coefficient and quantum efficiency, **2b** showed the highest blue emission appearance, and it was therefore selected for further investigation in sensing applications. The fluorescent responses of **2b** (1 µM) towards 14 metal ions (Na^+, Ca^{2+}, Zn^{2+}, Hg^{2+}, Co^{2+}, Ni^{2+}, Cu^{2+}, Ag^+, Fe^{2+}, Fe^{3+}, Cd^{2+}, Al^{3+}, Mn^{2+} and Pb^{2+}) were evaluated in aqueous PB solutions. Upon the addition of the metal ion (50 equiv) into a solution of **2b**, only Hg^{2+} caused a significant fluorescence quenching effect observed at 30 minutes (**Figure 3.15**). This highly selective fluorescence quenching was also observable by naked-eye (**Fig. 3.16**).
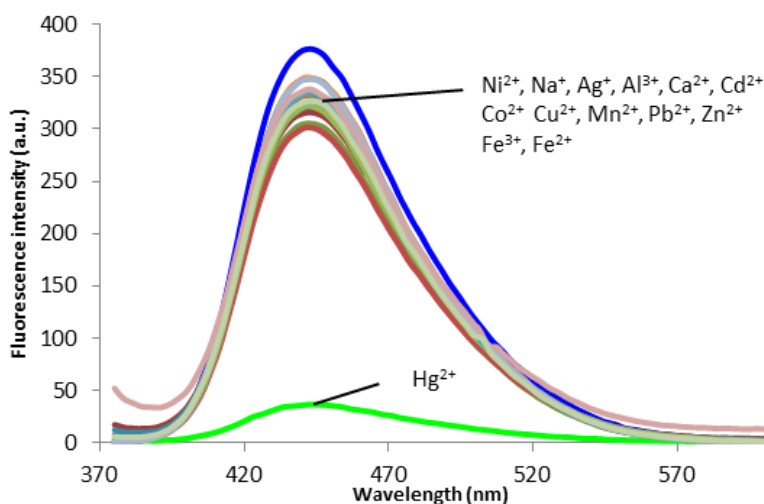
Figure 3.15 Fluorescence quenching profile of **2b** (1 µM)**,** 30 minutes after addition of each metal ion (50 µM) in PB solution pH 8.0 (λ_{ex} = 352 nm). Acetate salts were used except for $CdSO_4$, $FeSO_4$ and $Fe(NO_3)_3$.
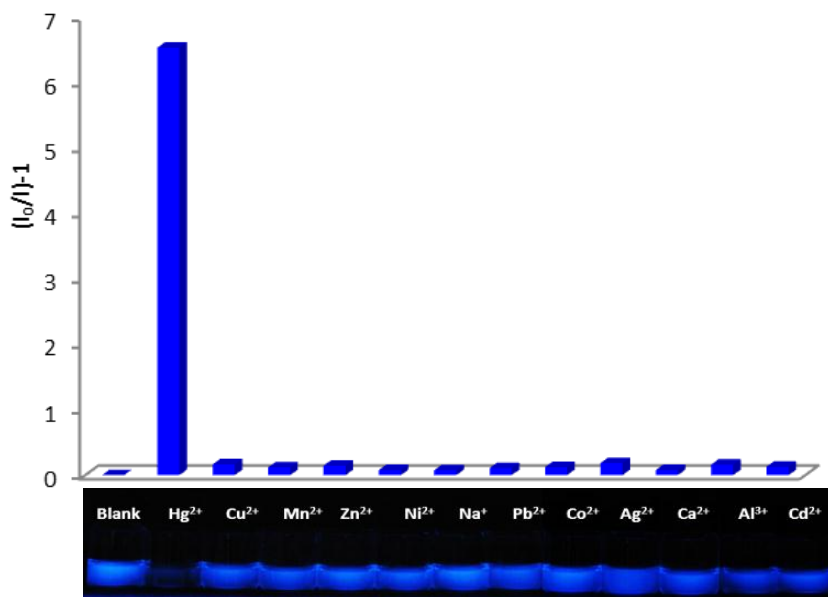
Figure 3.16 Fluorescence response (I_0/I)-1of **2b** (1 μM)**,** 30 minutes after addition of metal ion (50 μM) in PB solution pH 8.0 (λ_{ex} = 352 nm). The photograph shows fluorescence appearance under black light of **2b** (0.1 mM) upon addition of metal ion (1 mM).

3.3.2 Time-dependent quenching of 2b to Hg^{2+}

During the preliminary sensing study, we found that the fluorescence quenching by Hg^{2+} proceeded gradually, therefore, the fluorescence intensity was monitored for 60 minutes (**Figure 3.17**). The kinetic results showed that the intensity decreased and reached the minimum after 30 minutes. Since the quenching process was relatively slow, we hypothesized that it was a result of a chemical reaction rather than the fast dynamic or static quenching mechanism.
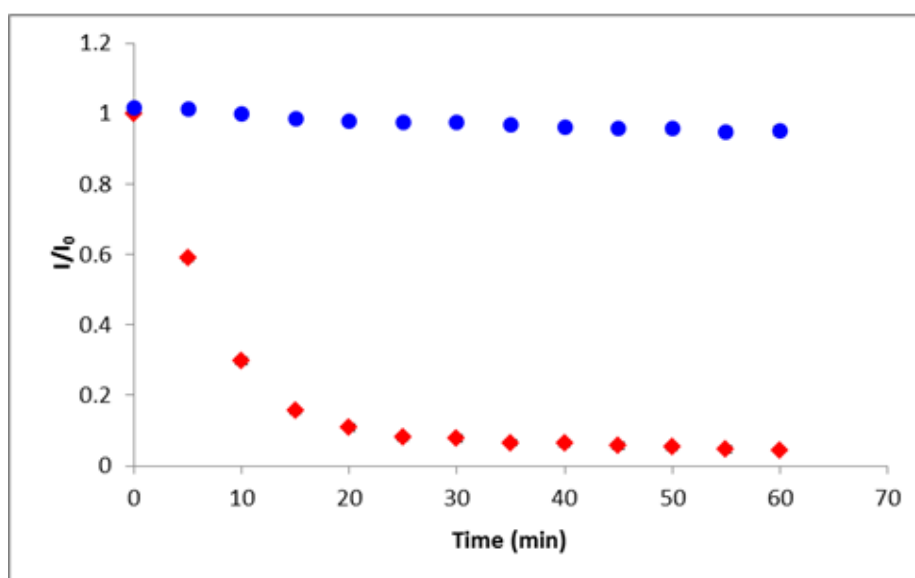

Figure 3.17 Fluorescence quenching profile of **2b** (1 µM) 0 to 60 min after addition of Hg^{2+} (♦) 0 and (●) 50 equiv in pH 8.0 PB solution (excitation at 352 nm, emission at 442 nm).

3.3.3 UV–vis spectral responses of 2b to Hg^{2+}

In order to gain insightful information about the quenching mechanism, time tracking UV–vis spectroscopy of 2b with 50 equiv of Hg^{2+} was carried out from 1 to 45 minutes. As a result, the absorbance spectrum of **2b** was altered significantly with time. The aromatic band at 281 nm gradually dropped, while the DHP band at 352 nm blue shifts by 17 nm confirming the possibility of structural change in the DHP ring (**Figure 3.18**). This hypsochromic shift is probably caused by the aromatization of the DHP ring to a pyridine ring, as the new band appears in the same area as the characteristic band of a pyridinium ring (around 325-342 nm).
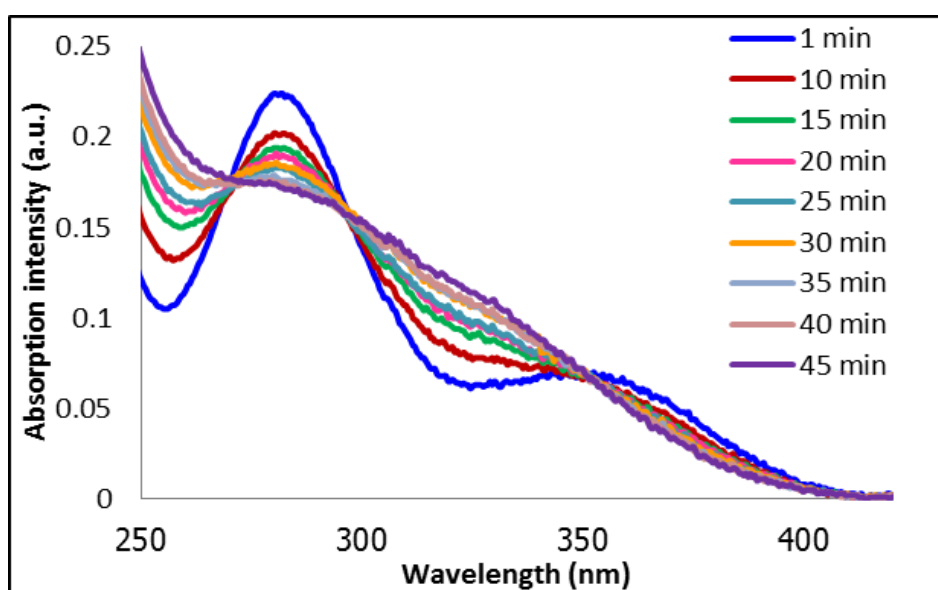

Figure 3.18 UV–vis spectra of **2b** in pH 8.0 PB solution (24 µM) 1 to 45 min after adding Hg^{2+} 50 equiv.

3.3.4 ^{1}H NMR experiment

^{1}H NMR experiment was conducted to seek more evidence to support the formation of a pyridine ring from the DHP ring. Due to the solubility limitation, only 1 equiv of Hg^{2+} could be used, and there was no significant change in the ^{1}H NMR spectrum within 30 minutes. After 2 days, the signals of the DHP olefinic and allylic protons at 7.4 and 4.0 ppm disappeared (**Figure 3.19**), signifying the lost of the DHP structure. The signal of methylene protons at 2.2 ppm and the aromatic signal at 7.0

ppm down field shifted to 3.7 and 7.6 ppm, respectively, suggesting that the DHP ring had turned into an electron withdrawing moiety. We thus believe that the DHP ring was oxidized into a pyridinium ring by Hg^{2+} (Scheme 2). The MS spectrum of the product also showed strong signal at $m/z = 332$ (**Figure A.38**) in good agreement with the molecular weight of the proposed pyridinium product **3b**. However, it is not clear to us at this moment for the observation of two ^{1}H NMR signals at 8.9 and 6.8 ppm for the two supposedly equivalent protons of pyridinium ring. The two observed proton signals theoritically fit better with the hydroxy pyridinium compound **4b**, another possible product resulted from the sequence of hydrolysis and oxidation of **3b**. However, only a small peak in the region corresponding to the formula weight of **4b** (m/z = 347) appeared in the MS spectrum (**Figure A.38**). Unfortunately, our attempt to isolate the product for better defined characterization has not yet been successful due to the instability of this product.
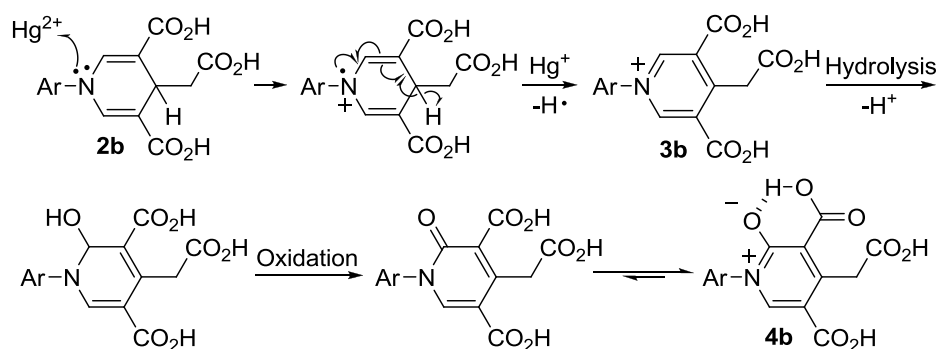
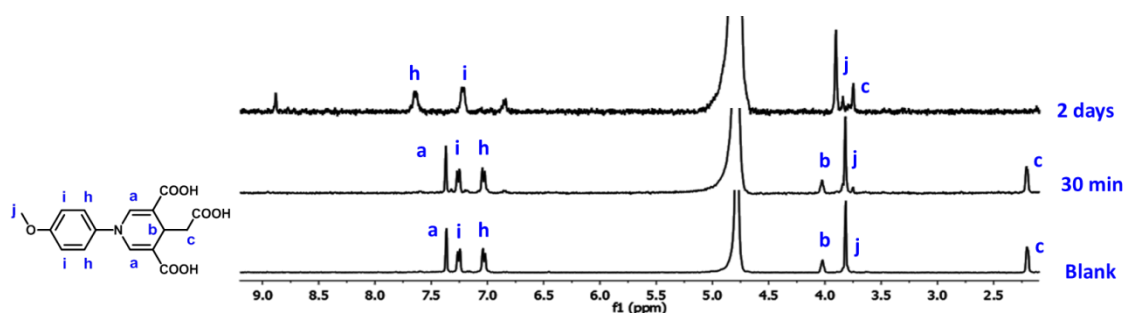**Scheme 3.2.** Proposed mechanism for the formation of **3b** and **4b**.

Figure 3.19 ^{1}H NMR spectra of **2b** in D_2O, 30 minutes to 2 days after adding of 1 equiv Hg^{2+}.

3.3.5 Fluorescence titration of 2b to Hg^{2+}

For further investigation of the interaction between sensor **2b** and Hg^{2+} ion, the fluorescent response of **2b** against different Hg^{2+} ion concentrations (1 to 100 μM) were individually operated in aqueous solution of **2b** (1 μM) (**Figure 3.20**). As the concentration for Hg^{2+} ions increased, the gradual quenching of **2b** started and completed from the ratio of 70 equiv of Hg^{2+} ion. The results show that the ratio of mercury ion to substrate has an effect to rate of the mercury-induced fluorescent quenching of **2b**. The long time mercury-induced fluorescent quenching of **2b** was probably from of structural change in DHP derivative. Furthermore, the addition of a strong chelating reagent, such as EDTA, did not regain the fluorescence signal (**Figure 3.24**). The result confirmed that the quenching was not caused by the complexation between **2b** and Hg^{2+} ion but by the chemodosimeter type Hg^{2+} induced structural transformation. The detection limits of **2b** for the analysis of Hg^{2+} ions were determined in the range of <1 μM from the titration spectra, which can be calibrated from the titration curve of **Figure 3.20**. From the fluorescence titration profiles, the association constant for **2b**·Hg^{2+} in water was calculated as 78,300 M^{-1}, also by a Stern–Volmer plot (**Figure 3.20 inset**).

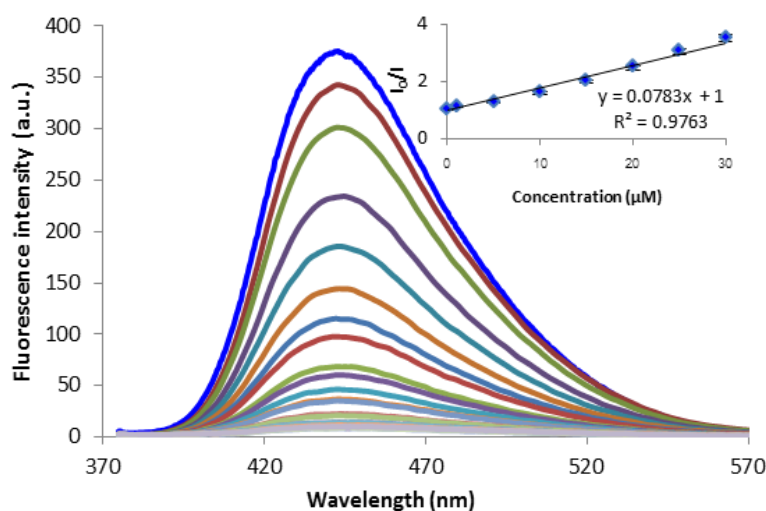**Figure 3.20** Fluorescence change of 2b (1 μM) with the addition of Hg^{2+} (0 to 100 equiv) in pH 8.0 PB solution at 30 minutes (λ_{ex} = 352 nm).

3.3.6 Effect of pH

In addition, the effect of pH on the fluorescence emission of solution **2b** in the absence and presence of Hg^{2+} (50 equiv. to **2b**) was also explored. As shown in **Figure 3.21**, the signal of DHP **2b** was gradually increased since the pH values is 6 and almost strong fluorescence between pH 8-9, whereas, its fluorescence was quenched when the pH value is 6. In the presence of Hg^{2+}, the fluorescence intensity of solution **2b** decreased dramatically between pH 6 and 10. These results demonstrate that Hg^{2+} induced transformation by sensor **2b** can appropriate for used as Hg^{2+} sensor at pH 6-10.
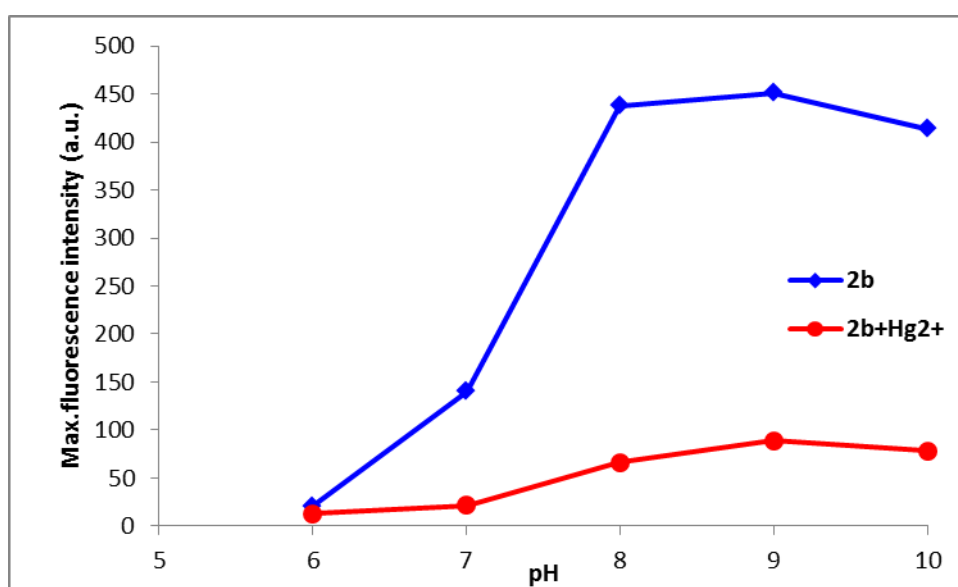
Figure 3.21 Effect of pH on fluorescence quenching response of **2b** in PB solution pH 8.0 without (♦) and with (●) Hg^{2+} 50 μM.

3.3.7 Competitive experiments over other metal ions

The selectivity toward Hg^{2+} ions was further ascertained by the competitive experiment employed with addition of the 100 equiv of competing metal ions to the $2b \cdot Hg^{2+}$ mixtures. The interference can be determined in bar diagram from plotting of $(I_{Hg} - I_0)/(I - I_0)$ and types of metal ion. Where I_0 = Maximum fluorescent intensity of $2b$ without metal ions, I_{Hg} = Maximum fluorescent intensity of $2b$ with Hg^{2+}, I = Maximum fluorescent intensity of $2b$ with Hg^2 and other metal ions. Therefore, without the interference from other metal ion, y axis is equal to 1. The fluorescence quenching efficiency of Hg^{2+} ions were affected a little in presence of Ni^{2+} and Na^+ (**Figure 3.22**), it is result from Ni^{2+} and Na^+ disturb the reaction from Hg^{2+}. The interference from Fe^{2+} and Fe^{3+} was found by Lee and Lohani. [15] As a result of the may be from absorbance of Fe^{3+} has a considerable interference effect on the excitation of the fluorophore with a short excitation wavelength range in UV light. In this case the absorbance of Fe^{3+} itself is much larger than that of the absorbance of the $2b$, resulted in a decrease of fluorescent intensity.
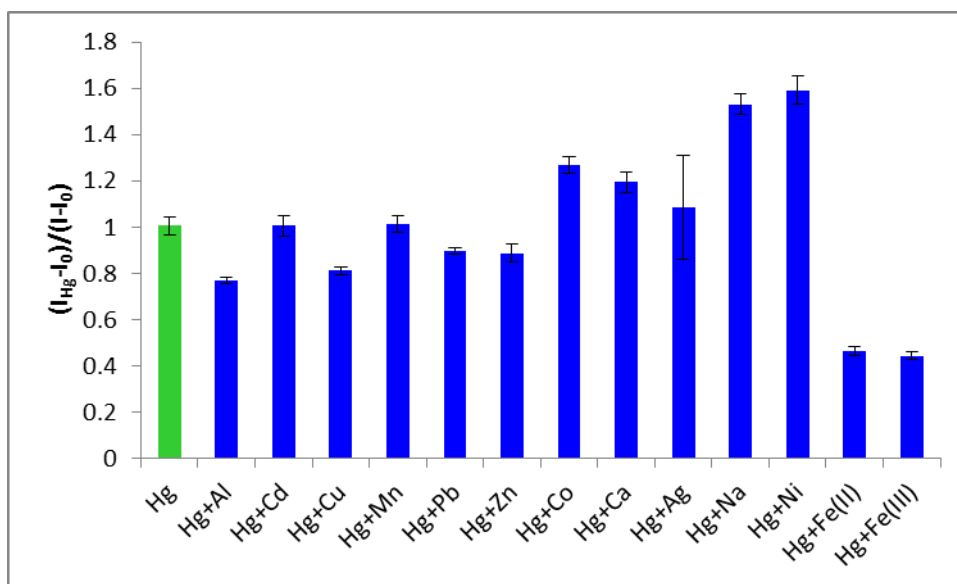

Figure 3.22 Competitive experiments in the $2b \cdot Hg^{2+}$ system with interfering metal ions. $[2b]$ = 1 μM, $[Hg^{2+}]$ = 10 μM, and $[M^{n+}]$ = 100 μM in pH 8.0 PB solution.

3.3.8 Job's method

Job's method of continuous variation was applied to determine the stoichiometry of **2b** and Hg^{2+}. To implement Job's Method experimentally, one prepares a series of solutions containing a fixed total number of moles of **2b** and Hg^{2+}, but in which their mole fractions are varied. An observable that is proportional to complex formation is plotted against the mole fractions of these two components. The maximum on the plot corresponds to the stoichiometry of the two species. A Job's plot, which exhibits a maximum at a 0.5 mol fraction, indicates that the structural change stoichiometrically and most efficiently occurred at the mixture ratio of 1:1 (**Fig 3.23**).
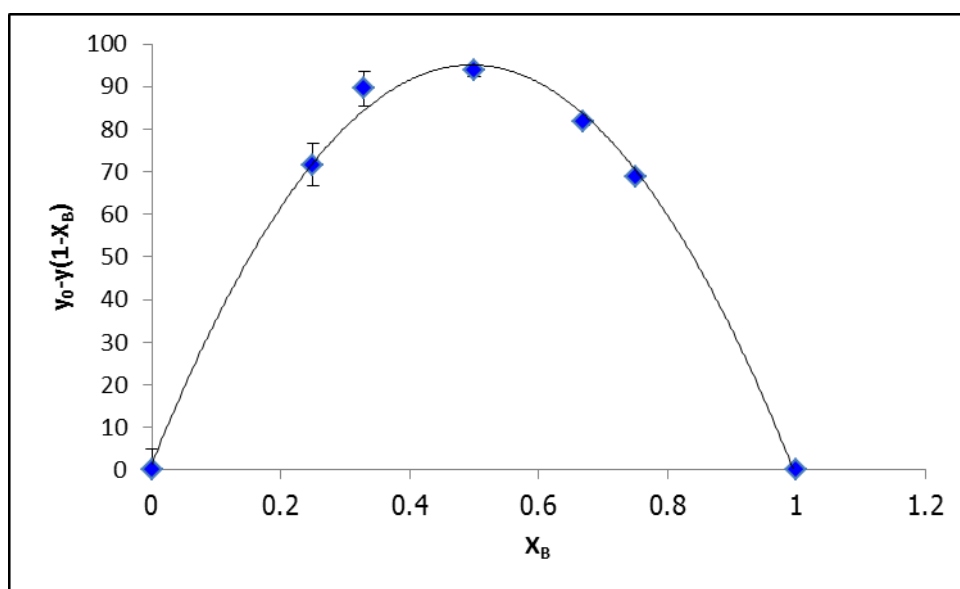
Figure 3.23 Job's plot of a **2b** in 1:1 stoichiometry with Hg^{2+}.
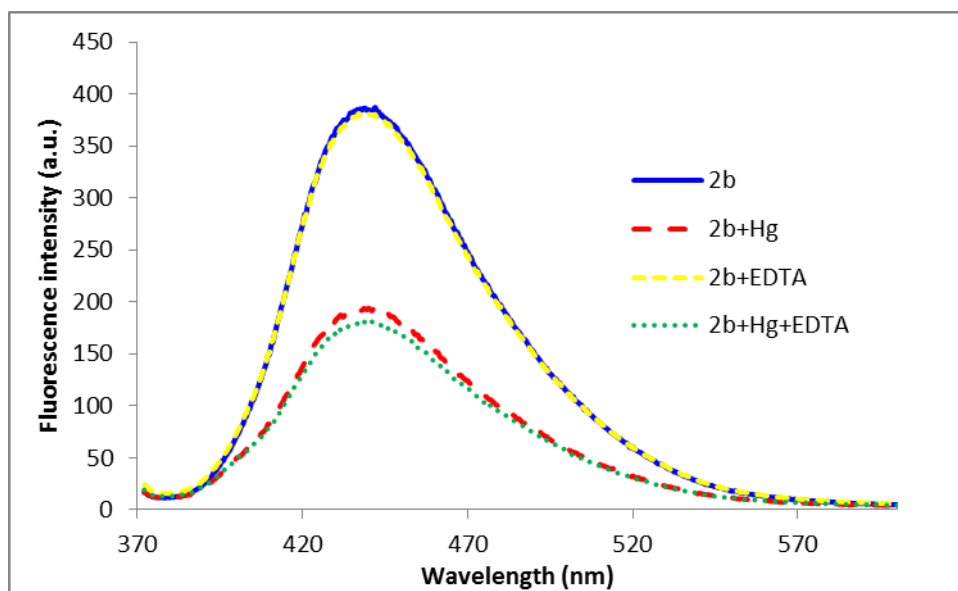
Figure 3.24 Emission spectra of **2b** (1µM) upon addition of Hg^{2+} (20 µM) and EDTA (250 µM) in pH 8.0 PB solution.

3.4 Surfactant sensor

We used compound **2a** for the sensing materials in a surfactant study. **Figure 3.25** shows the fluorescence spectra of DHP **2a** in the existence of surfactants. In these experiments, three anionic surfactants (SDS, SDC and SDBS), three cationic surfactants (TTAB, DTAB and HTAB) and three non-ionic surfactants (Tween 20, Triton X-100, Brij 58) were selected due to the viability and reliability of their literature Critical Micellar Concentrations (CMC) data.

In the presence of the surfactant at low concentration (0.1 mM), there was no change in an emission intensity of DHP **2a**. With slightly higher concentration (1 mM), only SDBS could considerably increase the emission intensity of DHP **2a**.
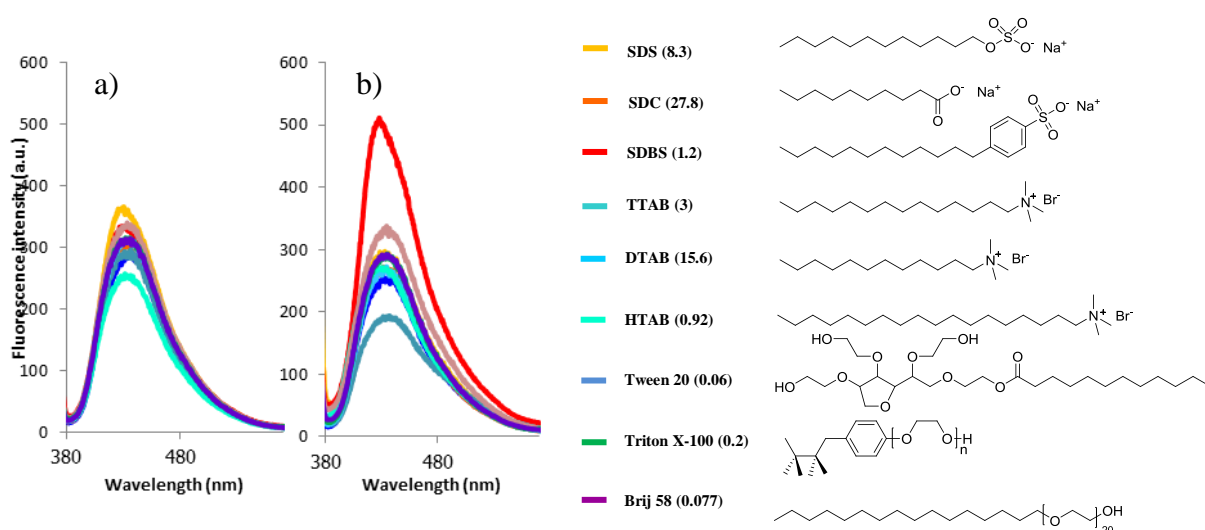
Figure 3.25 Fluorescent change of DHP **2a** in the presence of surfactant a) 0.1 mM and b) 1 mM. (The structures of all surfactants and CMC values are shown on the right.)
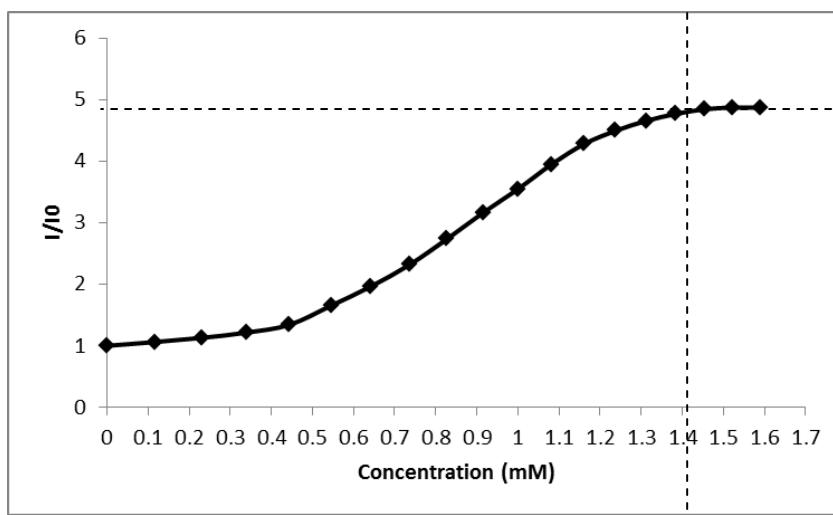
Figure 3.26 Variation of fluorescence intensity at λ_{max} 431 nm of DHP **2a** (1μM) as a function of SDBS concentration.

Addition of a little more SDBS (1.2 mM) led to an enhancement in the intensity (27% enhancement from 1 mM to 1.2 mM). Therefore we monitored various fluorescence intensity of λ_{max} 431 nm of DHP **2a** by varying the SDBS concentration (0 – 1.6 mM). As shown in **Figure 3.26**, the fluorescence intensity of the most intensive peak at λ_{max} 431 nm was plotted against the surfactant concentration. The resulting fluorescence intensity increased upon the addition of SDBS and started to become stable at the point above CMC (1.2 mM). According to this result, 1.4 mM was confirmed to be the end of the increasing point and in a good agreement with the literature values of 1.2 mM. This method might be useful in terms of the determination of CMC.

3.5 Explosive sensor

Moreover, DHP **2a** and **2b** were demonstrated in nitroaromatic sensing study. Two types of nitroaromatics were selected for the study; the nitrotoluene (NT) derivatives {4-nitrotoluene (4-NT), 2,4-dinitrotoluene (2,4-DNT) and 2,4,6-trinitrotoluene (TNT)} and nitrophenol (NP) derivatives (3-nitrophenol (3-NP), 2,4-dinitrophenol (2,4-DNP) and 2,4,6-trinitrophenol (TNP) or Picric acid) (**Figure 3.27**).
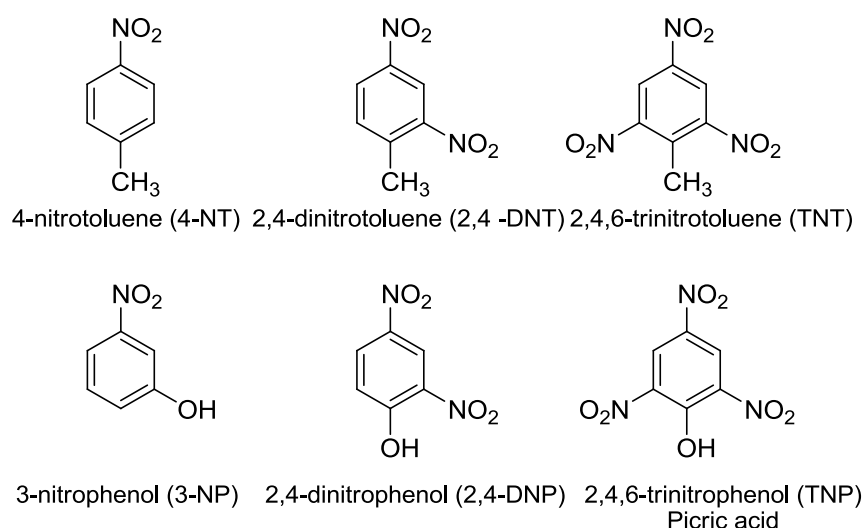

4-nitrotoluene (4-NT) 2,4-dinitrotoluene (2,4 -DNT) 2,4,6-trinitrotoluene (TNT)

3-nitrophenol (3-NP)   2,4-dinitrophenol (2,4-DNP) 2,4,6-trinitrophenol (TNP) Picric acid

Figure 3.27 Structures of nitroaromatic compounds.

The emission experiments of DHP **2a** and **2b** responding to all NTs and NPs were executed. Interestingly, DHP **2a** distinguished selectively NT cases (**Figure 3.28a**), and DHP **2b** could discriminate NP derivatives (**Figure 3.28b**). The emission intensity of DHP **2a** decreased in an approximate 10%, 25% and 40% quenching by 4-NT, 2,4-DNT and TNT, respectively with the well agreement of more nitro groups less emission. In the case of DHP **2b**, the differences in responses between 3 NPs are significant; NP approximately 30% enhancement for TNP, 4% enhancement accompanying with red shift about 5 nm for 2,4-DNP, and 30% quenching for 3-NP. The fluorescence intensity of DHP **2b**, on the contrary to that of the DHP **2a** results, was elevated as the number of nitro group increased. It should be repeatedly

emphasized that the change in an emission behavior of DHP **2a** and **2b** can be used for fluorescent sensors of NTs and NPs, respectively.
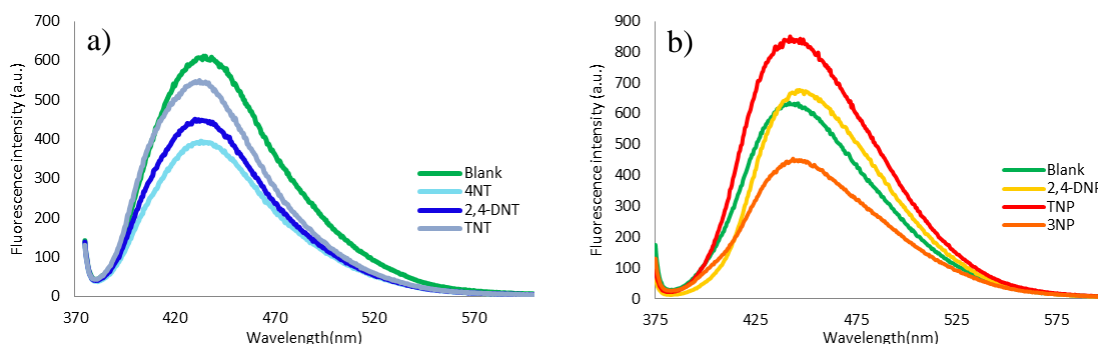

Figure 3.28 Fluorescent quenching profiles of DHP a) DHP **2a** and b) DHP **2b** in the presence of nitroaromatic compounds.

3.6 Protein/metal sensor

Additionally, bovine serum albumin protein (BSA) and metal ions was employed to study their effects on the fluorescence behavior of this DHP **2a**. According to the preliminary results, BSA could be used as the fluorescent signal enhancing agent to increase the sensitivity of DHP **2a**. The fluorescence intensity was increased two-fold higher in the presence of BSA. In **Figure 3.29a**, Fe^{n+} have a quenching effect more   than other metal ions and the addition of 10 µM Fe^{2+} extremely decreases fluorescence signal. On the other hand, 10 µM Fe^{3+} have no effect as shown in **Figure 3.29b**.
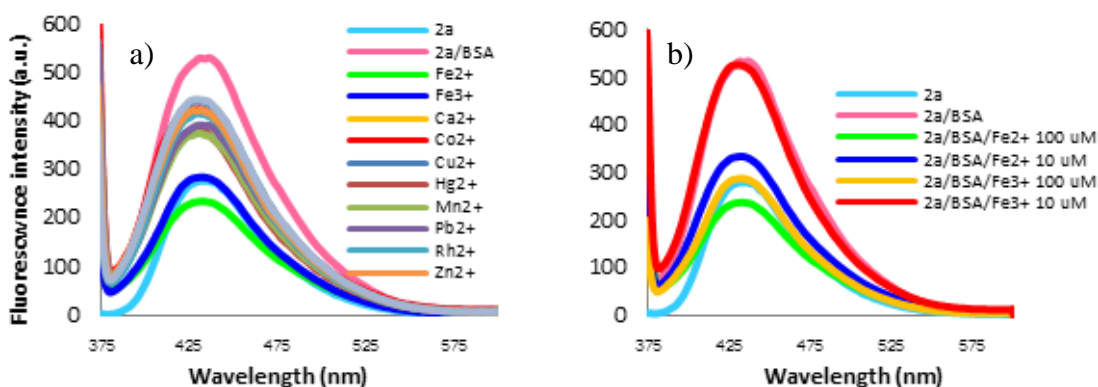
Figure 3.29 Fluorescence spectra of DHP **2a** (1 µM) in the presence of BSA (15 µM) a) added various metal ions (100 µM) and b) added Fe^{2+}, Fe^{3+} at 10 and 100 µM in pH 7.4 PBS 10 mM, excitation at 347 nm.

      The fluorescent quenching results can be explained by the possible mechanism from **Figure 3.30**. The reason that DHP **2a** gave a fluorescence enhancement in the presence of bovine serum albumin (BSA) was probably due to the result of the insertion of DHP **2a** into the protein pocket. After Fe^{n+} was added into the mixture, fluorescent intensity turned back to initial emission of DHP **2a**. This result that DHP **2a** in each protein pocket was replaced by the added Fe^{n+}, confirmed the fact that selectivity of BSA to Fe^{n+} was more than that to the DHP.
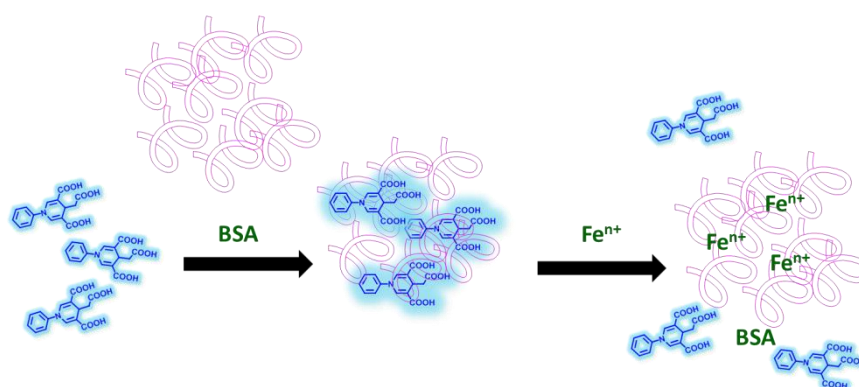
Figure 3.30 Possible quenching mechanism of DHP **2a**/BSA by Fe^{n+}.

CHAPTER IV

CONCLUSION

4.1 Conclusion

In conclusion, a series of 1,4-dihydropyridine (DHP) were successfully synthesized. The synthesis relied on the cyclotrimerization of β-amino acrylate by treatment of $TiCl_4$ at room temperature. These DHP derivatives were useful for sensing applications in aqueous media due to their water solubility and good fluorogenic responses. The comparison of photophysical properties of the compounds in pH 8.0 phosphate buffer solution indicated that the substituent of nitrogen atom was responsible for the maximum wavelength (λ_{max}) and quantum efficiency (Φ_f). One of these compounds, bearing the *p*-methoxyphenyl *N*-substituted group (**2b**), showed specific fluorescent quenching with mercuric ion (Hg^{2+}). The decrease of fluorescence signal was proportional to Hg^{2+} concentration with high quenching efficiency (K_{sv} = 78,300 M^{-1}) providing a detection limit of 0.2 μM. The quenching process involves an oxidation of the DHP into a pyridinium ring specifically induced by Hg^{2+} that brought about its remarkable selectivity over other metal ions. Moreover, **2b** was demonstrated in nitroaromatic sensing study. The different fluorescence behavior of compound **2** in THF by nitroaromatic explosives, such as trinitrotoluene, 4-nitrotoluene and 2,4-nitrotoluene might be useful for the explosive detection. Additionally, the fluorescent signal of **2a** was enhanced selectively by sodium dodecylbenzene sulfonate (SDBS). The increasing end point (1.4 mM) of the graph plotted between fluorescence intensity and the surfactant concentration is in good agreement with the literature CMC value of SDBS (1.2 mM). Bovine serum albumin protein (BSA) and metal ions was employed to study their effects on the fluorescence behavior of **2a**. The fluorescent signal of **2a** was greatly enhanced by BSA protein. This enhanced fluorophore/BSA system demonstrated the selective fluorescence quenching upon the addition of 10 μM of Fe^{2+} presenting a potentially sensitive bio-conjugate sensor for ferrous ion analysis. Lastly, fluorescent chemosensor for Hg^{2+} was successfully investigated. Fluorescence enhancements of DHP by BSA protein are useful for increase the sensitivity of Fe^{2+} and Fe^{3+} analysis. DHP derivatives used to find the CMC value of SDBS and provided a significant discriminating ability to nitroaromatic compounds.

4.2 Suggestion for future work

The future work should focus on fluorescence sensing applications of these DHP derivatives for real time monitoring system to detect mercury ions in living cells.

REFERENCES

[1]   Hantzsch, A. Uber die synthese pyridinartiger verbindungen aus acetessigather und aldehyammoniak. *Ann. Chem.* 215 (1882): 1–82.

[2]   Fukuzumi, S.; Koumitsu, S.; Hironaka, K.; Tanaka, T. Energetic comparison between photoinduced electron-transfer reactions from NADH model compounds to organic and inorganic oxidants and hydride-transfer reactions from NADH model compounds to *p*-benzoquinone derivatives. *J. Am. Chem. Soc.* 109 (1987): 305-316.

[3]   Mochizuki, A.; Fukuoka, T.; Kanada, M.; Kinjou, N.; Yamamoto, T. Development of photosensitive porous polyimide with low dielectric constant. *J. Photopolym Sci. Technol.* 15 (2002): 159-165.

[4]   Yamamoto, T.; Ohno, S.; Niwa, S.; Tokumasu, M.; Hagihara, M.; Koganei, H.; Fujita, S.; Takeda, T.; Saitou, Y.; Iwayama, S.; Takahara, A.; Iwata, S.; Shoji, M., Asymmetric synthesis and biological evaluations of (+)- and (-)-6-dimethoxymethyl-1,4-dihydropyridine-3-carboxylic acid derivatives blocking N-type calcium channels. *Bioorg. Med. Chem. Lett.* 21 (2011): 3317-3319.

[5]   Briede, J.; Daija, D.; Bisenieks, E.; Makarova, N.; Uldrikis, J.; Poikans, J.; Duburs, G. Effects of some 1,4-dihydropyridine Ca antagonists on the blast transformation of rat spleen lymphocytes. *Cell Biochem. Funct.* 17 (1999): 97-105.

[6]   Janis, R. A.; Triggle, D. J. New developments in Ca^{2+} channel antagonists. *J. Med. Chem,* 25 (1983): 775–785.

[7]   Manhold, R.; Jablonka, B.; Voigdt, W.; Schoenfinger, K.F.; Schravan, K. Calcium- and calmodulin-antagonism of elnadipine derivatives: comparative SAR. *Eur. J. Med. Chem.* 27 (1992): 229–235.

[8]   Striessnig, J.; Grabner, M.; Mitterdorfer, J.; Hering, S.; Sinnegger, M. J.; Glossmann, H. Structural basis of drug binding to L Ca^{2+} Channels. *Trends Pharmacol. Sci.* 19 (1998): 108–115.

[9]   Fasani, E.; Fagnoni, M.; Dondi, D.; Albini, A. Intramolecular electron transfer in the photochemistry of some nitrophenyldihydropyridines. *J. Org. Chem.* 71 (2006): 2037-2045.

[10]   Jimenez, A. J.; Fagnoni, M.; Mella, M.; Albini, A. Photoinduced Electron and Energy Transfer in Aryldihydropyridines. *Org. Chem. 74* (2009): 6615–6622.

[11]   Fasani, E.; Dondi, D.; Ricci, A.; Albini, A. Photochemistry of 4-(2-nitrophenyl)-1,4-dihydropyridines. Evidence for electron transfer and formation of an intermediate. *Photochem. Photobiol.* 82 (2006): 225-230.

[12]   Pavez, P.; Encinas, M. V. Photophysics and photochemical studies of.1,4-dihydropyridine derivatives. *Photochem. Photobiol.* 83 (2007): 722-729.

[13]   Yamaoka, T.; Yokoyama, S.; Omote, T.; Naitoh, K.; Yoshida, K. Photochemical behavior of nifedipine derivatives and application to photosensitive polyimide. *Polymeric Materials for Microelectronic Applications: Science and Technology.* 579 (1994): 253-270.

[14]   Chen, B.; Peng, M. L.; Wu, L. Z.; Zhang, L. P.; Tung, C. H.   Switch between charge transfer and local excited states in 4-aminophenyl-substituted Hantzsch 1,4-dihydropyridine induced by pH change and transition metal ions. *Photochem. Photobiol. Sci.,* 5 (2006): 943-947.

[15]   Lohani, C. R.; Lee, K. H. The effect of absorbance of Fe^{3+} on the detection of Fe^{3+} by fluorescent chemical sensors *Sens. Actuator B-Chem.* 143 (2010): 649–654.

[16] Fang, C.; Peng, M.; Li, G.; Tian, J.; Yin, D. New functions of glucosamine as a scavenger of the lipid peroxidation product malondialdehyde. *Chem. Res. Toxicol.* 20 (2007): 947-953.

[17] Sirijindalert, T.; Hansuthirakul, K.; Rashatasakhon, P.; Sukwattanasinitt, M., Ajavakom, A. Novel synthetic route to 1,4-dihydropyridines from β-amino acrylates by using titanium(IV) chloride under facile conditions. *Tetrahedron* 66 (2010): 5161-5167.

[18] Kikuchi, S.; Iwai, M.; Murayama, H.; Fukuzawa, S. i. Catalytic synthesis of 1,4-dihydropyridine derivatives using scandium(III) triflate. *Tetrahedron Lett.* 49 (2008): 114-116.

[19] Vohra, K. R.; Bruneau, C.; Renaud, J. Lewis Acid Catalyzed Sequential Transformations: Straight forward Preparation of Functional Dihydropyridines. Adv. Synth. Catal. 348 (2006): 2571-2574.

[20] Lakowicz, J. R. Principles of Fluorescence Spectroscopy; 3rd ed.; John Wiley & Sons, Inc, Kluwer, 2006.

[21] Kim, J. S.; Choi, M. G.; Song, K. C.; No, K. T.; Ahn, S.; Chang, S. K. Ratiometric determination of Hg^{2+} ions based on simple molecular motifs of pyrene and dioxaoctanediamide. *Org. Lett.* 9 (2007): 1129–1132.

[22] Jung, H. S.; Kwon, P. S.; Lee, J. W.; Kim, J. I. I.; Hong, C. S.; Kim, J. W.; Yan, S.; Kim, J. S. Coumarin-derived Cu^{2+}-selective fluorescence sensor: Synthesis, mechanisms, and applications in living cells. *Am. Chem. Soc*. 131 (2009): 2008-2012.

[23] Mandal, A. K.; Suresh, M.; Suresh, E.; Mishra, S. K.; Mishra, S.; Das, A. A chemosensor for heavy-transition metal ions in mixed aqueous–organic media. *Sensor Actuat. B-Chem.* 145 (2010): 32–38.

[24] Singh, N.; Kaur, N.; Dunn, J.; MacKay, M.; Callan, J. F. A new fluorescent chemosensor for iron(III) based on the β-aminobisulfonate receptor. *Tetrahedron Lett.* 50 (2009): 953-956.

[25] Xu, Z. C.; Baek, K. H.; Kim, H. N.; Cui, J. N.; Qian, X. H.; Spring, D. R.; Shin, I.; Yoon, J. Zn^{2+}-triggered amide tautomerization produces a highly Zn^{2+}-selective, cell-permeable, and ratiometric fluorescent sensor. *Am. Chem. Soc*. 132 (2010): 601-610.

[26] Mitra, A.; Ramanujam, B.; Rao, C. P. 1-(D-Glucopyranosyl-20-deoxy-20-iminomethyl)-2-hydroxynaphthalene as chemosensor for Fe^{3+} in aqueous HEPES buffer based on colour changes observable with the naked eye. *Tetrahedron Lett.* 50 (2009): 776-780.

[27] Sparano, B. A.; Koide, K. A Strategy for the Development of Small-Molecule-Based Sensors That Strongly Fluoresce When Bound to a Specific RNA. *J. Am. Chem. Soc.* 127 (2005): 14954-14955.

[28] Kim, J. S.; Choi, M. G.; Song, K. C.; No, K. T.; Ahn, S.; Chang, S. K., Chang, S. K. Ratiometric determination of Hg^{2+} ions based on simple molecular motifs of pyrene and dioxaoctanediamide. *Org. Lett.* 9 (2007): 1129–1132.

[29] Harris, H. H.; Pickering, I. J.; George, G. N. The chemical form of mercury in fish. *Science* 301 (2003): 1203– 1203.

[30] Tchounwou, P. B.; Ayensu, W. K.; Ninashvili, N.; Sutton, D. Environmental exposure to mercury and its toxicopathologic implications for public health. *Environ. Toxicol.* 18 (2003): 149– 175.

[31] Renzoni, A.; Zino, F.; Franchi, E. Mercury levels along the food chain and risk for exposed populations. *Environ. Res.*, 77 (1998): 68-72.

[32] Grandjean, P.; Weihe, P.; White, R. F.; Debes, F. Cognitive performance of children prenatally exposed to "Safe" levels of methylmercury. *Environ. Res.* 77 (1998): 165-172.

[33] Takeuchi, T.; Morikawa, N.; Matsumoto, H.; Shiraishi, Y. A pathological study of Minamata disease in Japan. *Acta Neuropathol.* 40 (1962): 40-57.

[34] Nendza, M.; Herbst, T.; Kussatz, C.; Gies, A. Potential for secondary poisoning and biomagnification in marine organisims. *Chemosphere* 35 (1997): 1875-1885.

[35] Johnson, D. W.*;* Lindberg, S. E. The biogeochemical cycling of Hg in forests: Alternative methods for quantifying total deposition and soil emission. *Water, Air, Soil Pollut.* 80 (1995): 1069-1077.

[36] Boening, D. W. Ecological effects, transport, and fate of mercury: A general review. *Chemosphere* 40 (2000): 1335-1351.

[37] Mercury Update: Impact of Fish Advisories. EPA Fact Sheet EPA-823-F-01-011; EPA, Office of Water: Washington, DC, 2001.

[38] Sardans, J.; Montes, F.; Penuelas, J. Determination of As, Cd, Cu, Hg and Pb in biological samples by modern electrothermal atomic absorption spectrometry. *Spectroc. Acta Pt. B-Atom. Spectr.* 65 (2010): 97-112.

[39] Sheremet, A.; Averyaskina, E.; Chekmeneva, E.; Ermakova, S., Standardless electrochemical method for mercury, cadmium, lead and copper determination in aqueous solution. *Electroanalysis* 19 (2007): 2222-2226.

[40] Beinrohr, E. Flow-through coulometry as a calibrationless method in inorganic trace analysis. *Accredit. Qual. Assur.* 6 (2001): 321-324.

[41] He, Q.; Zhu, Z. L.; Hu, S. H.; Jin, L. L. Solution cathode glow discharge induced vapor generation of mercury and its application to mercury speciation by high performance liquid chromatography-atomic fluorescence spectrometry. *J. Chromatogr. A* 1218 (2011): 4462-4467.

[42] Li, L.; He, B.; Jiang, G. B., Analysis of Hydrophilic Mercury-Binding Proteins in Medaka (Oryzias latipes) Using High Performance Liquid Chromatography Coupled with Inductively Coupled Plasma-Mass Spectrometry. *Chin. J. Anal. Chem.* 39 (2011): 623-627.

[43] Batista, B. L.; Rodrigues, J. L.; de Souza, S. S.; Souza, V. C. O.; Barbosa, F., Mercury speciation in seafood samples by LC-ICP-MS with a rapid ultrasound-assisted extraction procedure: Application to the determination of mercury in Brazilian seafood samples. *Food Chem.* 126 (2011): 2000-2004.

[44] Castillo, A.; Roig-Navarro, A. F.; Pozo, O. J. Method optimization for the determination of four mercury species by micro-liquid chromatography-inductively coupled plasma mass spectrometry coupling in environmental water samples. *Analytica Chimica Acta* 577 (2006): 18-25.

[45] Ghanthimathi, S.; Ibrahim, N. B.; Nasir, Z. B.; Lim, L.; Ong, K. Speciation: Determination of Methylmercury in Fish Samples with HPLC-ICP-MS. *Atom. Spectrosc.* 32 (2011): 85-89.

[46] Hong, Y. S.; Rifkin, E.; Bouwer, E. J. Combination of Diffusive Gradient in a Thin Film Probe and IC-ICP-MS for the Simultaneous Determination of CH_3Hg^+ and Hg^{2+} in Oxic Water. *Environ. Sci. Technol.* 45 (2011): 6429-6436.

[47] Li, J. H.; Lu, W. H.; Ma, J. P.; Chen, L. X. Determination of mercury(II) in water samples using dispersive liquid-liquid microextraction and back extraction along with capillary zone electrophoresis. *Microchim. Acta* 175 (2011): 301-308.

[48] Nolan, E. M.; Lippard, S. J., Tools and Tactics for the Optical Detection of Mercuric Ion. *Chem. Rev.* 108 (2008): 3443– 3480

[49] Youn, N. J.; Chang, S. K., Dimethylcyclam based fluoroionophore having Hg^{2+}- and Cd^{2+}-selective signaling behaviors. *Tetrahedron Lett.* 46 (2005): 125-129.

[50] Wang, L.; Zhu, X. J.; Wong, W. Y.; Guo, J. P.; Wong, W. K.; Li, Z. Y., Dipyrrolylquinoxaline-bridged Schiff bases: A new class of

fluorescent sensors for mercury(II). *Dalton Trans.* 19 (2005): 3235–3240.

[51] Caballero, A.; Martinez, R.; Lloveras, V.; Ratera, I.; Vidal-Gancedo, J.; Wurst, K.; Tarraga, A.; Molina, P.; Veciana, J. Highly selective chromogenic and redox or fluorescent sensors of Hg^{2+} in aqueous environment based on 1,4-disubstituted azines. *J. Am. Chem. Soc.* 127 (2005): 15666-15667.

[52] Ko, S. K.; Yang, Y. K.; Tae, J.; Shin, I. In vivo monitoring of mercury ions using a rhodamine-based molecular probe. *J. Am. Chem. Soc*. 128 (2006): 14150-14155.

[53] Ha-Thi, M. H.; Penhoat, M.; Michelet, V.; Leray, I. Highly selective and sensitive phosphane sulfide derivative for the detection of Hg^{2+} in an organoaqueous medium. *Organic Org. Lett.* 9 (2007): 1133-1136.

[54] Lee, M. H.; Lee, S. W.; Kim, S. H.; Kang, C.; Kim, J. S., Nanomolar Hg(II) Detection Using Nile Blue Chemodosimeter in Biological Media. *Org. Lett.* 11 (2009): 2101-2104.

[55] Li, H. W.; Wang, B.; Dang, Y. Q.; Li, L.; Wu, Y. Q. A highly selective fluorescent sensor for mercury ions in aqueous solution: Detection based on target-induced aggregation. *Sens. Actuator B-Chem.* 148 (2010): 49-53.

[56] http://home.fuse.net/clymer/buffers/phos2.html

[57] Skoog, A. D.; West, M. D.; Holler, F. J.; Crouch, S. R. Fundamental of analytical chemistry. 450-485.

APPENDIX
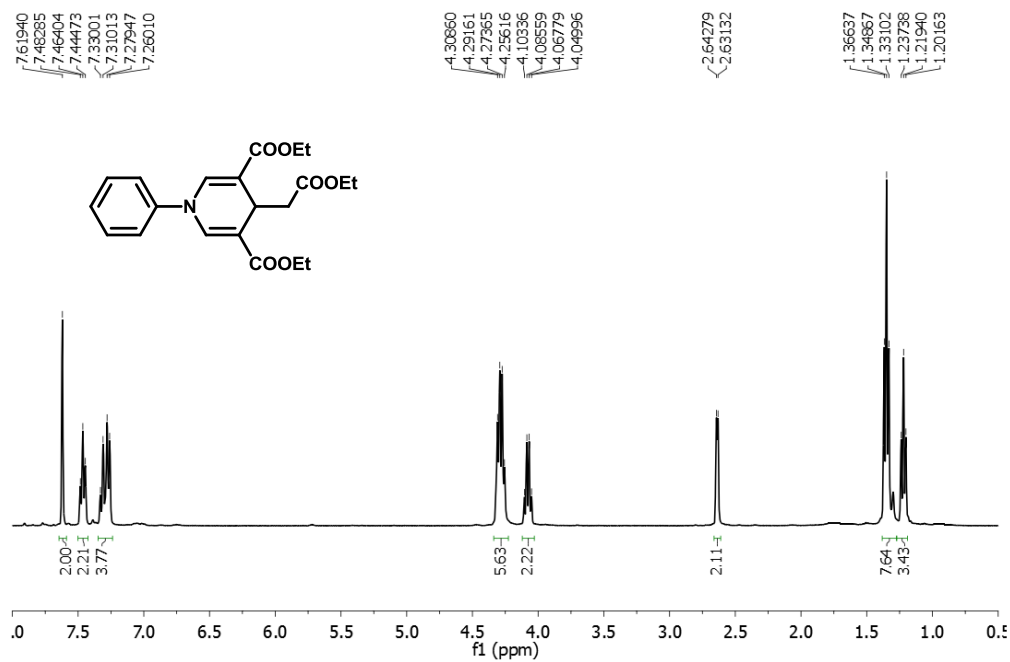
Figure A.1 The ^{1}H NMR of Diethyl-4-(2-ethoxy-2-oxoethyl)-1-phenyl-1,4-dihydropyridine-3,5-dicarboxylate (**1a**) in CDCl$_3$.
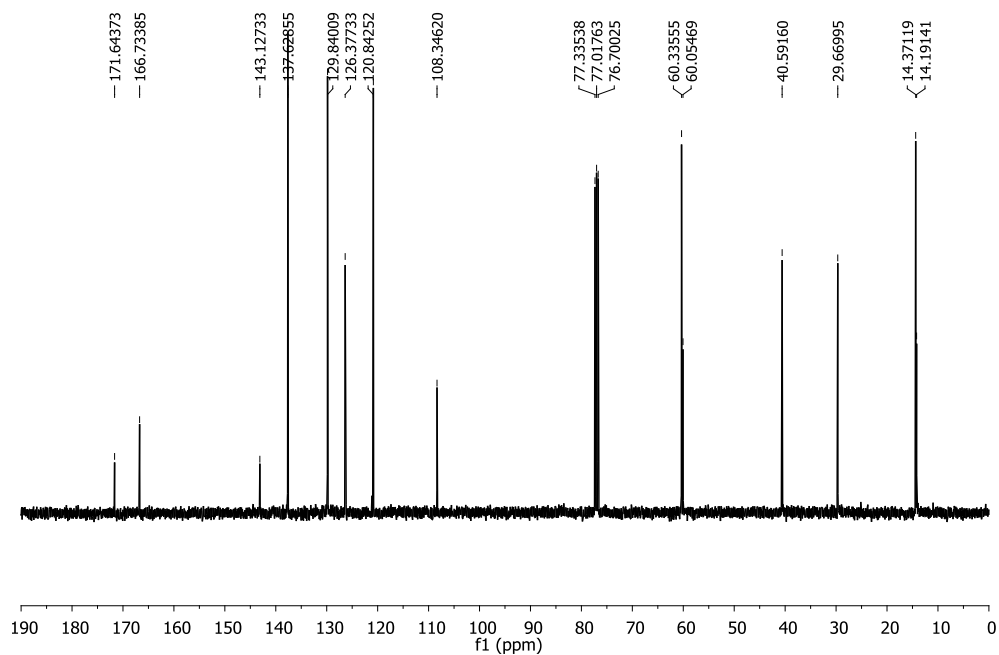
Figure A.2 The ^{13}C NMR of Diethyl-4-(2-ethoxy-2-oxoethyl)-1-phenyl-1,4-dihydropyridine-3,5-dicarboxylate (**1a**) in CDCl$_3$.
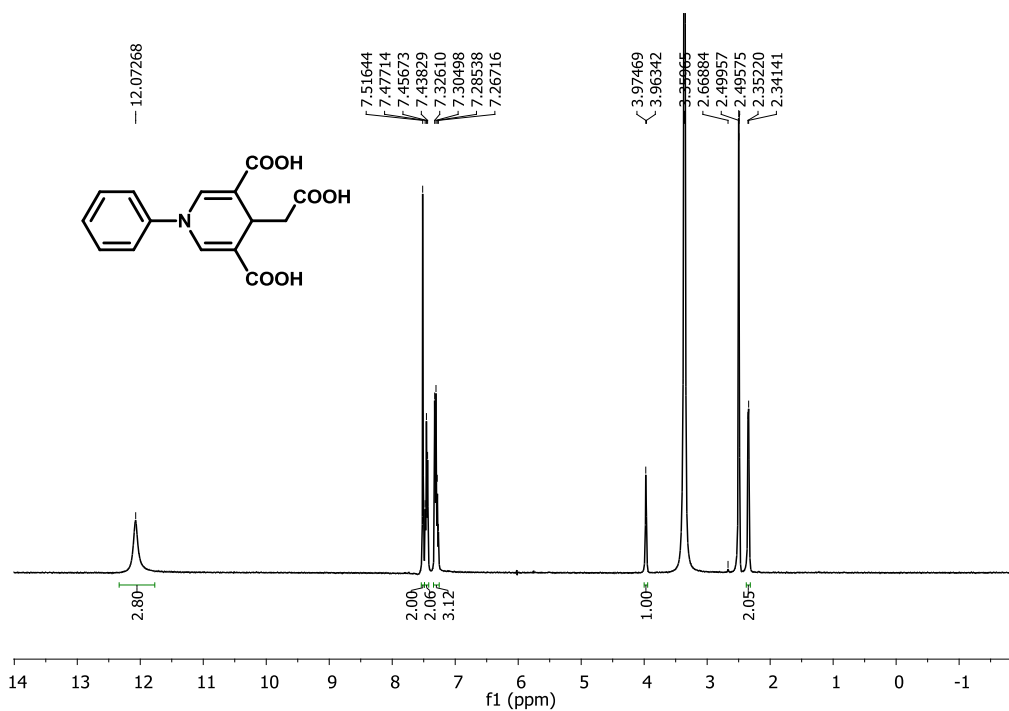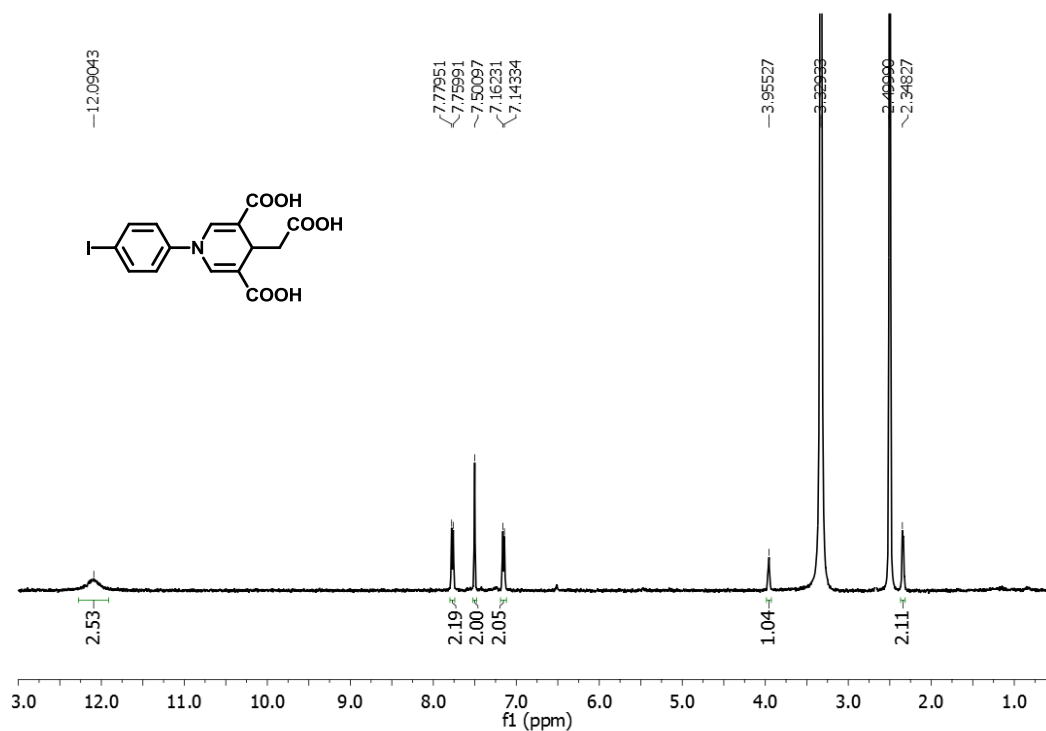
Figure A.3 The ^{1}H NMR of 4-(Carboxymethyl)-1-phenyl-1,4-dihydropyridine-3,5-dicarboxylic acid (**2a**) in DMSO.
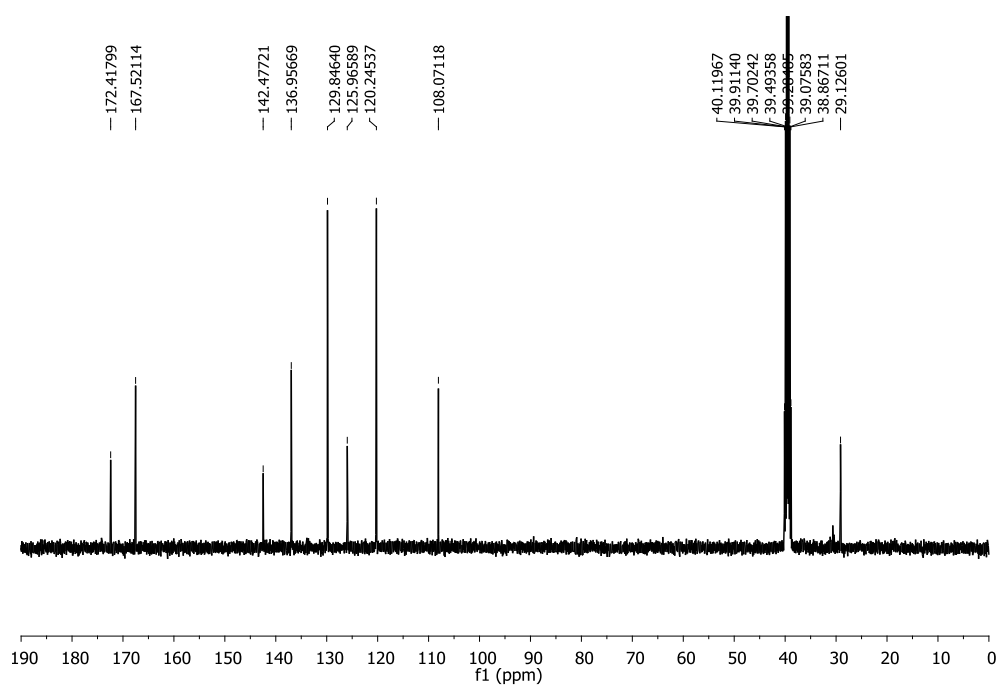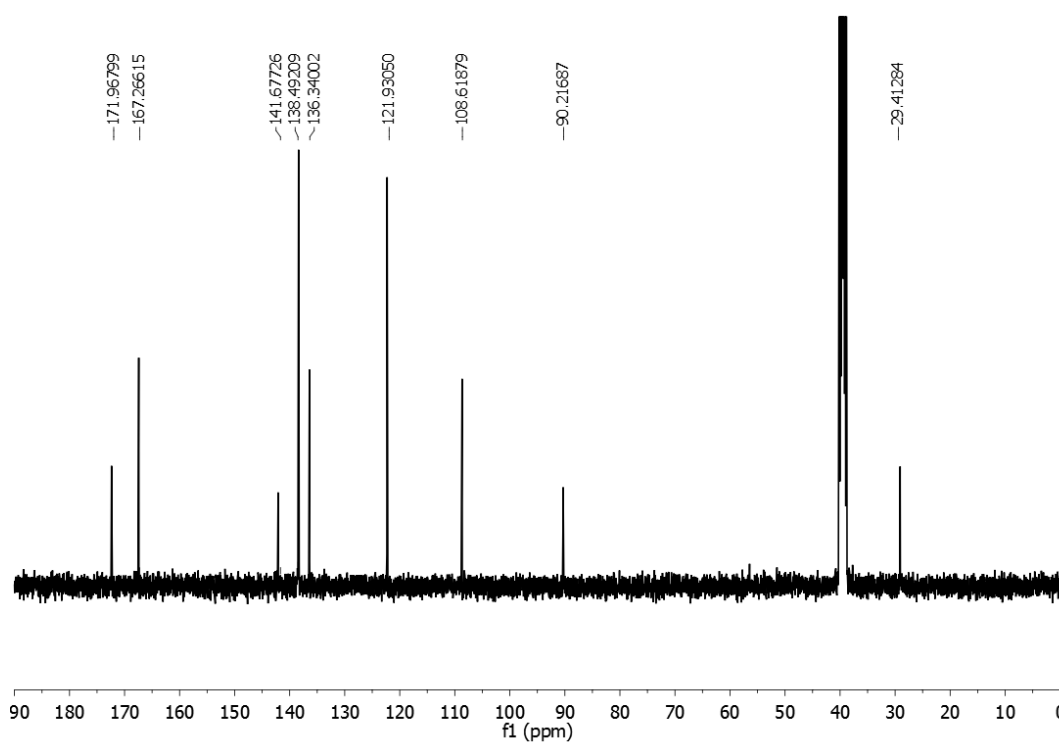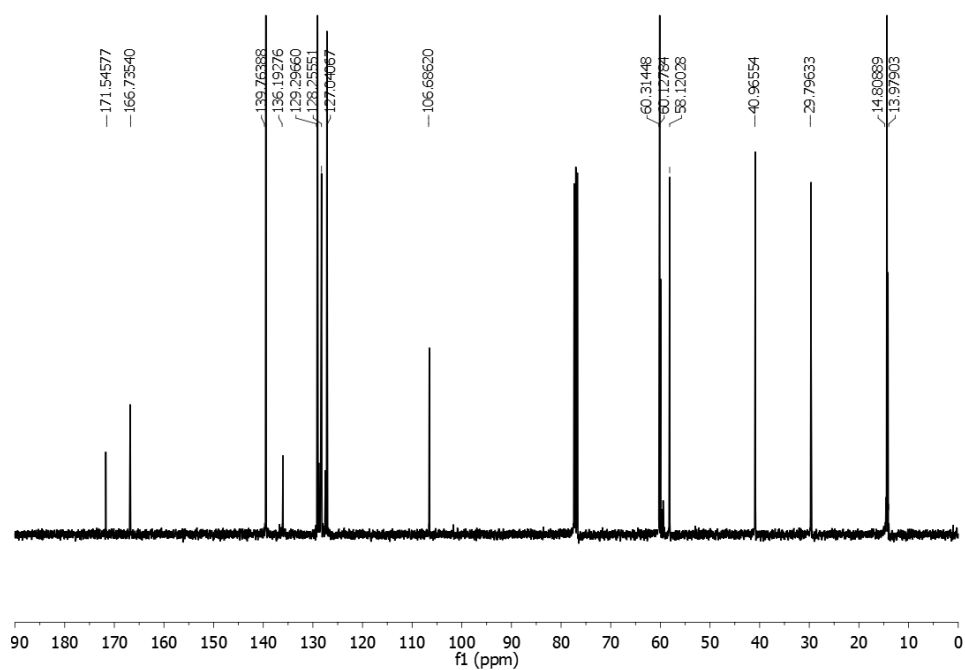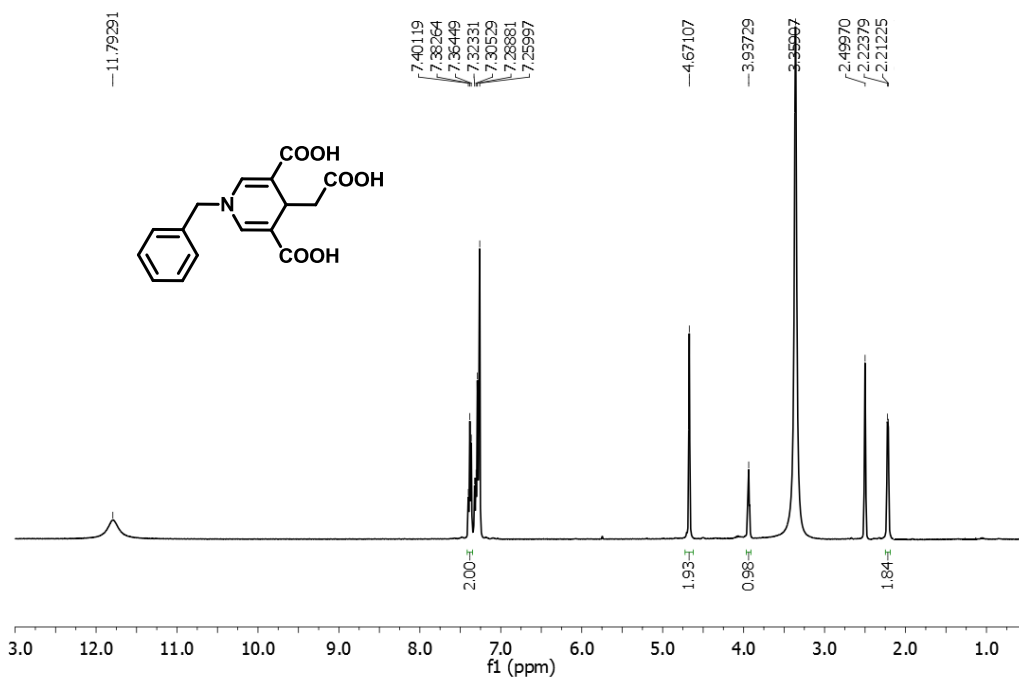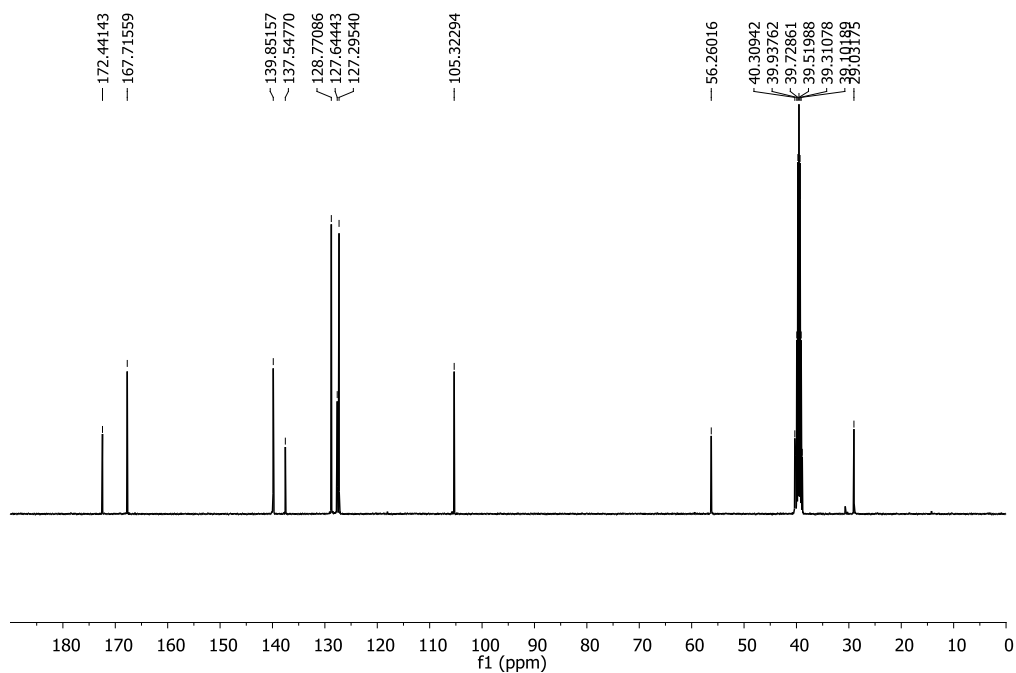

Figure A.4 The ^{13}C NMR of-(Carboxymethyl)-1-phenyl-1,4-dihydropyridine-3,5-dicarboxylic acid (**2a**) in DMSO.
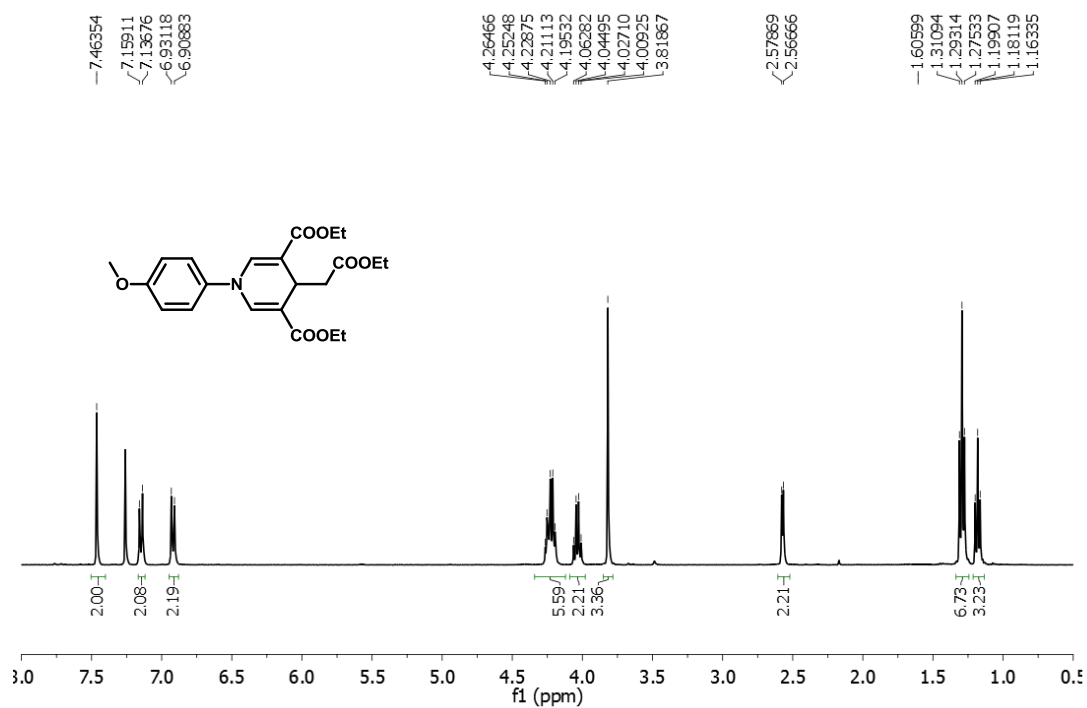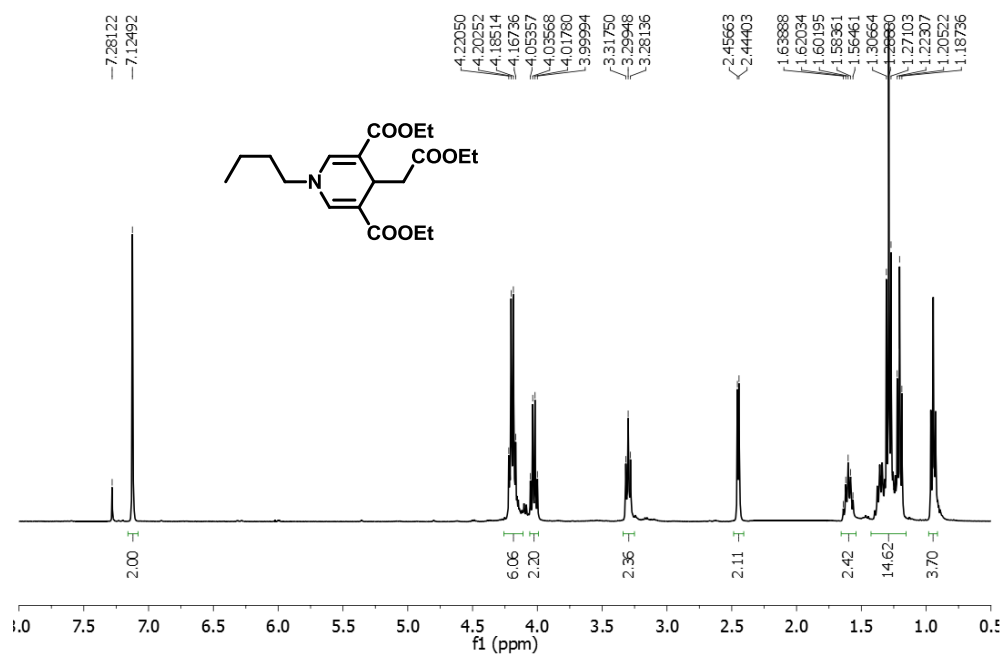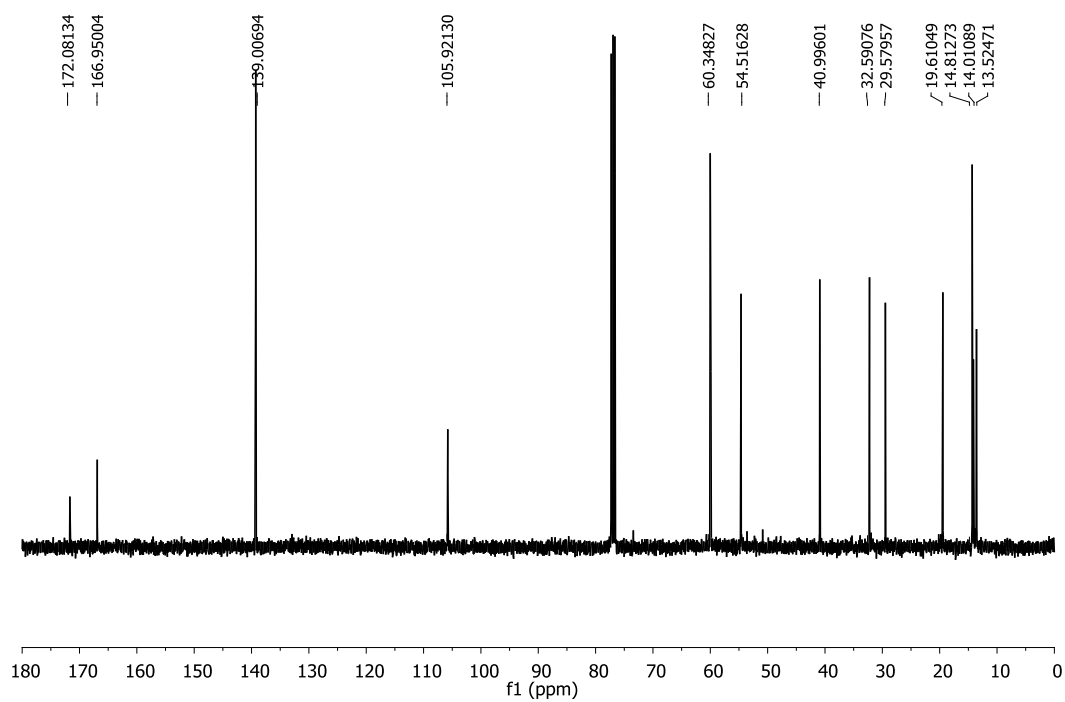
Figure A.5 The ¹H NMR of Diethyl-4-(2-ethoxy-2-oxoethyl)-1-(4-methoxyphenyl)-1,4-dihydropyridine-3,5-dicarboxylate (**1b**) in CDCl₃.
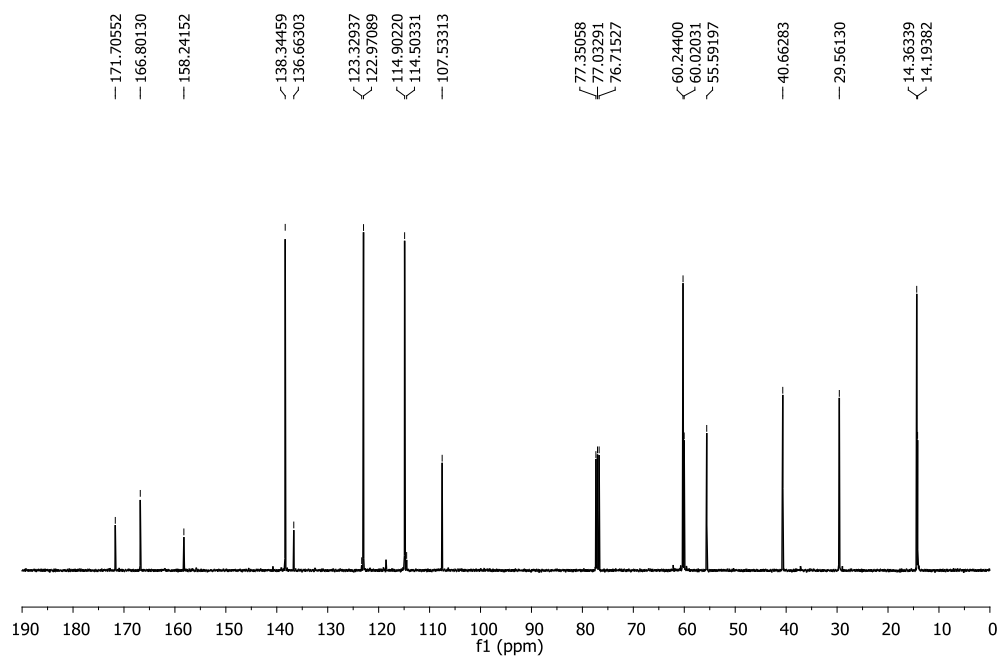
Figure A.6 The ¹³C NMR of Diethyl-4-(2-ethoxy-2-oxoethyl)-1-(4-methoxyphenyl)-1,4-dihydropyridine-3,5-dicarboxylate (**1b**) in CDCl₃.
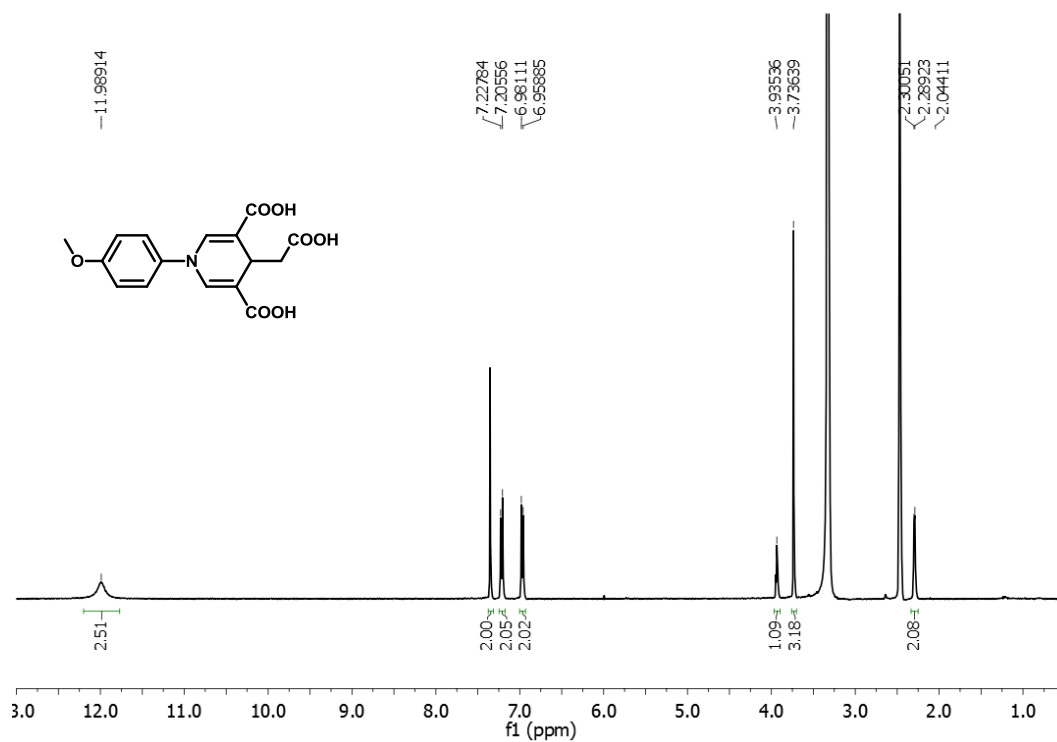
Figure A.7 The ^{1}H NMR of 4-(Carboxymethyl)-1-(4-methoxyphenyl)-1,4-dihydropyridine-3,5-dicarboxylic acid (**2b**) in DMSO.
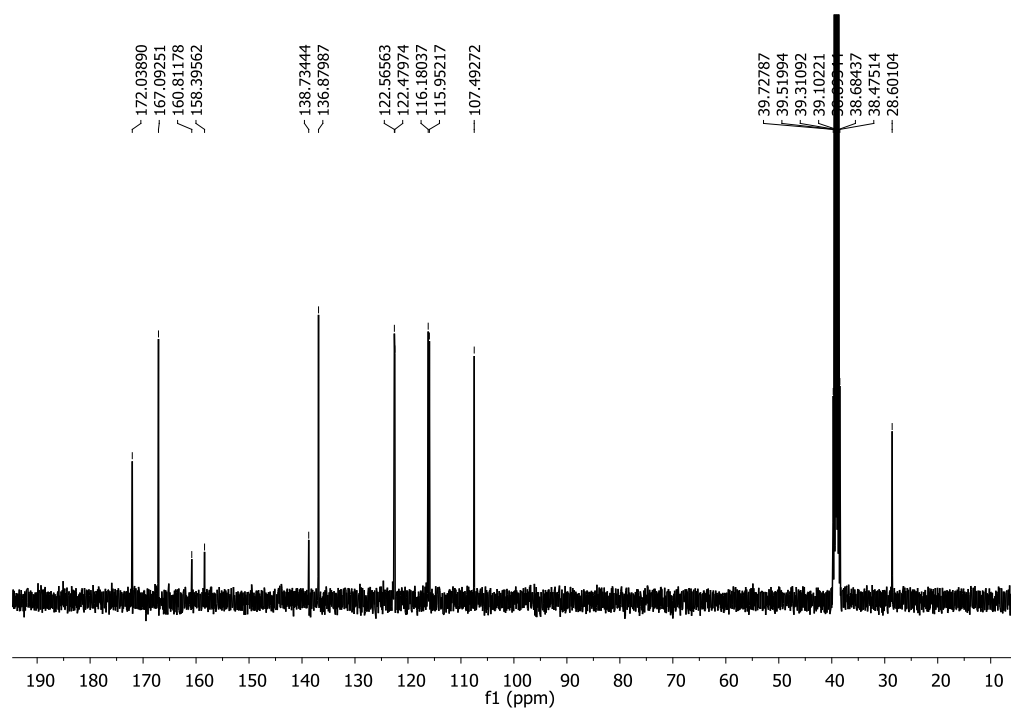
Figure A.8 The ^{13}C NMR of 4-(Carboxymethyl)-1-(4-methoxyphenyl)-1,4-dihydropyridine-3,5-dicarboxylic acid (**2b**) in DMSO.
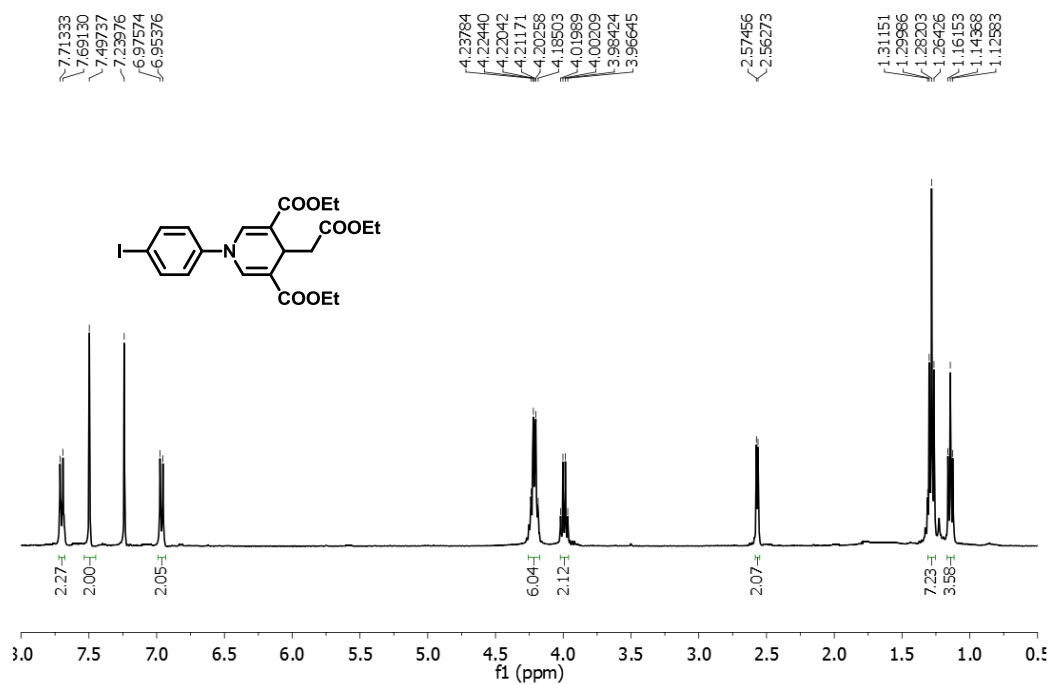
Figure A.9 The ^{1}H NMR of Diethyl-4-(2-ethoxy-2-oxoethyl)-1-(4-iodophenyl)-1,4-

dihydropyridine-3,5-dicarboxylate (**1c**) in CDCl$_3$.
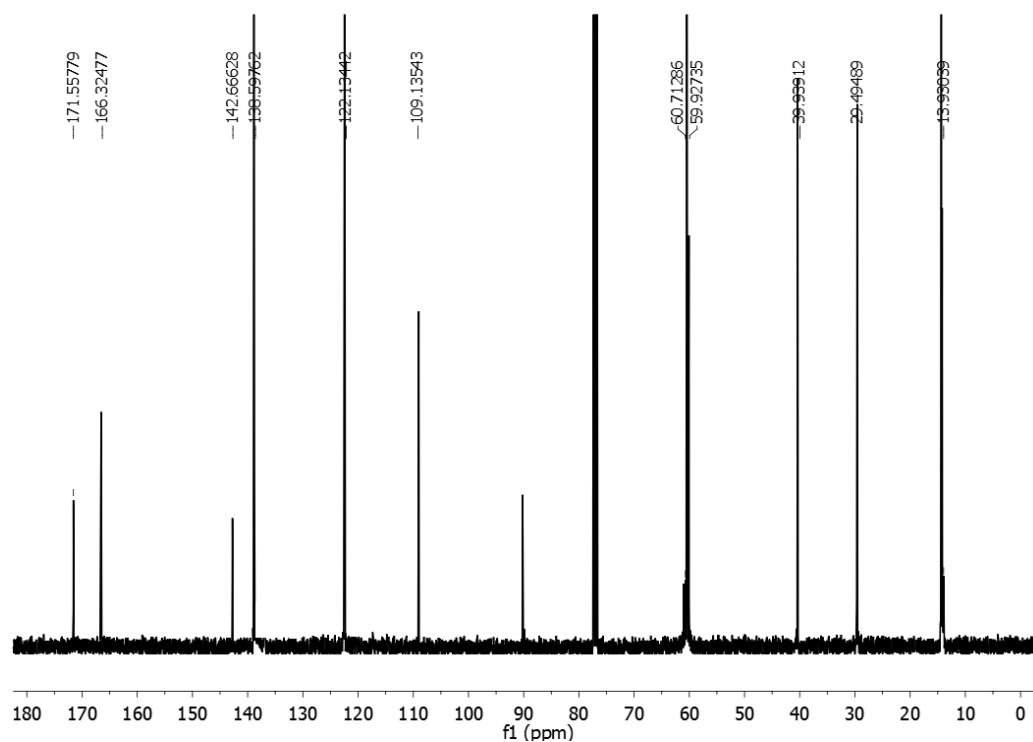
Figure A.10 The ^{13}C NMR of Diethyl-4-(2-ethoxy-2-oxoethyl)-1-(4-iodophenyl)-1,4-

dihydropyridine-3,5-dicarboxylate (**1c**) in CDCl$_3$.

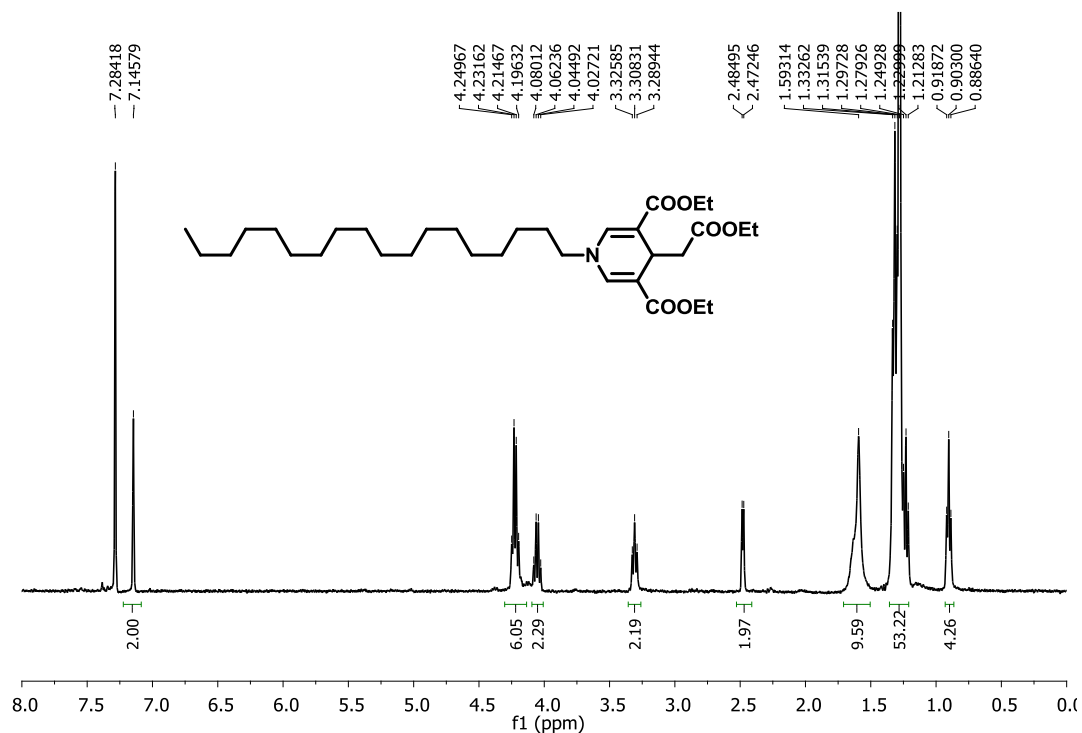**Figure A.11** The ¹H NMR of 4-(Carboxymethyl)-1-(4-iodophenyl)-1,4-dihydropyridine-3,5-dicarboxylic acid (**2c**) in DMSO.

Figure A.12 The ¹³C NMR of 4-(Carboxymethyl)-1-(4-iodophenyl)-1,4-dihydropyridine-3,5-dicarboxylic acid (**2c**) in DMSO.
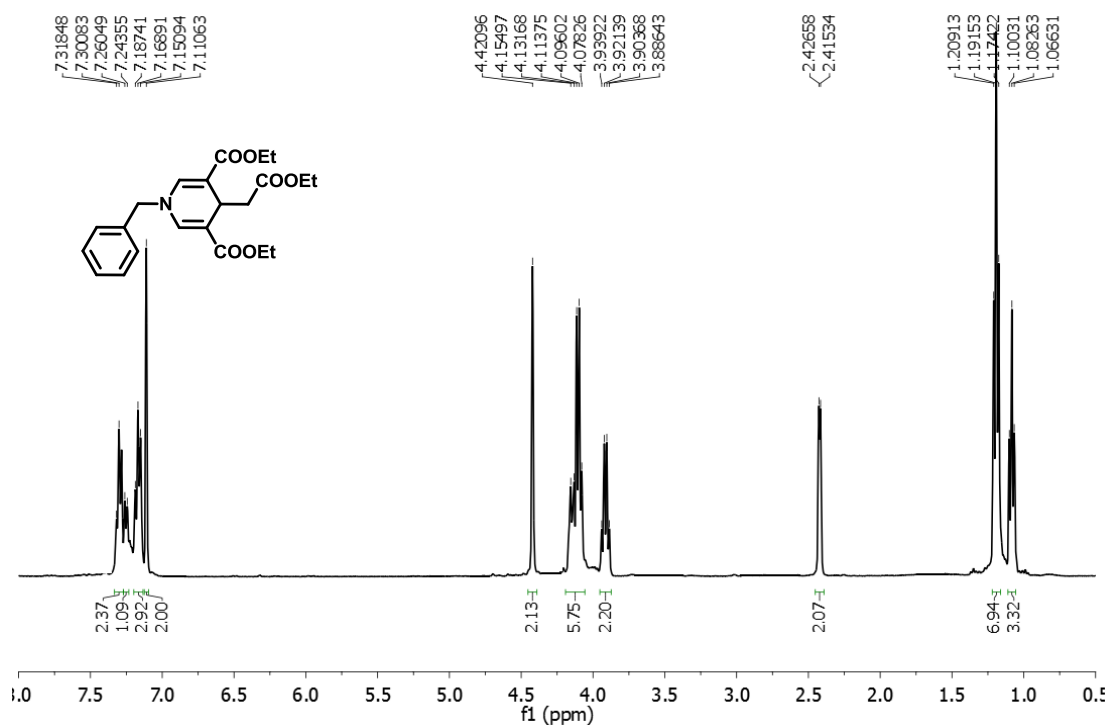
Figure A.13 The ^{1}H NMR of Diethyl-1-benzyl-4-(2-ethoxy-2-oxoethyl)-1,4-dihydropyridine-3,5-dicarboxylate (**1d**) in CDCl$_3$.
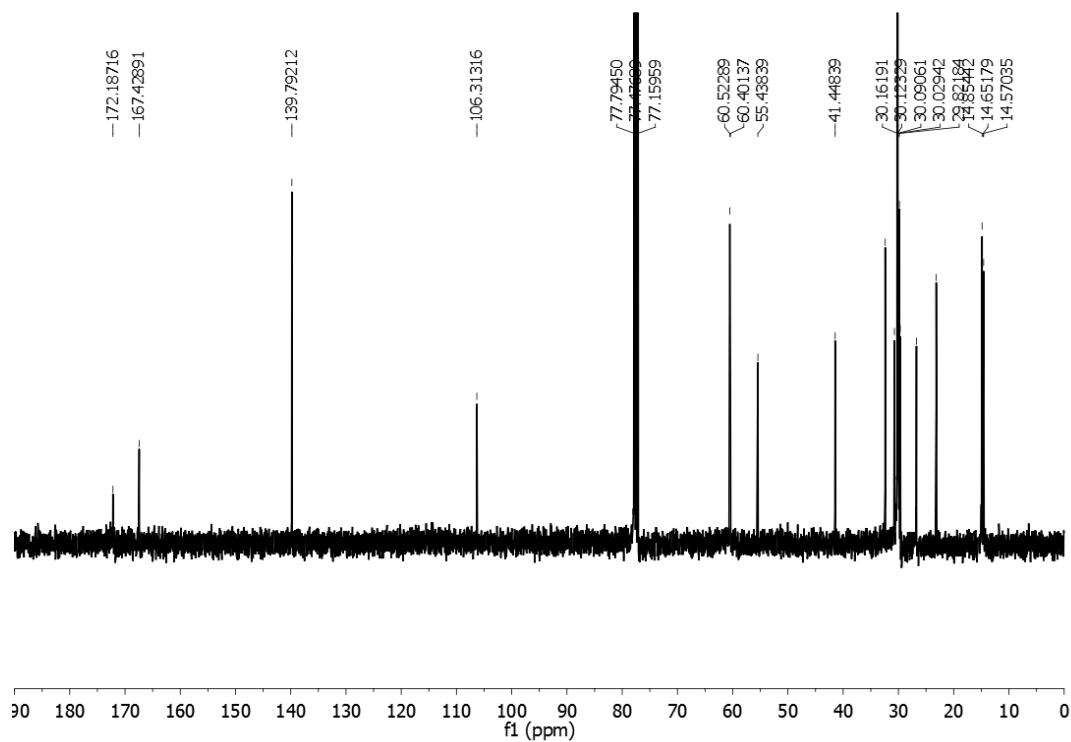

Figure A.14 The ^{13}C NMR of Diethyl-1-benzyl-4-(2-ethoxy-2-oxoethyl)-1,4-dihydropyridine-3,5-dicarboxylate (**1d**) in CDCl$_3$.
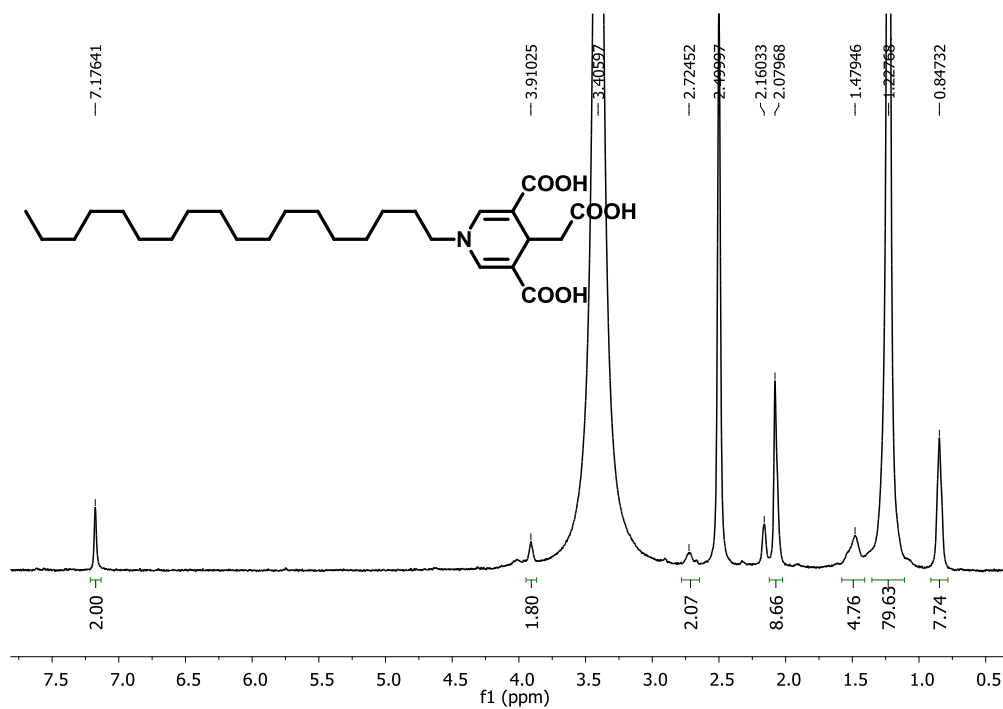
Figure A.15 The ^{1}H NMR of 1-Benzyl-4-(carboxymethyl)-1,4-dihydropyridine-3,5-dicarboxylic acid (**2d**) in DMSO.
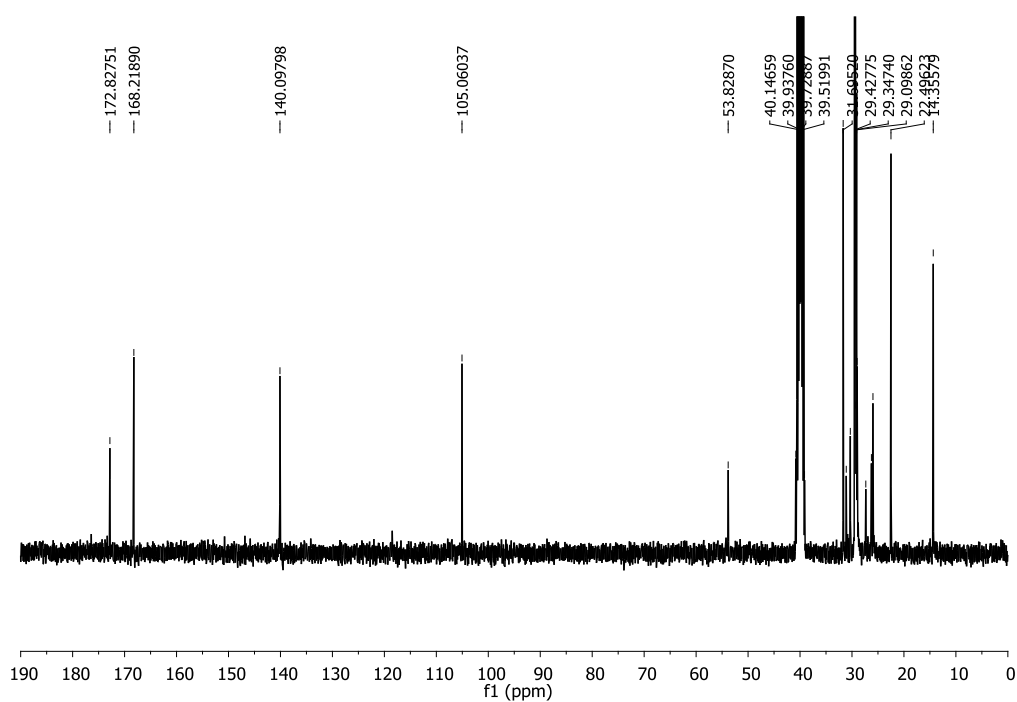

Figure A.16 The ^{13}C NMR of 1-Benzyl-4-(carboxymethyl)-1,4-dihydropyridine-3,5-dicarboxylic acid (**2d**) in DMSO.

Figure A.17 The ^{1}H NMR of Diethyl-1-butyl-4-(2-ethoxy-2-oxoethyl)-1,4-dihydropyridine-3,5-dicarboxylate (**1e**) in CDCl$_3$.

Figure A.18 The ^{13}C NMR of Diethyl-1-butyl-4-(2-ethoxy-2-oxoethyl)-1,4-dihydropyridine-3,5-dicarboxylate (**1e**) in CDCl$_3$.
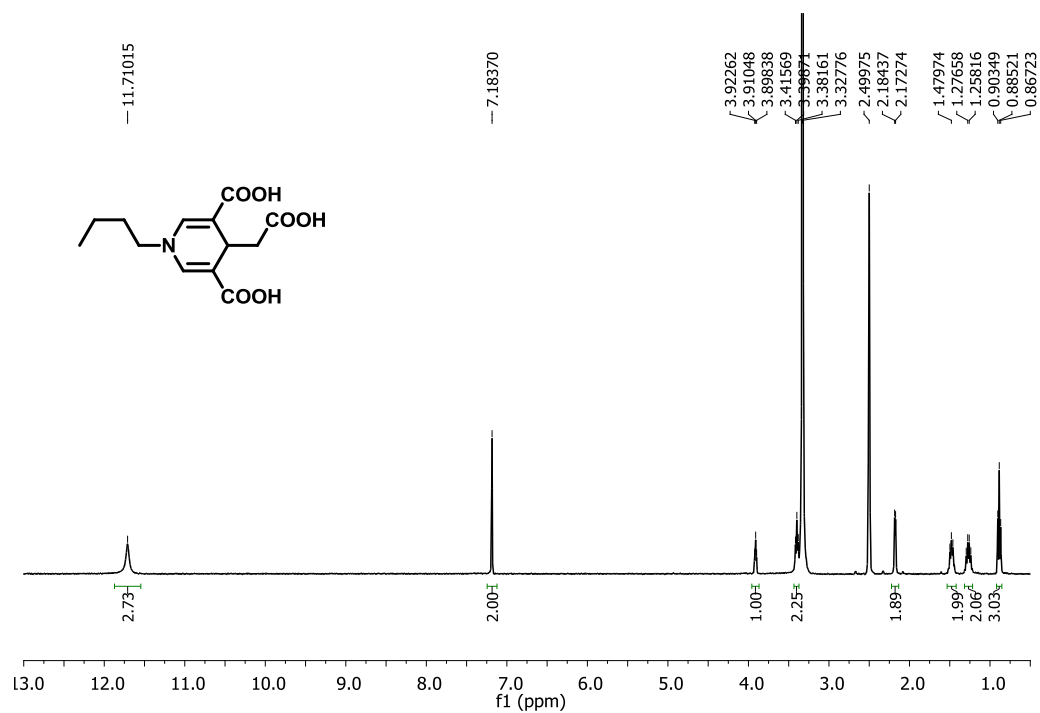
Figure A.19 The ^{1}H NMR of 1-Butyl-4-(carboxymethyl)-1,4-dihydropyridine-3,5-dicarboxylic acid (**2e**) in DMSO.
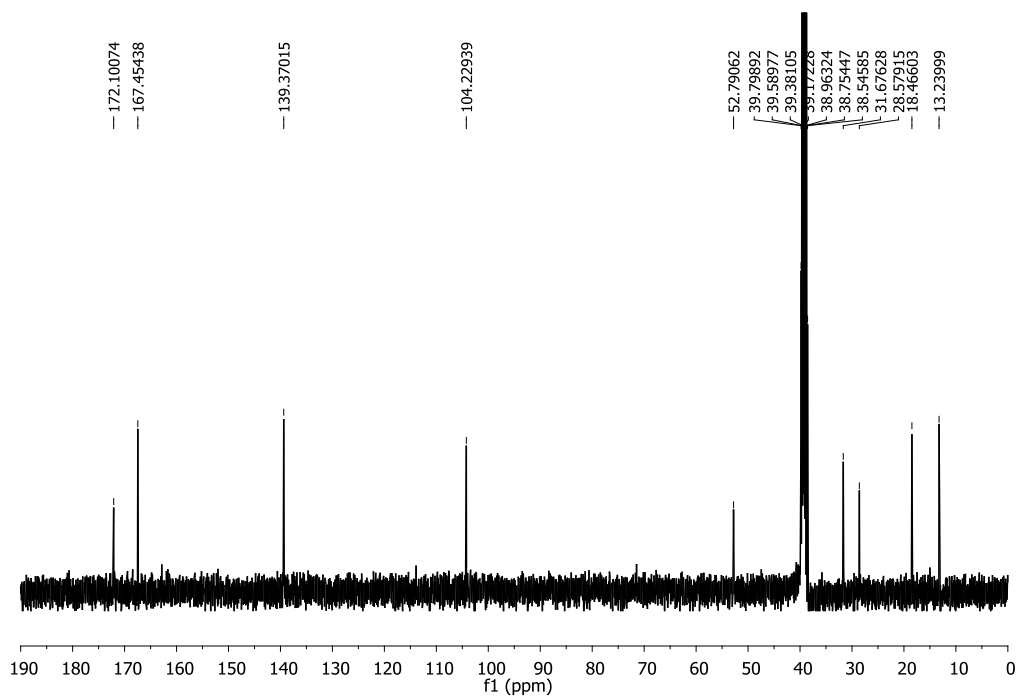
Figure A.20 The ^{13}C NMR of 1-Butyl-4-(carboxymethyl)-1,4-dihydropyridine-3,5-dicarboxylic acid (**2e**) in DMSO.

Figure A.21 The ^{1}H NMR of diethyl 4-(2-ethoxy-2-oxoethyl)-1-octadecyl-1,4-dihydropyridine-3,5-dicarboxylate (**1f**) in CDCl$_3$.

Figure A.22 The ^{13}C NMR of diethyl 4-(2-ethoxy-2-oxoethyl)-1-octadecyl-1,4-dihydropyridine-3,5-dicarboxylate (**1f**) in CDCl$_3$.

Figure A.23 The ^{1}H NMR of 4-(carboxymethyl)-1-octadecyl-1,4-dihydropyridine-3,5-dicarboxylic acid (**2f**) in DMSO.
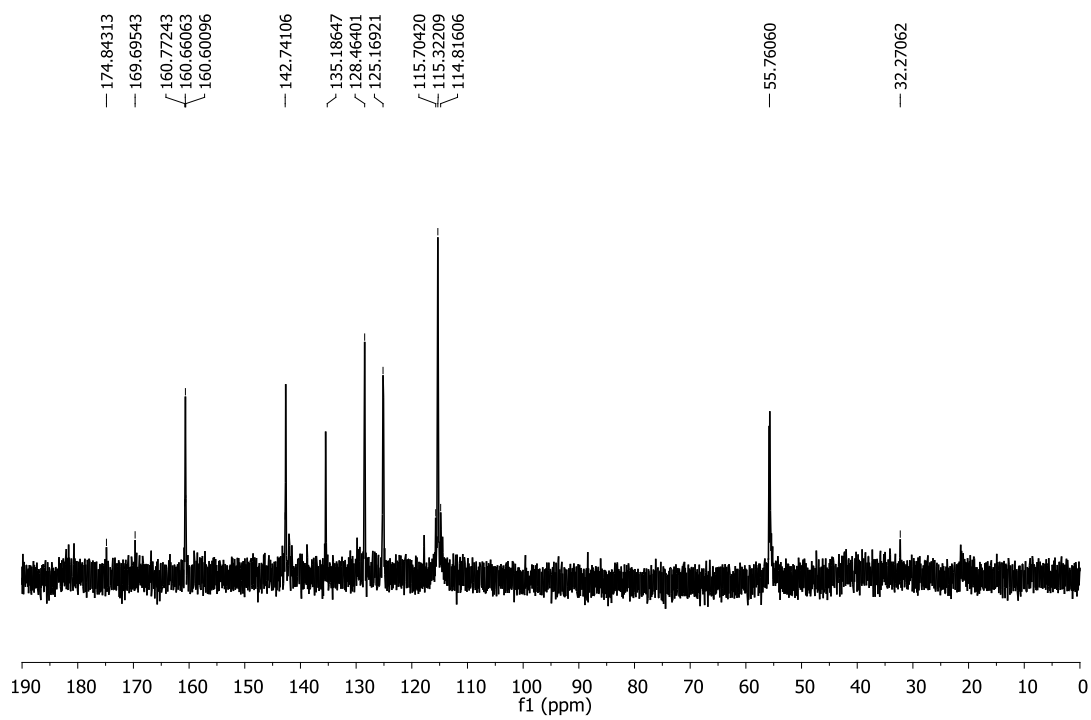

Figure A.24 The ^{13}C NMR of 4-(carboxymethyl)-1-octadecyl-1,4-dihydropyridine-3,5-dicarboxylic acid (**2f**) in DMSO.
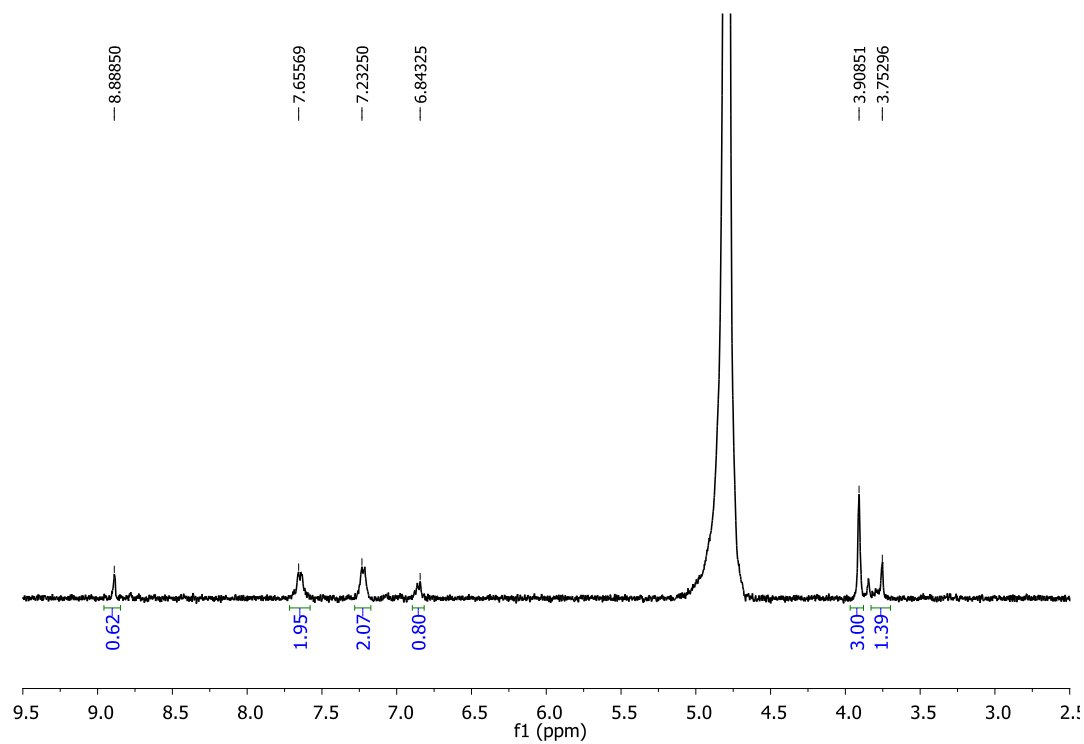
Figure A.25 The ^{1}H NMR of compound **3** in D$_2$O.

Figure A26 The ^{13}C NMR of compound **3** in D$_2$O.
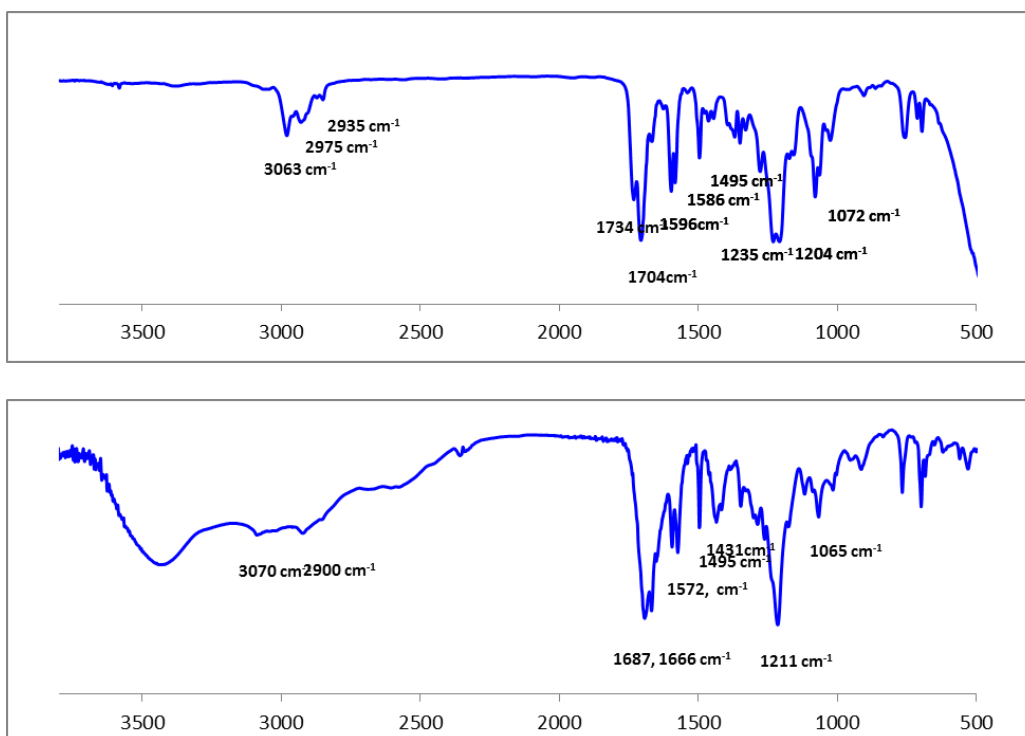
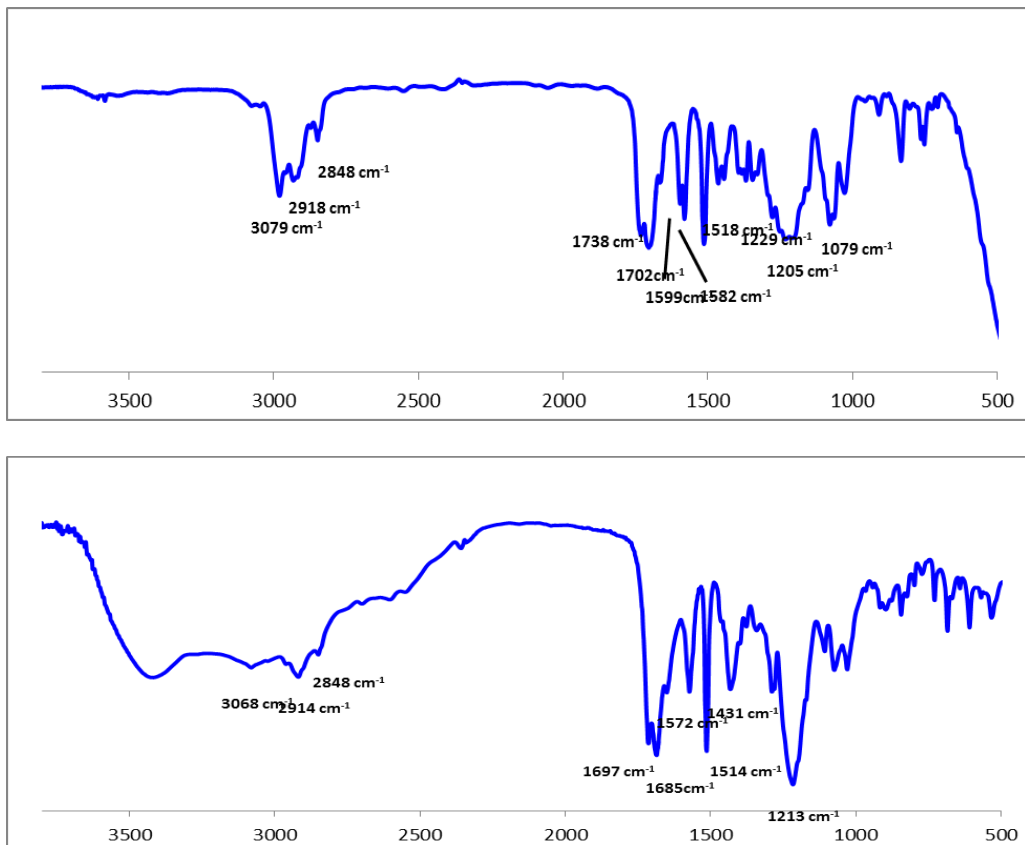**Figure A.27** The IR spectra of compound **1a** and **2a**.

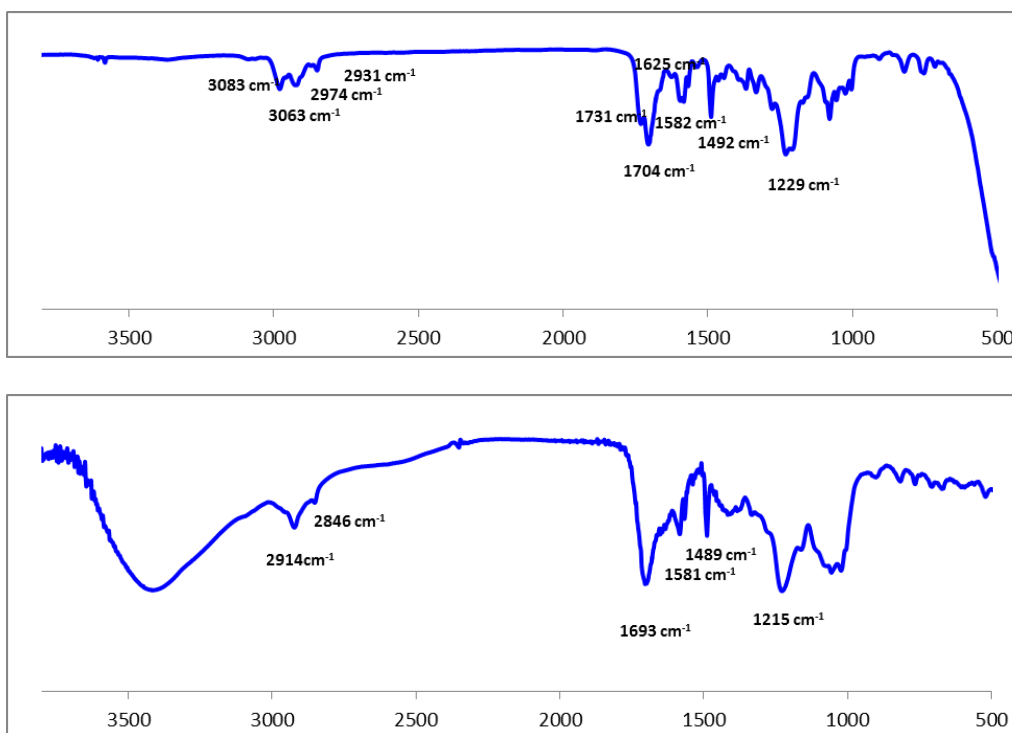
Figure A.28 The IR spectra of compound **1b** and **2b**.
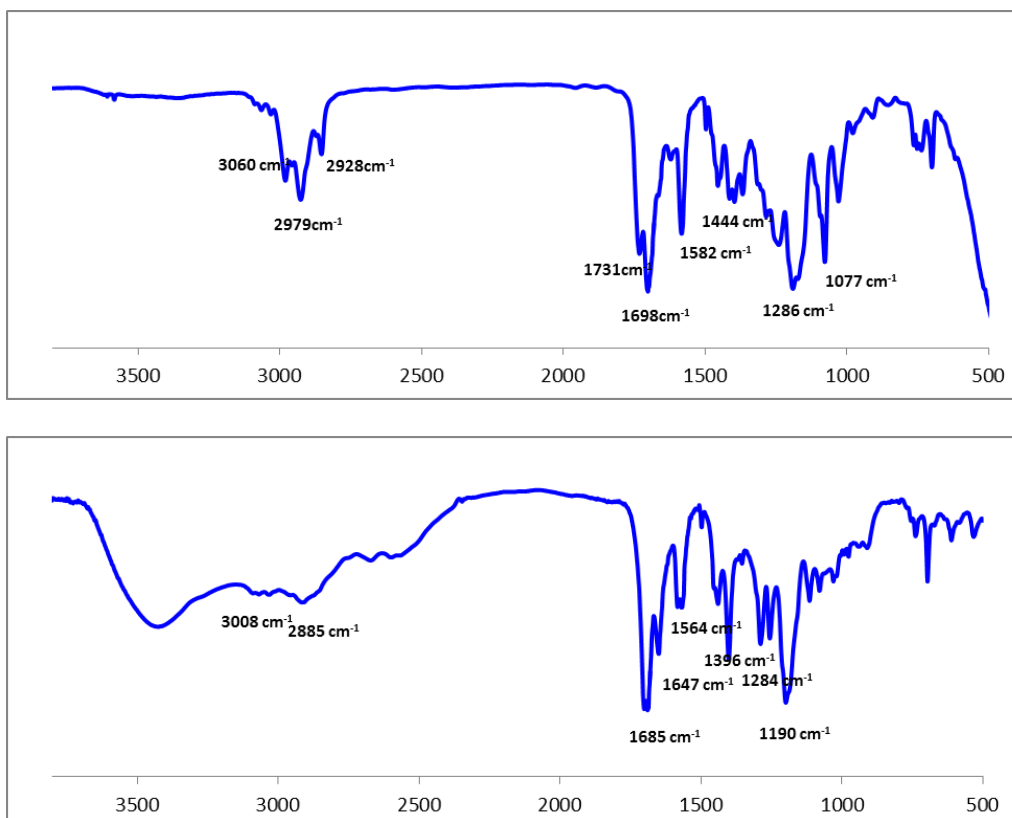
Figure A.29 The IR spectra of compound **1c** and **2c**.

Figure A.30 The IR spectra of compound **1d** and **2d**.
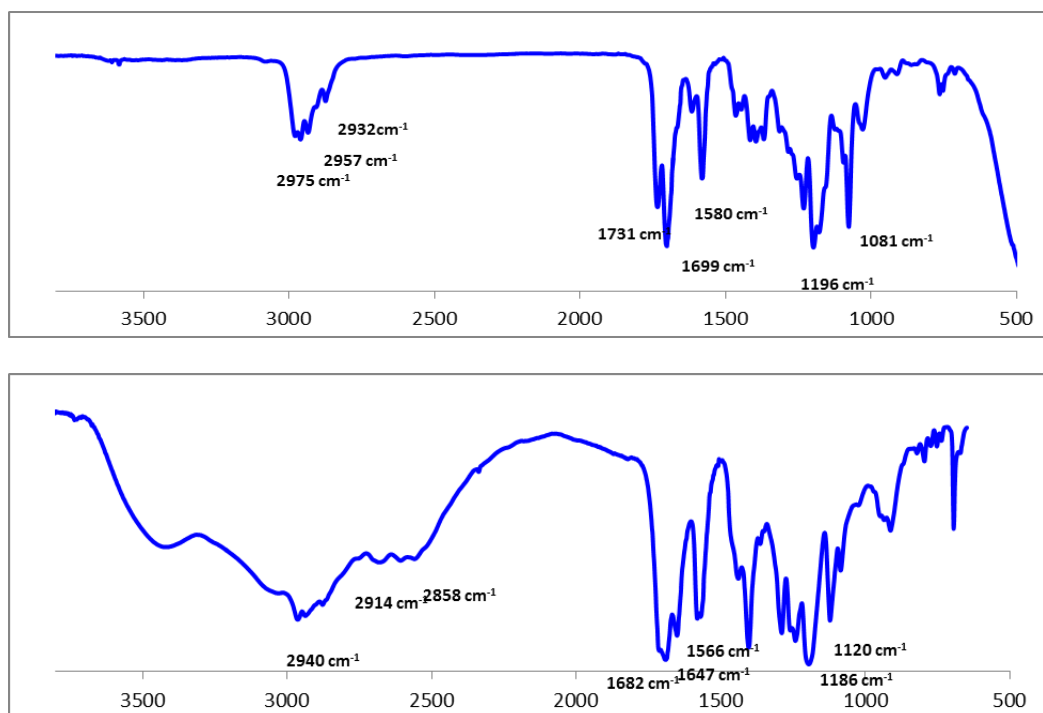
Figure A.31 The IR spectra of compound **1e** and **2e**.

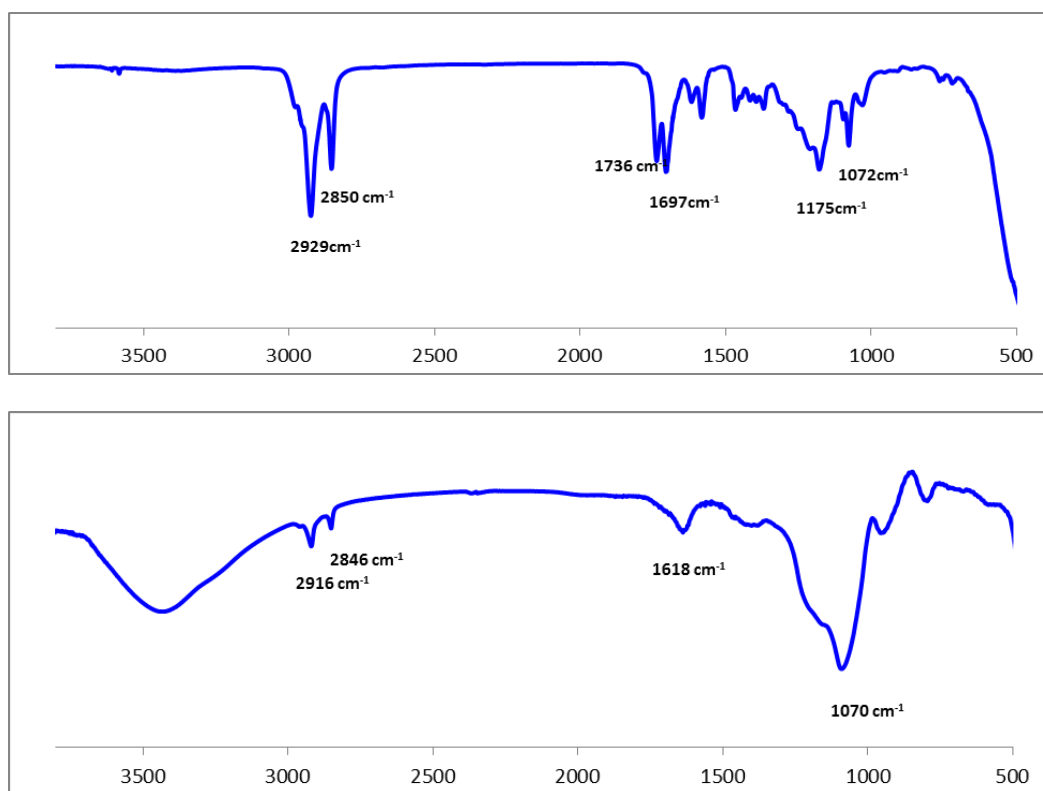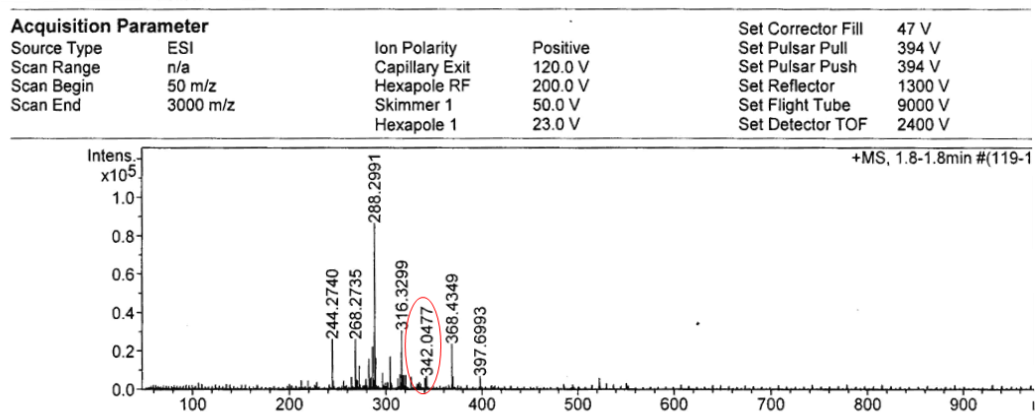**Figure A.32** The IR spectra of compound **1f** and **2f**.
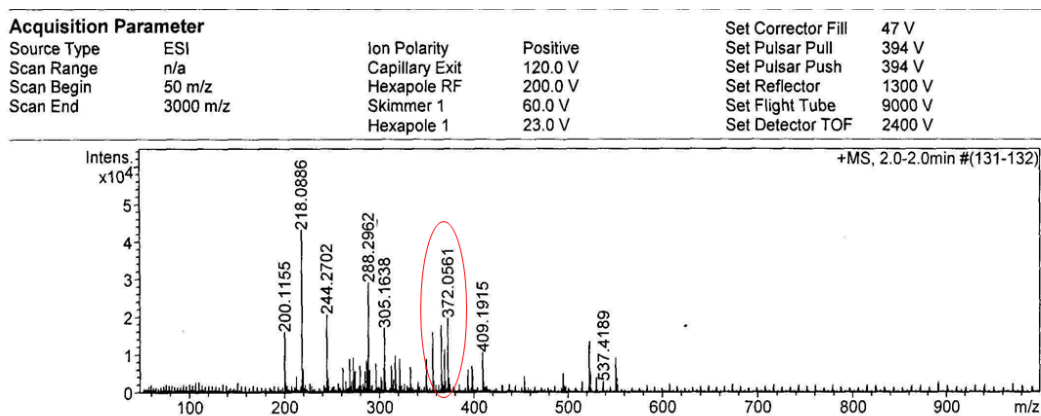
Figure A.33 MS spectra of **2a**.

Figure A.34 MS spectra of **2b**.
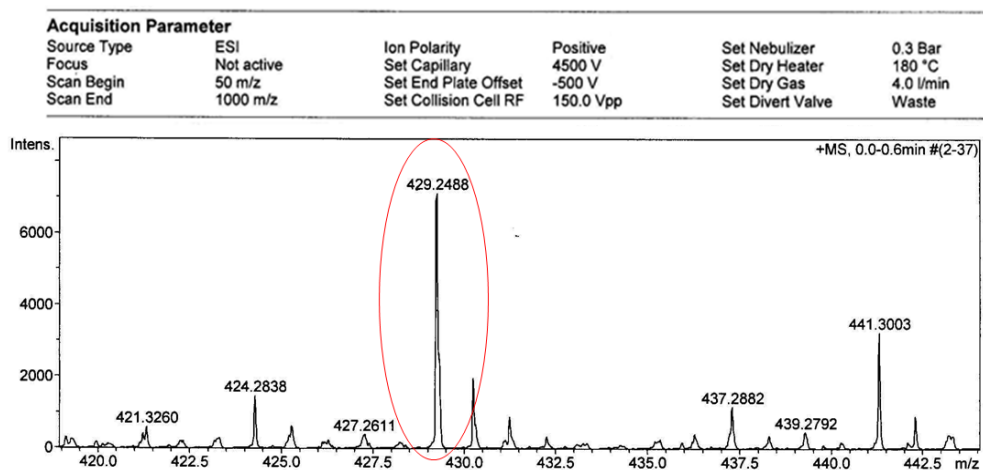
Figure A.35 MS spectra of **2c**.

Acquisition Parameter					
Source Type	ESI	Ion Polarity	Positive	Set Corrector Fill	47 V
Scan Range	n/a	Capillary Exit	120.0 V	Set Pulsar Pull	394 V
Scan Begin	50 m/z	Hexapole RF	300.0 V	Set Pulsar Push	394 V
Scan End	3000 m/z	Skimmer 1	50.0 V	Set Reflector	1300 V
		Hexapole 1	23.0 V	Set Flight Tube	9000 V
				Set Detector TOF	2400 V
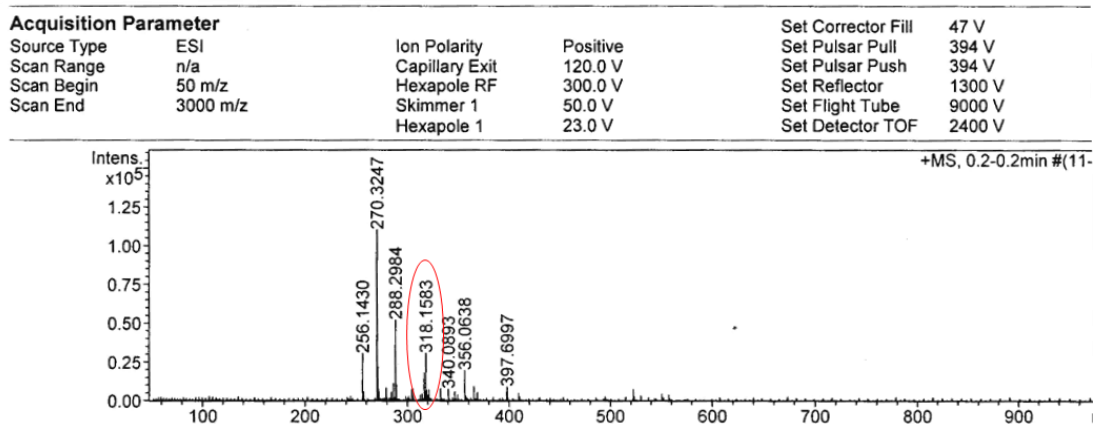
Figure A.36 MS spectra of **2d**.

Acquisition Parameter					
Source Type	ESI	Ion Polarity	Positive	Set Nebulizer	0.3 Bar
Focus	Not active	Set Capillary	4500 V	Set Dry Heater	180 °C
Scan Begin	50 m/z	Set End Plate Offset	-500 V	Set Dry Gas	4.0 l/min
Scan End	1000 m/z	Set Collision Cell RF	150.0 Vpp	Set Divert Valve	Waste
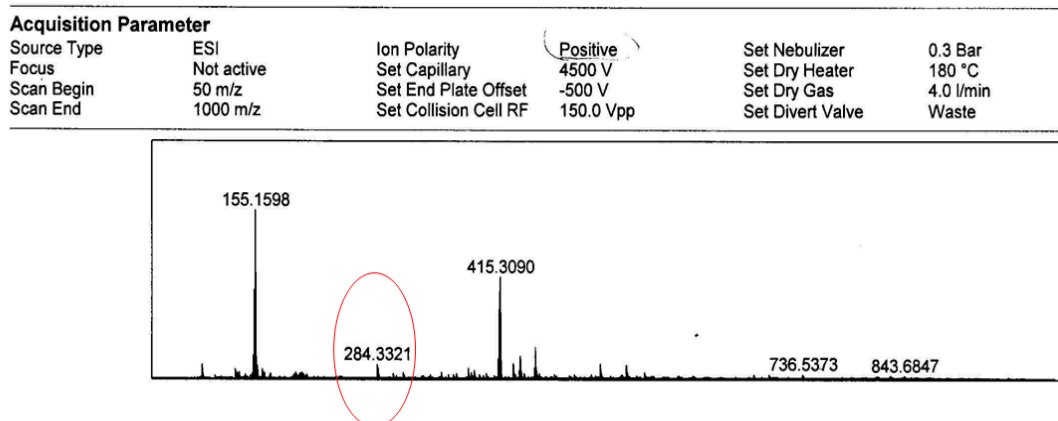
Figure A.37 MS spectra of **2e**.
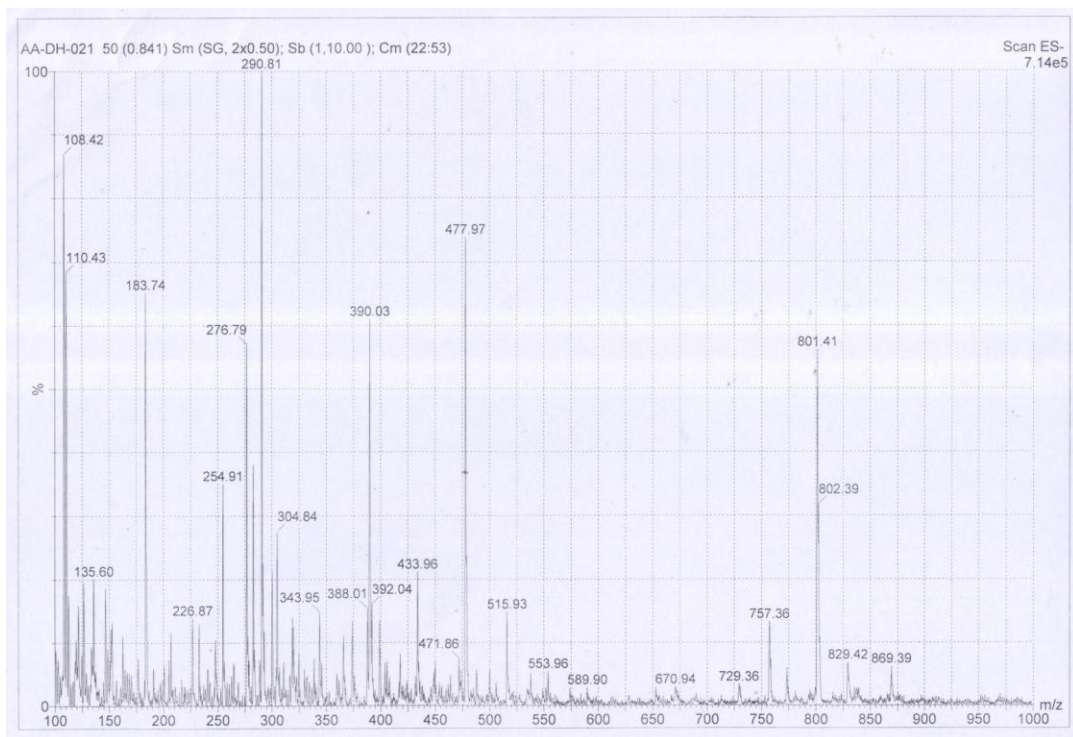
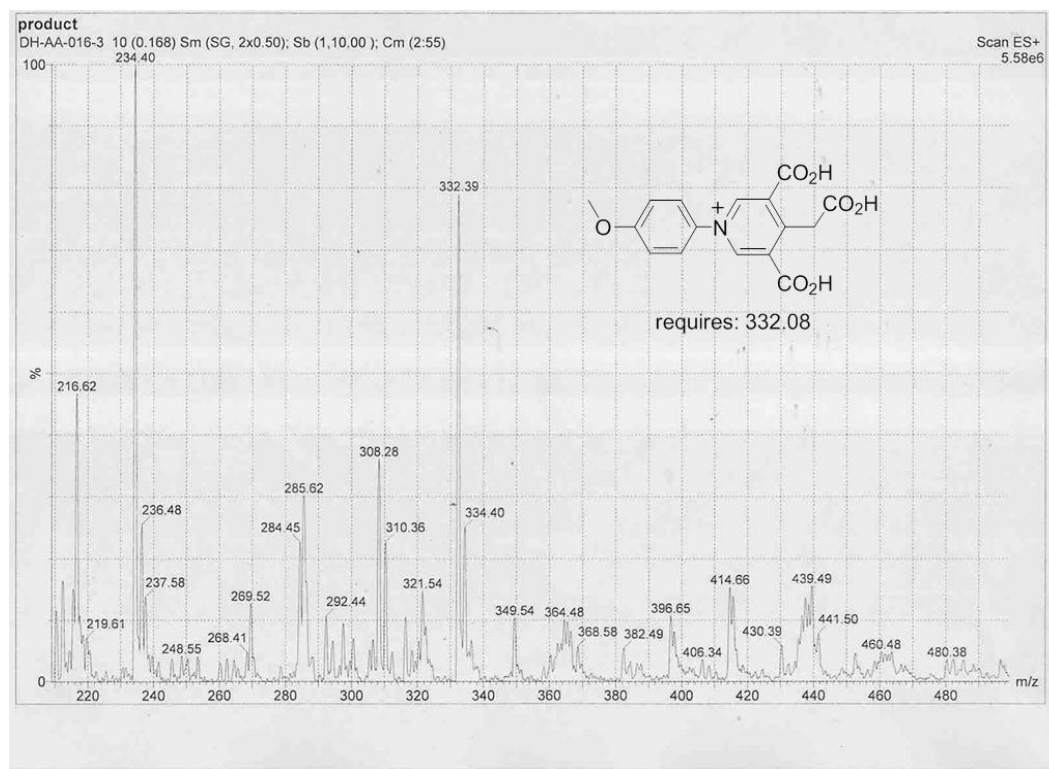**Figure A.38** MS spectra of **2f**.

requires: 332.08

Figure A. 39 MS spectra of compound **3b** and **4b**.

VITAE

Ms. Daranee Homraruen was born on November 19th, 1986 in Rayong, Thailand. She graduated with Bachelor Degree of Science, majoring in Chemistry from Mahidol University in 2009. In 2010, she further received a Master's Degree in Petrochemistry and Polymer Science program at Chulalongkorn University. During the course of study, she received the scholarship from the Center for Petroleum, Petrochemicals and Advanced Materials (ADB) and 90th anniversary of Chulalongkorn University Fund. She had presented her research in Pure and Applied Chemistry International Conference (PACCON 2011) and The 8th International Symposium on Advanced Materials in Asia-Pacific Rim (ISAMAP) and the 2nd International Work shop on Nanogrid Materials (IWNM).

Her present address is 54, Mabkha, Nikompattana, Rayong, Thailand 21180.